Dissertation

Investigations on IL-6Rα and IL-6 mediated signaling in cholangiocarcinoma

submitted by

Florian KLEINEGGER, BSc MSc

for the Academic Degree of

Doctor of Medical Science

(Dr. scient. med.)

at the

Medical University of Graz

Diagnostic and Research Institute of Pathology

under the Supervision of

Assoz. Prof. Priv.-Doz. Dr.med.univ. Dr.sc.nat. **Johannes HAYBAECK**

2019

Declaration

I hereby declare that this thesis is my own original work and that I have fully acknowledged by name all of those individuals and organizations that have contributed to the research for this thesis. Due acknowledgement has been made in the text to all other material used. Throughout this thesis and in all related publications I followed the "Standards of Good Scientific Practice and Ombuds Committee at the Medical University of Graz".

Graz, 28th of February 2019

Florian Kleinegger, BSc MSc

Parts of my thesis had been published in Kleinegger *et al.* Biochim Biophys Acta Mol Basis Dis. 2019 (1):

Pharmacologic IL-6Rα inhibition in cholangiocarcinoma promotes cancer cell growth and survival.

Florian Kleinegger[a], Eva Hofer[a], Christina Wodlej[a,b], Nicole Golob-Schwarzl[a,b], Anna Maria Birkl-Toeglhofer[a], Alexander Stallinger[c], Johannes Petzold[a], Anna Orlova[d,e], Stefanie Krassnig[a], Robert Reihs[a], Tobias Niedrist[f], Harald Mangge[f], Young Nyun Park[g], Michael Thalhammer[h], Ariane Aigelsreiter[a], Sigurd Lax[i], Christoph Garbers[j], Peter Fickert[k], Stefan Rose-John[j], Richard Moriggl[d,e,l], Beate Rinner[c], Johannes Haybaeck[a,b,m]

[a] Diagnostic & Research Center for Molecular BioMedicine, Institute of Pathology, Medical University of Graz, Austria

[b] Center for Biomarker Research in Medicine, Graz, Austria

[c] Department for Biomedical Research, Core Facility Alternative Biomodels and Preclinical Imaging, Medical University of Graz, Austria

[d] Ludwig Boltzmann Institute for Cancer Research, Vienna, Austria

[e] Institute of Animal Breeding and Genetics, University of Veterinary Medicine Vienna, Austria

[f] Clinical Institute of Medical and Chemical Laboratory Diagnostics, Medical University of Graz, Austria

[g] Department of Pathology, Brain Korea 21 PLUS Project for Medical Science, Yonsei University College of Medicine, Seoul, South Korea

[h] Department of General Surgery, Medical University of Graz, Austria

[i] Department of Pathology, Hospital Graz South-West, Austria

[j] Institute of Biochemistry, Kiel University, Germany

[k] Division of Gastroenterology and Hepatology, Medical University Graz, Austria

[l] Medical University of Vienna, Austria

[m] Department of Pathology, Medical Faculty, Otto von Guericke University Magdeburg, Germany

As first author, I confirm that all co-authors agreed to use the published data in my thesis.

“... I´m still standing better than I ever did ...”

Sir Elton John (1982)

Acknowledgements

First, I would like to thank my supervisor and PI Johannes Haybaeck for giving me the opportunity to work within his lab. He always pushed me forward and trained my skills to look at data critically, and he always pushed me beyond unknown limits.

I am grateful to my thesis committee, Peter Fickert and especially to Beate Rinner, who took care of me in desperate moments and who brought me down to earth but always cheered me up.

I want to thank Stefan Rose-John and Christoph Garbers, for providing me with Hyper-IL-6, sgp130Fc and sharing their experience in IL-6 trans-signaling with me.

Paul Baran and Juergen Scheller for providing me with the IL-6Rα antibody and for supporting any interpretative issues, not to forget Margit Gogg-Kammerer, Silvia Schauer, Ulrike Fackelmann, Daniela Pabst and Iris Kufferath for their experience, advices and for heaving a great time together.

I appreciate the help of all my collaborators. Without their assistance, this thesis would not have been possible.

I thank the Doctoral Program for Medical Science and the Doctoral School General and Clinical Pathophysiology of the Medical University of Graz for giving me the opportunity to write a dissertation.

My thanks go to all other members of the Diagnostic and Research Institute of Pathology for their help, guidance and nice meetings during the last years and to my colleagues in the labs, thank you so much.

After all this time, I would rather prefer to call you friends than colleagues.

Many thanks also go to my friends, who understood that I could not keep appointments because I was busy in the lab.

Pez, what would I do without your patience and your sympathy? I know, the last few years have been quite hard, but you always assured me that someday things would get better. You mean everything for me.

And last, but not least, Mum, thank you for everything!

Content

Abbreviations

4-11	IL-6Rα antibody
8-oxo-dG	8-Oxo-2'-deoxyguanosine
ADAM17	A disintegrin and metalloprotease 17
AJCC	Amercian Joint Committee on Cancer
APC	Allophycocyanin
Bcl-2	B-cell lymphoma 2
BSA	Bovine serum albumin
BTC	Biliary tract cancer
CAF	Cancer associated fibroblast
CCA	Cholangiocarcinoma
CD126	Cluster of differentiation 126
CDKN2A	Cyclin-dependent kinase inhibitor 2A
CEACAM	Carcinoembryonic antigen-related cell adhesion molecules
CIS	Cytokine-induced STAT inhibitor
CK	Cytokeratin
COX2	Cyclooxygenase 2
CXCR4	C-X-C chemokine receptor type 4
DAPI	4′,6-Diamidin-2-phenylindol
DEN	Diethylnitrosamine
DMEM	Dulbecco´s Modified Eagle´s Medium
DTT	Dithiothreitol
eCCA	Extrahepatic cholangiocarcinoma
ECLIA	Electrochemiluminescence immunoassay
EDTA	Ethylenediaminetetraacetic acid
EGFR	Epidermal growth factor receptor
EMT	Epithelial-to-mesenchymal transition
ERBB2	Avian erythroblastosis oncogene B2
FBS	Fetal bovine serum
FFPE	Formalin fixed paraffin embedded
FHIT	Fragile histidine triad
FOX	forkhead box
GAPDH	Glyceraldehyde 3-phosphate dehydrogenase

GAS	Interferon-γ activated sequence
GBC	Gallbladder cancer
gp130	Glycoprotein 130
gp80	Glycoprotein 80
HCC	Hepatocellular carcinoma
HER2	Human epidermal growth factor receptor 2
HIF-1α	Hypoxia-inducable factor 1-alpha
iCCA	Intrahepatic cholangiocarcinoma
IDH	Isocytrate dehydrogenase
IHC	Immunohistochemistry
IL-6	Interleukin 6
IL-6Rα	Interleukin 6 receptor alpha chain
iNOS	Inducable nitric oxide synthase
JAK	Janus kinase
JH	JAK homology
KRAS	Kirsten rat sarcoma viral oncogene
MAPK	Mitogen-activated protein kinase activated
Mcl-1	Myeoloid cell leukemia-1
mDNA	Mitochondrial deoxyribonucleic acid
mIL-6R	Membranous interleukin 6 receptor
MTT	3-(4,5-Dimethylthiazol-2-yl)-2,5-diphenyltetrazolium bromide
NF-κB	Nuclear factor kappa-light-chain-enhancer of activated B cells
NNT	Non-neoplastic, not inflammed GBC tissue
NO	Nitric oxide
NP-40	Nonidet P-40
p21	Cyclin-dependent kinase inhibitor 1
PAGE	Polyacrylamide gel electrophoresis
PBS	Phosphate buffered saline
PDAC	Pancreatic ductal adenocarcinoma
PDT	Population doubling time
PI	Propidium iodide
PIAS	Protein inhibitors of activates STATs
PTP	Protein tyrosine phosphatases
PVDF	Poly(1,1-difluoroethylene)

qRT-PCR	Quantitative real-time polymerase chain reaction
ROS	Reactive oxygen species
RPMI	Roswell Park Memorial Institute medium
SDS	Sodium-dodecyl-sulfate
SEM	Standard error of mean
SH2	Src homology 2
sIL-6R	Soluble interleukin 6 receptor
SOCS3	Supressor of cytokine signaling
STAT	Signal transducer and activator of transcription
STR	Short tandem repeat
TAD	Transactivation domain
TBS	Tris buffered saline
TBS-T	0.1% TBS-Tween 20
TCA	Trichoracetic acid
TCGA	The Cancer Genome Database
TMA	Tissue microarray
TNF-α	Tumor necrosis factor alpha
TSG	Tumor supressor gene
TYK2	Non-receptor tyrosine-protein kinase 2
UICC	Union for International Cancer Control's

List of tables

List of figures

Abstract

Biliary tract cancer (BTC) is the second most frequent primary liver cancer. Due to high mortality rates and missing therapy options, constant research is necessary to provide insights into BTC pathogenesis. BTCs are classified based on their anatomical location in intrahepatic cholangiocarcinoma (iCCA), extrahepatic CCA (eCCA) and gallbladder cancer (GBC), whereas the latter is the most common form worldwide.

Chronic inflammation is one of the most leading causes for BTC. The cytokine interleukin 6 (IL-6) is one of the major mediators for inflammatory signals. IL-6 transduces signals via the IL-6 receptor (IL-6Rα). This receptor can occur either in membrane-bound (mIL-6R) form or in soluble form (sIL-6R). The presence of a sIL-6R form enables IL-6 to influence cells lacking IL-6Rα expression. This IL-6 signaling process was termed IL-6 trans-signaling, whereas signal transduction mediated by mIL-6R is termed IL-6 classic signaling.

The present study was based on the hypotheses that IL-6Rα has a pivotal role in the carcinogenesis of BTC and that IL-6 classic signaling and IL-6 trans-signaling influence CCA cells differently. Therefore, we presume that the form of IL-6 signaling plays a role for CCA cells.

To test these hypotheses, GBC tissues were analyzed regarding IL-6Rα expression as tissue microarray and fresh frozen tissues. Non-neoplastic, not inflamed gallbladders served as controls. The results of this study showed a significantly reduced expression of IL-6Rα in GBC on protein and RNA level. Moreover, a significant association between high IL-6Rα expression and better overall survival of GBC patients was found.

In vitro experiments on different CCA cell lines showed that activation of IL-6 trans-signaling plays a rather minor role in the cellular processes observed in CCA. In contrast, activation of IL-6 classic signaling induced increased cell proliferation and reduced apoptosis. Similar results were achieved by specific inhibition of IL-6 trans-signaling. These observations indicate a superior role of both, activation of IL-6 classic signaling and inhibition of IL-6 trans-signaling.

In conclusion, this study describes an association between IL-6Rα and BTC, suggesting an important role of IL-6Rα in cholangiocarcinogenesis. Furthermore, differentiation between IL-6 classic signaling and IL-6 trans-signaling brought more information about the different forms of IL-6 signal transduction in CCA. Therefore, the data obtained in this study make an important contribution to the understanding of BTC and might be used for the development of new therapeutic strategies in the near future.

Zusammenfassung

Karzinome der Gallengänge sind die zweithäufigsten primären Leberkarzinome. Aufgrund ihrer hohen Mortalitätsraten und fehlender Therapiemöglichkeiten ist die Erforschung potentieller Mechanismen, die zur Pathogenese dieser Krankheit führen von besonderer Wichtigkeit. Gallengangskarzinome werden anhand ihrer anatomischen Lokalisation in intrahepatisches cholangiozelluläres Karzinom (iCCA), extrahepatisches cholangiozelluläres Karzinom (eCCA) und Gallenblasenkarzinom (GBC) eingeteilt. Davon stellt das Gallenblasenkarzinom die häufigste Form weltweit dar.

Zur Entwicklung eines Gallengangskarzinoms kommt es häufig durch chronische Entzündung. Entzündungen sind komplexe Prozesse, bei welchen Interleukin 6 (IL-6) als eines der wichtigsten Signalmoleküle dient. Zur Signalübertragung interagiert IL-6 mit dessen Rezeptor (IL-6Rα), welcher entweder membrangebunden (mIL-6R) oder in löslicher Form (sIL-6R) vorliegt. Durch die Interaktion zwischen IL-6 und dem sIL-6R können auch jene Zellen beeinflusst werden, die keine Rezeptorexpression aufweisen. Diese als IL-6 *trans-signaling* bezeichnete Signalübertragung ermöglicht IL-6 daher prinzipiell jede Zelle des menschlichen Körpers zu beeinflussen. Die über den mIL-6R vermittelte Signalübertragung wird im Gegensatz dazu als klassisches IL-6 *signaling* bezeichnet.

Grundlage dieser Dissertation bildete die primäre Hypothese, dass der IL-6Rα einen wesentlichen Beitrag zur Entstehung des Gallengangskarzinoms leistet. Eine weitere Hypothese war, dass klassisches IL-6 *signaling* und IL-6 *trans-signaling* CCA Zellen unterschiedlich beeinflussen und daher die Art der IL-6 Signaltransduktion eine wesentliche Rolle spielt.

Zur Überprüfung dieser Hypothesen wurde Gewebe von Gallenblasenkarzinom-patienten analysiert und mit pathologisch unauffälligem Gallenblasengewebe verglichen. Diese Untersuchungen zeigten eine reduzierte Expression des IL-6Rα im Tumormaterial. Ebenso konnte ein signifikanter Zusammenhang zwischen einer starken IL-6Rα Expression und längerem Überleben von GBC Patienten festgestellt werden.

In vitro Versuche an verschiedenen CCA Zelllinien ergaben, dass die Aktivierung des IL-6 *trans-signaling* eine eher untergeordnete Rolle im CCA spielt. Die Aktivierung

des klassischen IL-6 *signaling* führte hingegen zu einer erhöhten Zellproliferation und zu reduziertem Zelltod. Ähnliche Resultate wurden durch die Inhibierung des IL-6 *trans-signaling* erzielt. Diese Beobachtungen weisen auf eine übergeordnete Rolle von sowohl der Aktivierung des klassischen IL-6 *signaling* als auch der Inhibierung des IL-6 *trans-signaling* hin.

Zusammenfassend beschreibt diese Studie eine Assoziation zwischen dem IL-6Rα und dem Gallengangskarzinom. Dies deutet auf eine potentiell wichtige Rolle des IL-6Rα im Zuge der cholangiozellulären Karzinogenese hin. Des Weiteren wurde neue Erkenntnisse über die unterschiedlichen Formen der IL-6 Signaltransduktion und deren Rolle im CCA gewonnen. Die im Zuge dieser Studie gewonnenen Daten liefern daher einen wichtigen Beitrag zum Verständnis des Gallengangskarzinoms und können für die Entwicklung neuer Wirkstoffe genutzt werden.

1. Introduction

1.1 Function of the biliary tree

With a weight of 1 200 to 1 500 g, the liver is the largest organ of the human body (2). Besides many functions, hepatocytes produce about 500 to 600 mL bile each day, which is drained by the bile ducts from the liver to the duodenum. The biliary tree (Figure 1) is categorized by anatomical location in intrahepatic bile ducts and extrahepatic bile ducts, whereas the origin of the biliary tree is located in the Canals of Hering (3).

This hepatocellular-ductular junction is lined by hepatocytes on one side and by cholangiocytes, the epithelial cells of the bile ducts, on the other side. Distal of the Canals of Hering, bile ducts are lined exclusively by cholangiocytes and are called ductules with a size smaller than 15 µm in diameter. The ductules congregate into small intrahepatic (interlobular and septal) ducts and large intrahepatic bile ducts (area, segmental and hepatic), forming the intrahepatic part of the biliary tree.

The intrahepatic part ends as right and left hepatic ducts surrounded by peribiliary glands (4,5). These ducts emerge from the liver in the porta hepatis, forming the common hepatic bile duct (*ductus hepaticus communis*). This part of the extrahepatic biliary tree is joined by the cystic duct (*ductus cysticus*) of the gallbladder, where bile is stored, forming the common bile duct (*ductus choledochus*). The common bile duct passes through the head of the pancreas and ends surrounded by the sphincter of Oddi penetrating the duodenum at the ampulla Vateri (2,4).

The gallbladder is a thin pear-shaped, approximately 9 cm long, sac with a capacity of nearly 50 mL. It is located inferior to the liver lobes in the gallbladder fossa and consists of fundus, corpus and infundibulum. The cystic duct connects the infundibulum of the gallbladder to the extrahepatic bile ducts (2,6). Histologically, the gallbladder consists of a muscular lining with a single columnar epithelium layer, a lamina propria and a serosal layer, whereas no submucosa or muscular mucosae are present.

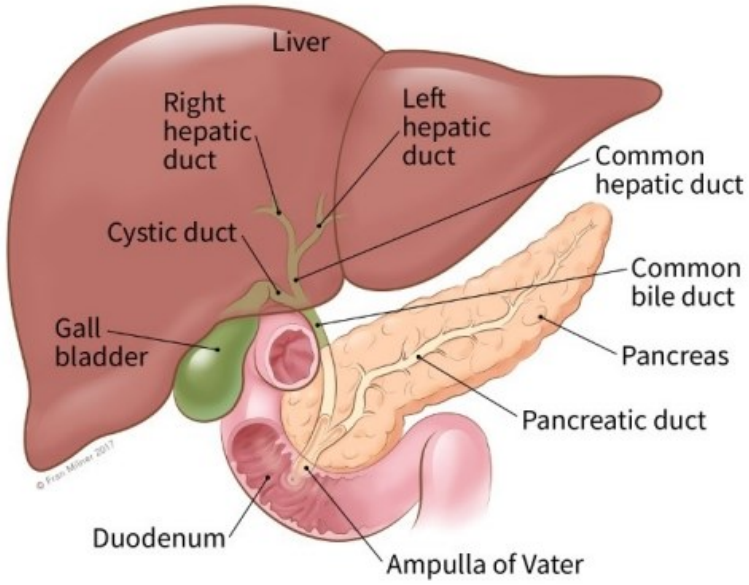

Figure 1: Anatomy of the biliary tree. ©American Cancer Society 2017. All rights reserved.

The epithelium forms interlacing folds to increase its surface (7). Bile and bile acids are stored in the gallbladder and modified by absorption of water and electrolytes. Release of the bile into the duodenum is triggered by the gastrointestinal hormone cholecystokinin (2,8).

Cholangiocytes have a dual origin: cholangiocytes lining the intrahepatic biliary tree originate from hepatoblasts, whereas cholangiocytes forming the extrahepatic bile ducts have endodermal origin (3,9). Within the intrahepatic bile ducts, cholangiocytes are diverse in size, morphology and function. Small cholangiocytes in small bile ducts are cuboidal or flattened, have a high nucleus to cytoplasm ratio and are poorly specialized. Large cholangiocytes lining large intrahepatic bile ducts are columnar, have plenty of organelles in the cytoplasm and a small nucleus to cytoplasm ratio (3,10–12).

In general, cholangiocytes are polarized cells possessing a single primary cilium that differs in length within the biliary tree and acts as chemosensory organelle (13). Besides cell morphology, gene and protein expression constitute a significant difference between small and large cholangiocytes, providing a mechanistic basis for their functional heterogeneity (3,10). Small cholangiocytes show increased expression of proliferation-associated genes and hepatocyte transcription factors. In contrast, large cholangiocytes express proteins involved in secretory processes and reabsorption of water (14,15).

1.2 Biliary tract cancers

Biliary tract cancers (BTCs) or bile duct cancers are rare, highly lethal tumor types arising from cholangiocytes. Between 10-25% of liver cancers are biliary tract cancers, making this tumor entity the second most common primary hepatobiliary cancer and the third most common gastrointestinal neoplasia worldwide (16–18). BTCs are classified according to their anatomical location in intrahepatic cholangiocarcinoma (iCCA), extrahepatic cholangiocarcinoma (eCCA) and gallbladder cancer (GBC). Two-thirds of all BTCs are GBCs, making it the most common form of BTC (19,20). The clinical presentation of patients suffering from BTC is non-specific. Usually, early stage BTCs are symptom-free. At advanced stages, patients show symptoms like abdominal pain, weight loss, bile duct obstruction and jaundice (21–23).

Most BTCs are adenocarcinomas showing tubular and/or papillary structures combined with a variable fibrous stroma. Adenocarcinomas consist of short or long tubular glands surrounded by cells varying in morphology from cuboidal to columnar. Mucinous BTCs contain more than 50% extracellular mucin and are either lined by columnar cells or are arranged in small groups or clusters. Two malignant components are present in the adeno-squamous BTC subtype. This subtype contains unequivocal squamous features mixed with characteristics of an adenocarcinoma (22,24,25).

Besides grading, according to the differentiation status of BTC, the American Joint Committee on Cancer (AJCC) and the Union for International Cancer Control (UICC) developed a staging system for BTC based on their primary side using the TNM system. Intrahepatic CCAs have 6 different stages (0, I, II, III, IVA, IVB), whereas eCCAs and GBCs have seven stages, including subclasses in stage II, III and IV. Generally, the higher the stage, the wider the cancer has spread (21,26).

All classifications have distinct clinical, therapeutic and remarkable epidemiological differences (16,27).

The incidences of iCCA are increasing in Asia, Japan, Australia, North America and Europe (Figure 2). Compared to eCCA (1.3 per 100 000/year), the incidence of iCCA (1.6 per 100 000/year) is significantly higher in the United States (27). Generally, CCA affects more men than women and is race-dependent. For instance, the highest incidence of CCA is among Hispanics and Asians in the US (27).

Worldwide, Thailand has the highest incidence of CCA, with 113 per 100 000/year in men and 50 per 100 000/year in women. This high incidence rate correlates with the presence of liver fluke infections caused by *Opisthorchis viverrini* and *Clonorchis sinensis* (28). The Agency for Research on Cancer considers a *Opisthorchis viverrini* infection *is* "carcinogenic to humans" (29). Inflammation caused by several diseases (e.g. parasitic infections, viral hepatitis, primary sclerosing cholangitis, Caroli´s disease, hepatolithiasis and liver cirrhosis) is the main risk factor for CCA. It creates a tumorigenic environment, leading to the malignant transformation of cholangiocytes.

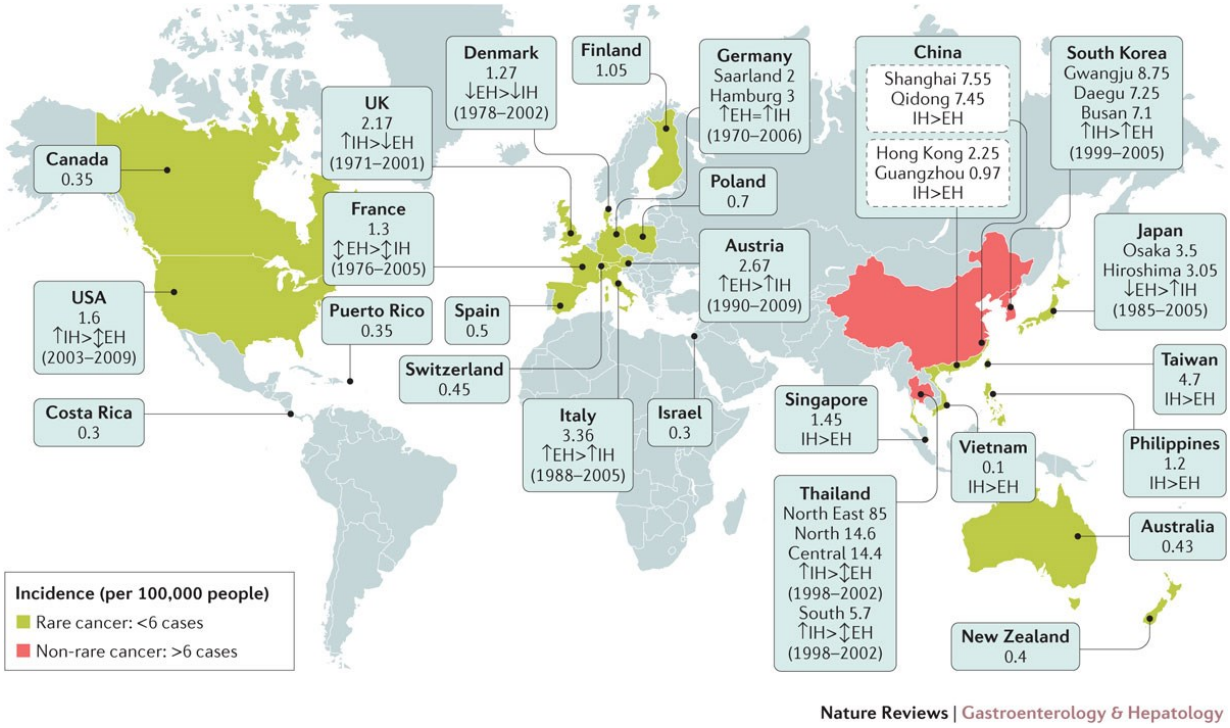

Figure 2: Worldwide incidences of cholangiocarcinoma. Incidence rates are given as 100 000 cases between 1971 and 2009. The green color refers to incidences lower than 6 per 100 000 cases (rare cancer). The red color refers to incidences greater than 6 per 100 000 cases (no rare cancer). IH = intrahepatic; EH = extrahepatic; ↑increasing trend; ↕ stable trend; ↓decreasing trend. Used with the publisher´s permission (30).

Genetically, molecular profiles of CCA samples identified mutations in, for example, *TP53*, *KRAS*, *CDKN2A* and *IDH1/2,* however, alterations were found in different CCA subtypes (19,31). Other risk factors for CCA are smoking, obesity, diabetes and other biliary-tract disorders, such as bile duct cysts (18,19,32–34). According to the American Cancer Society and the statistics from the National Cancer Institute´s (SEER) program, cholangiocarcinoma survival rates vary according to stage and location. For iCCA, the 5-year survival rates are 15% for stage I, 6% for stage II and III, and only 2% for stage IV iCCA. Patients with eCCA have a 5-year overall survival

rates of 30% with stage I tumors, 24% with stage II and III tumors, and only 2% with stage IV eCCA (19,35,36).

Globally, the highest rates of GBC are reported for Chile (27 per 100 000/year) and India (21.5 per 100 000/year) (37–39). In the Western world, incidences of GBC (0.4-1.4 per 100 000/year) are decreasing, probably as a result of routine cholecystectomy (40). Incidences of GBC are up to three times higher in women compared to men. The main risk factor for GBC is cholelithiasis, with the presence of gallstones larger than 3 cm in size (38). Gallstones damage the gallbladder mucosa, leading to inflammation of the gallbladder and chronic cholecystitis. Diseases like gallbladder polyps, pancreaticobiliary maljunction anomalies and infections are associated with GBC (37). Other risk factors are gravidity and parity, age, and obesity. Genetic analyses of GBC samples revealed that e.g. *TP53, CDKN2A, KRAS* and *COX2* are pathogenic mechanisms involved in gallbladder carcinogenesis (Figure 3) (19,37). According to data of the National Cancer Database, the 5-year survival rate for stage I GBCs is 50%, stage II 28%, stage III 8-7% and stage IV 4-2% (19,41).

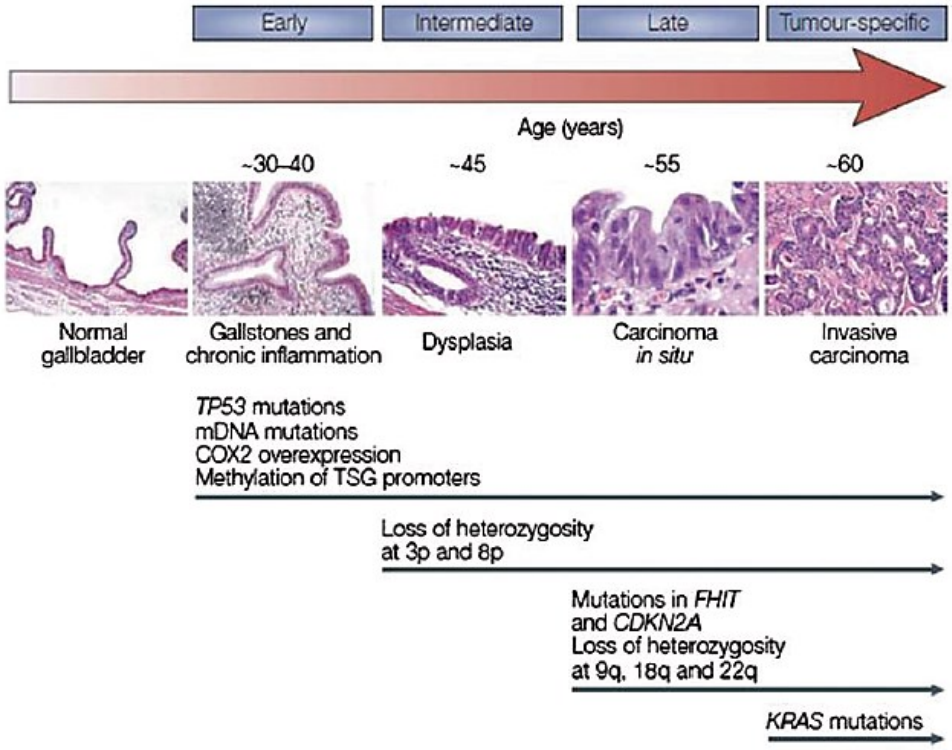

Figure 3: Mechanism of gallbladder carcinogenesis. FHIT, fragile histidine triad; TSG, tumor suppressor gene; COX, cyclooxygenase; mDNA, mitochondrial deoxyribonucleic acid. Used with the publisher´s permission (42).

Nowadays, surgical resection of the affected tissue is still the most promising treatment option. If a tumor is not resectable, neoadjuvant therapy using chemotherapy (gemcitabine, 5-fluorouracil) or irradiation (transcatheter arterial chemoembolization or transarterial radioembolization) is considered. Unfortunately, the management/treatment for patients with advanced or metastatic BTCs consists of systemic palliative chemotherapy in combination with best supportive care (21,43). Interestingly, a meta-analysis of twenty studies, including 6 712 patients, revealed that compared to surgery, any adjuvant therapy did not significantly improve the survival of BTC patients (44).

At the time of thesis preparation, 216 interventional clinical trials for BTCs are listed (https://clinicaltrials.gov/), highlighting the urgent need for new effective therapy strategies.

1.3 Inflammation in biliary tract cancers

Inflammation is a complex and essential response of the immune system to harmful stimuli, like infections, tissue damages or pathogens. The main goal of this process is to destroy pathogens and to prepare the damaged tissue for repair (45). Acute inflammation is the immediate response to tissue damage. If the immediate response of the immune system fails and the inflammation is continuing, chronic inflammation can arise. However, chronic inflammation may start due to low grade infections or autoimmune reactions (45,46). The condition of permanent, dysregulated and unresolved inflammation is often associated with neoplastic progression (47,48).

In 1863, the German pathologist Rudolf Virchow was the first to describe the association between chronic inflammation and cancer due to the presence of leukocytes in tumorous lesions (49,50). Today, this hypothesis is evident and, moreover, listed as one of the hallmarks of cancer (51). It is known that cancer and inflammation are connected by extrinsic and intrinsic pathways. The extrinsic pathway is present if inflammatory conditions increase the risk of cancer development. In contrast, if endogenous genetic alterations (e.g. oncogenes) lead to inflammation and cancer, the intrinsic pathway is present (52).

Infectious diseases and chronic inflammation are the cause for up to 25% of cancer, including BTC (29,53).

Long-term inflammation induces DNA damage in cholangiocytes giving raise to CCA. *In vitro* studies proved the activation of inducible nitric oxide synthase (iNOS) as a response to an inflammatory cytokines cocktail (54). This enzyme produces large amounts of nitric oxygen (NO) from L-arginine, which is associated with DNA damage by oxidation, nitration and deamination (55,56). NO and its associated reactive oxygen species (ROS) were proven to inhibit global and 8-oxo-dG base excision repair mechanisms which are reversed by NO scavengers. The failure to repair 8-oxodG promotes DNA mutation by adenine incorporation on the opposite DNA strain, giving a strong link between carcinogenesis of the biliary tree and inflammation (56,57).

Typically, iCCA exhibit extreme desmoplastic reaction (58). The tumor microenvironment consist of various types of stromal cells and the extracellular matrix (59). The communication of cancer cells and the tumor microenvironment is dynamic and bi-directional. Tumor cells secrete factors to recruit and activate stromal

cells. These recruited cells are able to produce and secrete several factors influencing tumor growth and survival (59). Extracellular matrix degradation for tumor-associated angiogenesis is mainly coordinated by tumor cells and cancer-associated fibroblasts (CAF), also known as myofibroblasts. Proteinases like matrix metalloproteinases and plasminogen activators are secreted by CAFs (60). Moreover, the presence of CAFs was found to correlate with lymph node metastasis, advanced TNM stage and poorer overall survival of iCCA patients (61).

Tumor-associated macrophages (TAM), are besides tumor-associated neutrophils (TAN), prominent cells found within the tumor microenvironment (59). These cells can switch from an activated, anti-tumor phenotype (N1 or M1) to a pro-tumor phenotype (N2 or M2), which is mainly regulated by NF-κB, TGF-β, IL-4, IL-13 respectively. (62–64). In eCCA an correlation of TANs and TAMs were found to positively correlate with enhanced eCCA growth and metastases (65). In GBC a correlation between low $CD15^+$ cell infiltration and better overall survival was found (66). Moreover, Lipopolysaccharide-activated human macrophages were found to increase EMT-related genes, like E-cadherin, in a CCA cell line (67).

A study on tumor-infiltrating immune cells on BTC showed $CD8^+$ and $CD4^+$ T-lymphocytes as the most prevalent inflammatory cell type. $CD8^+$ T-lymphocytes were seen more frequent in the tumor epithelium compared to $CD4^+$ T-lymphocytes (68). Interestingly, total count of these T-lymphocytes subtypes decreases from pre-tumorous lesions to metastases, whereas the number of TAMs significant increased (68). This finding highlights that BTCs are able to evade the activation of the adaptive immune response, which is beneficial to BTC patients shown by a positive correlation of $CD8^+$ and $CD4^+$ T-lymphocytes and overall survival (68,69). Controversially, a study focusing on GBC revealed no significant correlation between $CD8^+$ T-lymphocytes, but $CD3^+$ T-lymphocytes and GBC patients' overall survival emphasizing the differenced of BTC depending on the anatomical location (66).

All invading cells of the tumor microenvironment can secrete inflammatory mediators to interfere with tumor cells and *vice versa*. This includes cytokines (e.g. IL-1β, IL-6, TNF-α), transcription factors (e.g. NF-κB, STAT3), or chemokine receptors (e.g. CXCR4) (46,52).

High IL-6 levels have been reported in patients suffering from various cancer types, indicating an important role during carcinogenesis and disease progression (70). How IL-6 mediates inflammatory signals will be elucidated in the next chapters.

1.4 The interleukin 6/JAK/STAT pathway

As BTC is discussed to be an inflammatory driven cancer, it is important to investigate inflammatory signaling pathways in this malignant tumor entity (See Chapter 1.3).

The Janus kinase (JAK) and activators of transcription (STAT) signaling pathway have a wide range of functions, including influence of cell differentiation, cell proliferation, cell migration and apoptosis (71). The JAK/STAT pathway is stimulated by a variety of ligands and their receptors. Generally, for signal transduction, the intracellular domains of two receptor subunits must associate with Janus tyrosine kinases (71). Four different JAK family members are known in mammals: JAK1, JAK2, JAK3 and TYK2. JAK3 expression is limited to lymphoid tissue, whereas JAK1, JAK2 and TYK2 are found in most tissues (72,73) Biochemically, all JAK members consist of seven JAK homology (JH) domains (74). The first JH domain at the C-terminus harbors kinase activity, whereas the second is a pseudokinase domain. All other JH domains (JH3-7) are involved in cytokine receptor interaction (75).

For signal transduction, two JAK molecules have to be in close proximity to allow trans-phosphorylation. Therefore, critical tyrosine residues must be phosphorylated to inactivate the blockage of the catalytic domain (73). Subsequently the activated JAKs phosphorylate substrates including the receptors and the transcription factors STAT (71). Seven STAT protein family members (STAT1-6, 5a & 5b) are known in mammals (72). All STAT proteins contain a conserved tyrosine residue in near proximity to the C-terminus. This specific residue is phosphorylated by JAKs. After tyrosine phosphorylation, the STAT proteins are able to dimerize by interacting with a conserved Src homology 2 (SH2) domain. The phosphorylated STAT dimers then enter the nucleus in an importin α-5 and RAN nuclear import pathway dependent mechanism (71,76–78). In the nucleus, the STAT dimers activate or repress the transcription of target genes by binding to interferon-γ activated sequences (GAS) (72,79).

For the regulation of JAK/STAT signaling, three major classes of regulators are known: suppressor of cytokine signaling (SOCS), protein inhibitors of activated STATs (PIAS) and protein tyrosine phosphatases (PTP). PTP family members (e.g. SHP-1) reverse the phosphorylation of JAKs, thus reducing kinase activity. PIAS proteins have a Zn-binding RING-finger domain and bind to phosphorylated STAT dimers preventing them from DNA binding. The SOCS protein family consists of at least eight members (SOCS1-7 and cytokine-induced STAT inhibitor (CIS)). All contain a SH2 domain and a short C-terminal domain, the SOCS box and an N-terminal domain. Three possible mechanisms are known how SOCS can inhibit JAK/STAT signaling. First, these proteins bind to phosphorylated tyrosine residues of receptors preventing the recruitment of substrates allosterically. Second, SOCS protein family members can bind JAKs directly leading to JAK kinase activity block. Third, SOCS facilitate the ubiquitination of JAKs and their receptors leading to decreased protein stability and proteasomal degradation (71,80,81).

Interleukin 6 (IL-6) is member of the IL-6-type cytokine family, has pro-inflammatory and anti-inflammatory properties and, activates genes influencing survival, differentiation, proliferation and apoptosis of cells (77,82). Biochemically, IL-6 consists of 186 amino acids, forming a four α-helix bundle linked via loop regions in an up-up-down-down topology (Figure 4) (83).

To mediate signaling, IL-6 specifically binds to its non-signaling receptor (IL-6Rα, CD126, gp80), resulting in an IL-6/IL-6Rα complex. This complex recruits the ubiquitously expressed signal transducing receptor gp130 (CD130, IL-6Rβ), causing gp130 homodimerization. Interestingly, gp130 has no affinity to IL-6 nor IL-6Rα (84).

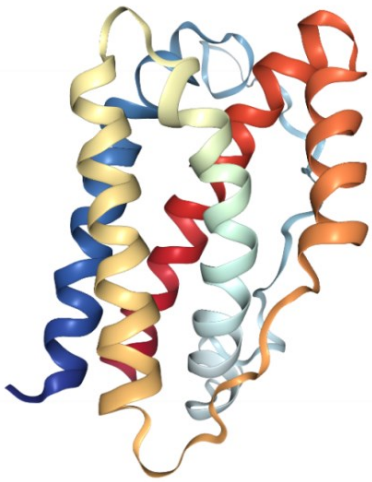

Figure 4: Three dimensional structure of recombinant expressed human IL-6. The image was created by NGL Viewer (85) (PDB: 1IL6) using data of solution NMR analysis and cartoon style to visualize the α-helices in the structure (86).

The activated IL-6R complex has a hexameric structure consisting of two molecules IL-6, IL-6Rα and gp130 each and adopt α-helical conformational changes in transmembrane and intracellular regions (70,87,88). The secondary receptor gp130 is essential for IL-6 signaling because the short 82 amino acids long intracellular domain of the IL-6Rα lacks the motifs for intracellular signal transduction (70,89). The gp130 molecule contains several of these motifs but lacks a kinase domain (89). Therefore, gp130 can recruit JAKs after conformational changes to mediate downstream signaling. These kinases phosphorylate cytoplasmic regions of gp130 to create binding sites with the consensus sequence YXXQ for the SH2 domains of STATs. In turn STATs, function as substrates for JAKs (79). For IL-6 induced signaling, JAK3 plays a minor role, while of the remaining three kinases, JAK1 is the predominant one (72,82,90,91). Amongst all STAT family members, IL-6 predominately activates STAT3, which was initially identified as IL-6 transcription factor in hepatocytes as acute-phase response factor, and to a minor extent STAT1 (72).

STAT3 is activated by tyrosine phosphorylation at a single site (Y705) in the SH2 domain in near proximity to the C-terminus, mediated mostly by JAK1, as well as serine phosphorylation (S727) in a mitogen-activated protein kinase domain within the transactivation domain (TAD) (79,91,92). Main dimerization of STAT3 is triggered by p-Y705 and stabilized by TAD due to binding of p-Y705 of the other monomer (93). The function of STAT3 as transcription factor has been studied extensively.

However, STAT3 was found to be localized in a small amount in the mitochondrion, where it influenced the electron transport chain (94,95). Deletion of STAT3 led to embryonic lethality, whereas all other STAT protein family members led to viable mice with limited phenotypes (96).

Moreover, STAT3 is involved in germinal center maintenance (97), B-cell development (98), self-renewal of pluripotent embryonic stem cells (99,100), the control of acute-phase response of the liver (101) and oncogenesis (102). In the latter, STAT3 is able to regulate both, oncogenes and TSG. As examples, STAT3 regulates a variety of other tumor supporting transcription factors (e.g. c-Fos, c-Myc and HIF-1α) (103–105), apoptosis by suppressing the expression of anti-apoptotic Bcl-2 protein family members (106) and evasion of the immune system by regulating COX-2 expression (107). Tumor suppressing function of STAT3 are, for instance, the regulation of p21 (CIP1/WAF1) and the family of FOX transcription factors, which regulate cell cycle and proliferation (108,109).

Moreover, dominant-negative STAT3 has been proven to induce apoptosis in breast cancer (110), non-small cell lung cancer (111) and prostate cancer (112).

STAT3 has several isoforms due to alternative splicing or proteolytic processing. Altogether, four isoforms have been identified so far: STAT3α (92 kDa), STAT3β (83 kDa), STAT3γ (72 kDa) and STAT3δ (64 kDA) (113,114).

STAT3α is the full-length form of STAT3 (Figure 5) and only its loss is lethal to mice, whereas deletion of STAT3β did not influence mice viability (115). STAT3β is truncated at the C-terminus of STAT3, lacking the TAD (Figure 5). It has the ability to suppress specific STAT3 functions and has therefore been considered as dominant negative factor. It can be phosphorylated at Y705 and forms more stable dimers leading to stronger DNA-binding activity compared to STAT3α (114,115).

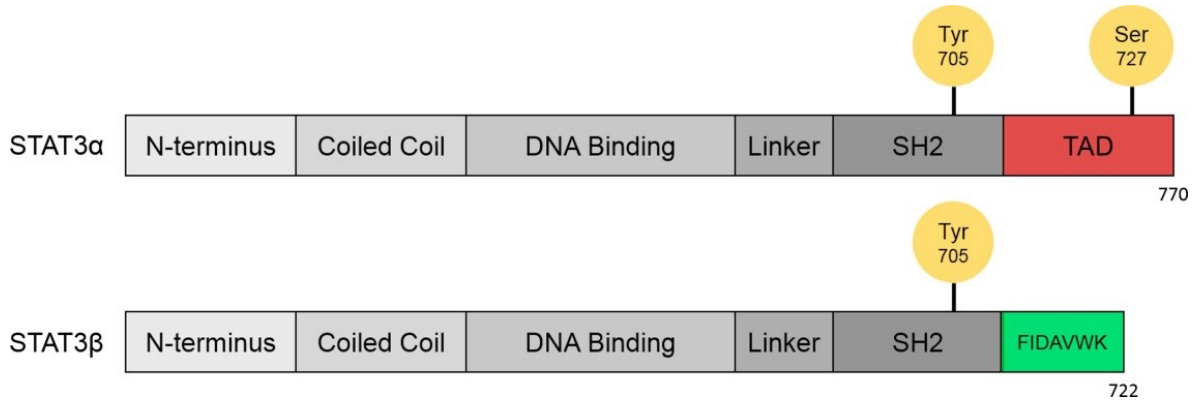

Figure 5: Schematic overview of the two alternatively spliced STAT3 variants. Both isoforms (STAT3α and STAT3β) share the N-terminal domain as well as the coiled coil domain (which allows protein-protein interactions) and the DNA binding domain which is linked to the Src homology 2 domain (SH2). The tyrosine 705 residue lies within the SH2 domain and is responsible for dimerization and activation of STAT3. Due to alternative splicing, STAT3β is missing the transactivation domain (TAD). Instead it carries seven amino acids. Used with the publisher´s permission (113).

STAT3γ originates from proteolytic cleavage STAT3α and carries a truncated C-terminus, leading to a dominant-negative variant of STAT3 (116). STAT3δ is generated like STAT3γ, but its specific function remains undefined (117).

Amongst all possible mechanism of IL-6 signaling termination by STAT3 deactivation, the SOCS family member SOCS3 is the predominant protein found to inhibit STAT3 signaling (118). The expression of SOCS3 is STAT3 dependent, leading to a negative feedback loop. SOCS3 is able to bind JAKs and/or gp130 by their central SH2 domain. The N-terminal kinase inhibitory region of SOCS3 is responsible for blocking the catalytic activity of JAKs leading to termination of IL-6 mediated signaling (81,119). Illustration of the activation and inhibition of IL-6 mediated signaling is shown in Figure 6 schematically.

IL-6 is able to stimulate cells lacking the IL-6Rα, indicating that another mechanism leads to IL-6 induced STAT3 signaling (82,120).

1.5 IL-6 trans-signaling

Expression of IL-6Rα was proven in hepatocytes, monocytes, neutrophils and some subtypes of lymphocytes (121). However, IL-6 is able to activate cells that do not express IL-6Rα. The full length IL-6Rα (mIL-6R) has a molecular weight of 80 kDa, harbors a transmembrane domain and binds to IL-6 with nanomolar affinity (122,123).

Interestingly, an additional IL-6Rα form with 50-55 kDa was detected first in human urine (124,125). Many cytokine receptors have soluble forms (126). In fact, the 50-55 kDa IL-6Rα is a soluble form (sIL-6R). In contrast to many other soluble receptors, sIL-6R has an agonistic function (127). The sIL-6R can be generated by alternative splicing or proteolytic cleavage at the Gln357/Asp358 in close proximity to the transmembrane domain by a disintegrin and metalloprotease 17 (ADAM17), a process called ectodomain shedding (128–132). Interestingly, no different splice variants of the IL-6Rα mRNA have been detected mice (133). Nowadays, it is believed that ectodomain shedding is the superior mechanism for sIL-6R generation (134). Shedding of the IL-6Rα is triggered by pore forming toxins (135), cholesterol depleting in plasma membranes (136), bacterial metalloproteinases (137), apoptosis (138) and, most importantly, by activation of protein kinase c (139).

For signal transduction, sIL-6R interacts with IL-6 with comparable affinity to the mIL-6R, forming an IL-6/sIL-6R complex (126). Subsequently, the complex interacts with gp130 inducing JAK/STAT signaling (See Chapter 1.4.) The signal transduction through the sIL-6R was named IL-6 trans-signaling, whereas the mIL-6R mediates IL-6 classic signaling (Figure 6) (126).

The possibility of targeting cells by IL-6 trans-signaling largely increases the spectrum of IL-6 signaling and opens new therapeutic approaches in several diseases. To study differences between IL-6 classic signaling and IL-6 trans-signaling, diverse agents (See Chapter 3.2) are necessary (Figure 6). Tocilizumab is a monoclonal antibody raised against all forms of the IL-6Rα and it blocks both types of IL-6 signaling. The antibody sgp130Fc is only capable of inhibiting the interaction between the IL-6/sIL-6R complex and it blocks IL-6 trans-signaling specifically (84). For specific activation of IL-6 trans-signaling, the designer cytokine Hyper-IL-6 is used (140). This protein mimics the IL-6/sIL-6R complex.

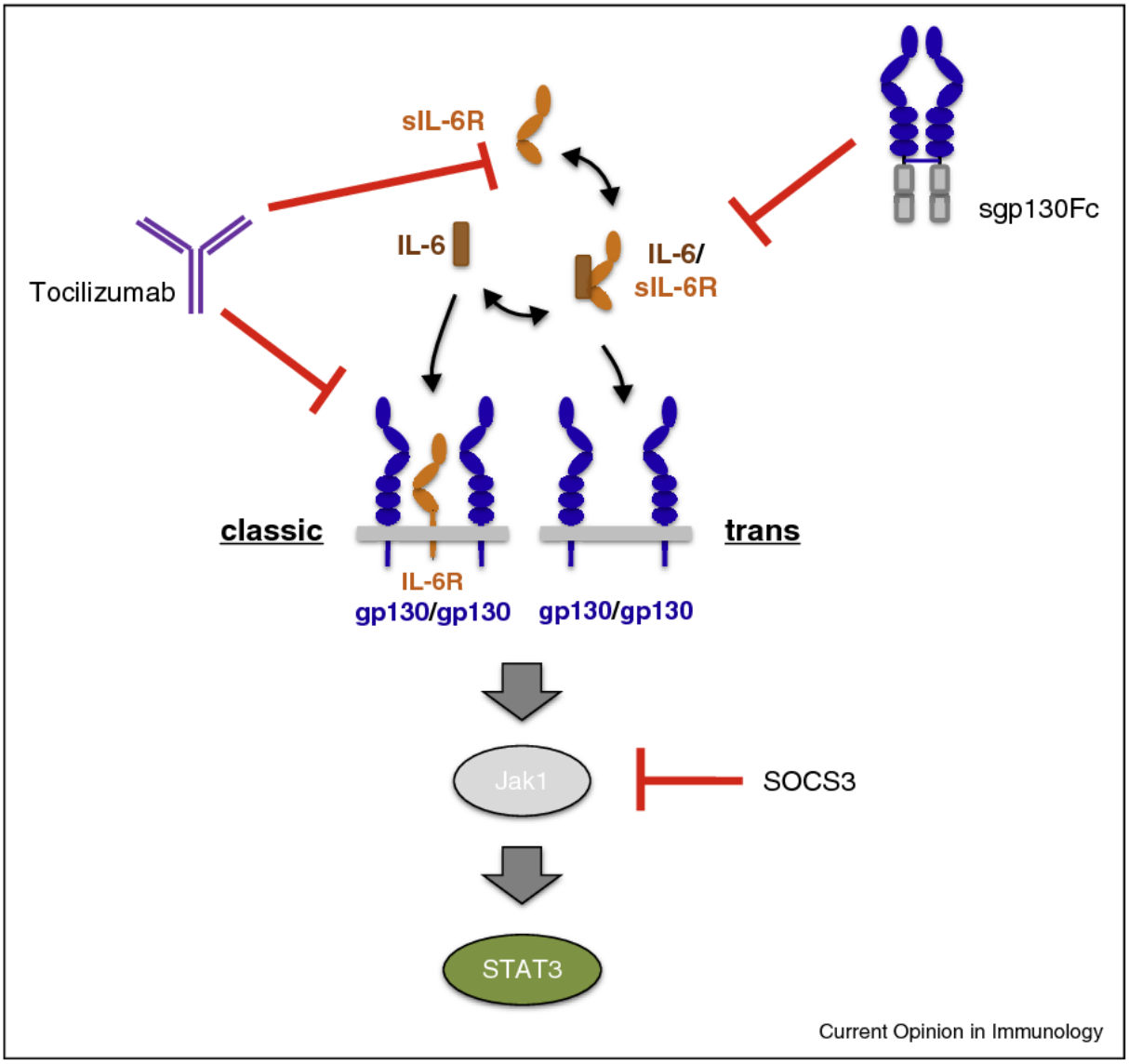

Figure 6: Principles of IL-6 signaling activation and inhibition. IL-6 activates STAT3 via interaction with membranous IL-6Rα (= IL-6 classic signaling) or by interacting with a soluble IL-6R (= IL-6 trans-signaling). Tocilizumab blocks the interaction of IL-6 and IL-6Rα independent of its form. The protein sgp130Fc inhibits IL-6 trans-signaling specifically. A natural feedback loop of STAT3 activation is performed by suppressor of cytokine signaling 3 (SOCS3). Used with the publisher´s permission (141).

Differences between IL-6 classic signaling and IL-6 trans-signaling were intensively studied in several diseases (123,142). Double transgenic mice for IL-6/sIL-6R had massive extramedullary hematopoiesis in liver and spleen and increased hepatocellular proliferation, not seen in single IL-6 or sIL-6R transgenic mice (143–145). Constant dividing hepatocytes are usually seen during liver regeneration. After 50% hepatectomy, Hyper-IL-6 treated mice showed increased liver regeneration compared to IL-6 treated mice (146). Even animals with sever hepatic damage

induced by D-galactosamine survived upon Hyper-IL-6 treatment but not by IL-6 alone (147,148).

Blocking of IL-6 trans-signaling is performed by a natural soluble form of gp130 (sgp130) under steady-state conditions. Serum levels of sIL-6R (40-70 ng/mL) and sgp130 (400 ng/mL) are approximately 10 000 times higher than IL-6 (1-5 pg/mL) levels under normal conditions (123,149). This implies that secreted IL-6 will bind to sIL-6R forming an IL-6/sIL-6R complex, which is neutralized by sgp130. Only dramatic IL-6 plasma levels, as seen under septic conditions, will allow IL-6 to act systemically (123,150). This is valid for paracrine secreted IL-6, depending on the proximity of cells. For instance, activated Kupffer cells influence neighboring hepatocytes and cholangiocytes by IL-6 secretion (142).

For dissection of IL-6 classic signaling and IL-6 trans-signaling, mice were injected with either the recombinantly expressed sgp130Fc, or the protein was synthesized in transgenic mice *in vivo.* Data of these studies showed that sgp130Fc was able to block the inflammatory process of rheumatoid arthritis (151–153), intestinal inflammation as seen in Crohn´s disease (154) and inflammation associated cancers like colon cancer (155), pancreatic cancer (156) and malignant ascites of ovarian cancer (157).

1.6 IL-6/JAK/STAT3 signaling in biliary tract cancers

The role of IL-6 is complex in cancer. Cancer cells can produce large amounts of all receptor subunits (IL-6R, gp130) and IL-6, which allows them to respond, on the one hand, to IL-6 classic signaling and, on the other hand, to stimulate surrounding cells via IL-6 trans-signaling (158).

Various tumor entities have been studied regarding IL-6 signaling (70). It was proven that IL-6 plays an important role in cellular processes like proliferation, survival, angiogenesis, chemotherapy resistance and the formation of metastasis (158,159). This pivotal role of IL-6 in cancer makes it a promising target for cancer therapy, whereas over the last decades, the IL-6Rα became more and more the focus of interest as potential target. In lung adenocarcinoma and ovarian cancer, it was shown that the *IL-6Rα* gene expression significantly correlates with patients´ overall survival, highlighting its prognostic value (160,161).

Cholangiocytes express little amounts of IL-6, IL-6Rα and gp130. If stimulated with lipopolysaccharide, phorbol esthers or forskolin cholangiocytes secret high amounts of IL-6, leading to increased proliferation (162–164).

Many studies highlight the role of IL-6 in BTC (165). In human malignant cholangiocytes, it was proven that over-expression of IL-6 promotes tumor growth *in vitro* and *in vivo* via the activation of p38 or p44/p42 MAPK signaling and the downregulation of the cell cycle regulator p21(WAF/CIP1) (166–168). In vitro experiments of IL-6 over-expressing CCA cell lines proved the involvement of IL-6 signaling in DNA methylation of promoter regions encoding for factors influencing carcinogenesis like p53 and epidermal growth factor receptor (EGFR) (169,170). A positive feedback loop of the EGFR was proven to be responsible for prolonged STAT3 activation independent of SOCS3 inhibition (171).

Over-expression of SOCS3 was shown to regulate IL-6 induced EMT in CCA cell lines by increasing E-cadherin expression due to inhibition of STAT3 tyrosine phosphorylation. This results in reduced cell invasion and *in vivo* metastasis (172). Activated STAT3 and SOCS3 were found to negatively correlate in CCA tumor, suggesting an inactivation of this negative feedback loop (173). The inactivation of SOCS3 is rather due to promotor methylation of the CpG island, leading to epigenetic silencing than due to mutations (173). This finding allows IL-6 to permanently induce STAT3 signaling in CCA.

Another example for the tumor supporting function of IL-6/JAK/STAT3 signaling in CCA is that IL-6 was found to enhance CCA cancer cell survival specifically through the JAK/STAT3 pathway. Activated STAT3 was shown to bind to a specific motif in the promoter of the anti-apoptotic Bcl-2 protein family member myeloid cell leukemia-1 (Mcl-1) in a CCA cell line (174).

Elevated IL-6 bile and serum levels of patients suffering from CCA were found compared to hepatocellular carcinoma, other biliary diseases and metastatic colorectal cancer patients (175). Quantification of IL-6 levels in serum of CCA patients has been proven to correlate with tumor mass and patients´ overall survival (176). Analysis of the epithelial and stromal transcriptomic profiles in CCA tissues identified 1 442 differentially expressed genes, including IL-6. Gene expression of *IL-6* was found to be significantly elevated in tumor stroma compared to matching CCA epithelium (177).

Expression pattern analysis of all STAT family members in 223 human CCA specimens and in the *Opisthorchis viverrini* infected CCA hamster model, revealed that p-STAT3 (Tyr705) was mainly detected in the nuclei of cholangiocytes during carcinogenesis (178). In more detail, it was frequently seen in the inflammatory state, the precancerous stage and in the final tumor stage. The expression of STAT3 was proven to increase along with CCA carcinogenesis suggesting an association between STAT3 and CCA progression (178). Over-expression of STAT3 was found to increase the metastatic potential of iCCA cell lines *in vitro* and *in vivo*. Moreover, STAT3 expression correlated with tumor size, vascular invasion, metastasis and TNM stage in iCCA Survival analysis of iCCA patients revealed an association between lower STAT3 expression and longer disease-free survival (178,179).

The impact of IL-6 trans-signaling was demonstrated in some cancer types. In pancreatic ductal adenocarcinoma (PDAC), IL-6 trans-signaling was demonstrated to be the form of IL-6 signal transduction involved in PDCA development. If IL-6 trans-signaling was genetically manipulated by inducing sgp130 in $Kras^{G12D}$ mice nearly no pancreatic intraepithelial neoplasia was seen (156).

Different murine models were used to study IL-6 trans-signaling in lung adenocarcinoma. A comparison of mice harboring mutated gp130 (which inhibits SOCS3 mediated STAT3 inhibition) with $Kras^{G12D}$ mice showed impaired lung

carcinogenesis. This effect was suppressed by pharmacological inhibition of IL-6 trans-signaling or crossing the mice with mice sgp130Fc transgenic mice (180).

In the murine diethylnitrosamine (DEN) model for hepatocellular cancer (HCC), the most common primary liver cancer, it was proven that IL-6 trans-signaling is able to prevent p53-dependent hepatocyte apoptosis. Kupffer cells were identified as the source of sIL-6R, leading to IL-6 trans-signaling and not IL-6 classic signaling. Protection of HCC development was seen in sgp130Fc transgenic mice to the same extent as IL-$6^{-/-}$ mice, leading to the conclusion that IL-6 trans-signaling is essential for HCC development (142,181).

In a murine model of colon cancer, it was shown that rather IL-6 trans-signaling than IL-6 classic signaling controls tumor growth due to STAT3 activation in intestinal epithelial cells, which usually show low to near IL-6Rα expression (182). Moreover, IL-6 trans-signaling was found to be responsible for the increased expression of carcinoembryonic antigen-related cell adhesion molecules (CEACAM) 5 and 6 in colon cancer, which are widely used in tumor diagnostics (183).

Besides the findings of single nucleotide polymorphism in the IL-6Rα of *Opisthorchis viverrini* associated CCA patients, no investigations on the receptor obligatory for IL-6 signal transduction and its association to BTC have been performed so far (184).

Moreover, dissection between IL-6 classic signaling and IL-6 trans-signaling was never included in studies regarding IL-6 in all types of BTC.

Therefore, this thesis focuses on IL-6Rα and its two ways of signal transduction in BTC.

2. Hypothesis

1. The IL-6Rα has a pivotal role in BTC.

Therefore, analyses of GBC tissues in form of a tissue microarray and as fresh frozen specimens were performed to gain information about a correlation of IL-6Rα with overall survival. Moreover, analysis of GBC tissue samples was used to provide insights into alterations of IL-6Rα mediated signaling during cholangiocarcinogenesis.

2. IL-6 classic signaling and IL-6 trans-signaling differentially impact malignant cholangiocytes *in vivo*.

Therefore, different pharmacological approaches were used to answer the following question: which form of IL-6 signaling is predominant in CCA and harbors tumor-promoting activity?

The following scheme gives an overview about the performed experiments to clarify the hypothesis of this study.

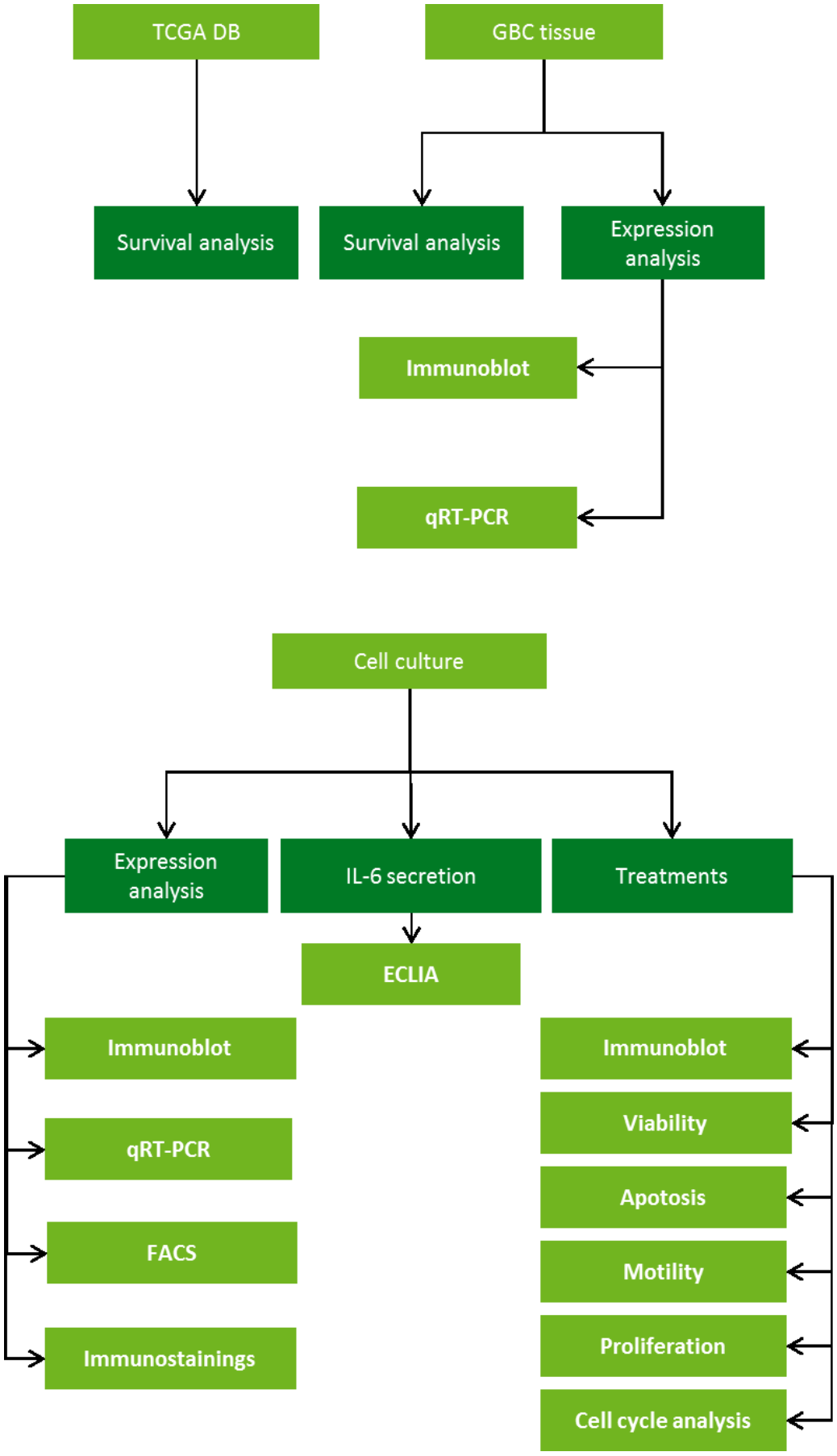

Figure 7: Schematic overview of the used analyses within this study.

3. Materials and methods

3.1 Cell culture

The cell lines TFK-1 (185) and EGI-1 (186), established from a primary eCCA, were kindly provided by Prof. Kai Breuhahn (University Hospital of Heidelberg, Germany). TFK-1 cells were cultivated in Roswell Park Memorial Institute (RPMI) - 1640 medium supplemented with 10% fetal bovine serum (FBS; Gibco, Life Technologies, Darmstadt, Germany). The cell line EGI-1 was cultured in Dulbecco´s Modified Eagle´s Medium (DMEM; Gibco, Life Technologies, Darmstadt, Germany), supplemented with 10% FBS and 1x MEM non-essential amino acids (Gibco, Life Technologies, Darmstadt, Germany).

The cell lines Mz-ChA-1 (derived from GBC abdominal wall metastasis), Mz-ChA-2 (established from GBC liver metastasis) and SK-ChA-1 (cultivated from malignant ascites of an eCCA) were a kind gift from Prof. Alexander Knuth (University of Zurich, Switzerland) and cultured in RPMI-1640 supplemented with 10% FBS, 2 mM L-Glutamine (Gibco, Life Technologies, Darmstadt, Germany) and 1x MEM non-essential amino acids (187).

All five cell lines were supplemented with 100 U/mL penicillin / 100 µg/mL streptomycin (Gibco, Life Technologies, Darmstadt, Germany) and maintained at 37°C in a humid atmosphere with 5% CO_2. All cell lines were routinely tested for *mycoplasma* contamination (PCR Mycoplasma Kit, Promocell GmbH, Heidelberg, Germany).

3.2 Compounds

3.2.1 Hyper-IL-6

First described in 1996, Hyper-IL-6 is a 408 amino acid long fusion protein that activates IL-6 trans-signaling. The non-helical N-terminal residues of IL-6 are linked by a flexible loop to the C-terminus of the sIL-6R. Hence, Hyper-IL-6 mimics the IL-6/sIL-6R complex (140). Recombinantly expressed Hyper-IL-6 was kindly provided by Prof. Stefan Rose-John[1] (University Kiel, Germany).

[1] Stefan Rose-John is an inventor of patents and a shareholder of the CONARIS Research Institute AG, which develops soluble glycoprotein 130 fusion proteins as therapeutics.

3.2.2 sgp103Fc

In 2010, the group around Stefan Rose-John[1] was able to express gp130Fc recombinantly. Therefore, the extracellular portion of gp130 was fused to the constant region of a human IgG1 heavy chain. Functional analysis of sgp130Fc proved its selective inhibitory effects for IL-6 trans-signaling without affecting IL-6 classic signaling (84). The inhibitor sgp130Fc was a kind gift from Prof. Stefan Rose-John[1] (University Kiel, Germany).

3.2.3 Interleukin 6

IL-6 is a member of the IL-6-type cytokines consisting of 186 amino acids arranged in four-helical protein domains (Figure 4). IL-6 activates the JAK/STAT pathway by interaction with its receptor (IL-6Rα) and gp130 (82). For this study in *Escherichia coli* expressed human IL-6 was purchased from Peprotech (Rocky Hill, USA).

3.2.4 Tocilizumab

Tocilizumab is a humanized anti-IL-6Rα monoclonal antibody that blocks the soluble and membrane-bound IL-6Rα form, leading to total IL-6 signal transduction inhibition. First approved in 2005 for Castlemans´s disease, Tocilizumab was approved for the treatment of rheumatoid arthritis by the European Medicines Agency in 2009 and the US Food and Drug Administration in 2010 (188,189). Tocilizumab (RoActemra®) was purchased from Roche Diagnostics (Risch-Rotkreuz, Switzerland).

3.3 Patient derived tissue specimens

3.3.1 FFPE tissue and tissue microarray generation

After approval of the ethics committee of the Medical University of Graz (28-294 ex 15/16) and the institutional review board of the Severance Hospital Seoul (no. 4-2014-0421), formalin-fixed, paraffin embedded (FFPE) GBC samples (n=367) and non-neoplastic, not inflamed gallbladder samples (NNT; n=61) were collected retrospectively from the Medical University of Graz (43%), the Hospital Graz South-West (6%), the Medical University of Innsbruck (11%) and the University Hospital of Seoul (40%) according to the ethical guidelines of the 1975 Declaration of Helsinki. In total, 428 specimens were used in this study. For tissue microarray (TMA) generation, the tumor areas were marked on the paraffin block, and tissue cones of 0.6 mm in diameter were punched out of the tumor area. These cones were embedded as TMA in a fresh paraffin block in triplicates (Beechers Instruments, Sun

Prairie, USA). The clinicopathological characteristics of the patient-derived FFPE specimens are listed in Table 1.

3.3.2 Frozen tissue samples

Frozen tissues of GBC (n=14) and NNT specimens (n=12) were collected immediately after surgery or provided by the Biobank Graz. Therefore, the tissue was cut into small pieces, snap frozen in liquid nitrogen and stored at -80°C prior to biochemical analysis. The patients' characteristics of frozen tissue samples are listed in Table 1.

Table 1: Clinicopathological characteristics of patient-derived tissue. [Published in Kleinegger *et al.*, 2019]

	Frozen tissue (n = 26)		TMA (n = 428)	
	GBC (n = 14)	NNT (n = 12)	GBC (n = 367)	NNT (n = 61)
Age (± SD)	70.4 (8.5)	57.8 (8.1)	68.8 (10.7)	64.2 (9.6)
Gender				
Female	9	2	268	36
Male	5	10	99	25
Subtype				
Adenocarcinoma	14		336	
Adenosquamous	4		13	
Tubulary	4		77	
Mucinous	1		6	
Tubulo-papillary	4		25	
Mixed	1		32	
Papillary	0		11	
Solid	0		7	
Unknown	0		165	
Squamous cell carcinoma	0		6	
Without subtyping	0		25	
Grading				
Low	7		221	
High	6		137	
Unknown	1		9	

3.4 Immunohistochemistry

For immunohistochemical staining (IHC), the TMAs were cut in 3 µm thick sections. After de-paraffinization, antigen retrieval was performed either with 0.01 M citrate buffer (pH 6) or 1 mM Tris-EDTA buffer (pH 9). The primary antibody (Table 2) was incubated overnight at 4°C. Detection was performed using the Super Stain System-HRP AEC detection kit (Empire Genomics, Buffalo, USA) following the manufacturer's instructions. Evaluation of the TMAs was performed by independent, blinded, board-certified pathologists. Staining intensity was scored as no (score 0), weak (score 1), moderate (score 2) and strong (score 3) immunoreactivity. For survival analysis, no and weak staining intensities were grouped as "low expression", and strong and moderate staining intensities were grouped as "high expression". Analysis of tumor marker expression of CCA cell lines was also performed by immunohistochemistry. Therefore, cells were prepared as described in Chapter 3.11. Subsequently, cells were fixed with 3.7% formalin in PBS followed by immunohistochemical staining. IHC was performed by Margit Gogg-Kammerer and Eva Hofer.

3.5 Survival analysis

Based on staining intensities and patients´ characteristics of TMAs, Kaplan-Meier analysis was performed using the R survival package. Therefore, the Cox proportional hazards regression model, including the Likelihood ratio test, was used. This analysis was performed by Robert Reihs.

Gene expression data of 28 CCA patients from The Cancer Genome Atlas (TCGA; http://cancergenome.nih.gov/) was analyzed regarding patients´ overall survival. The data was stratified by median to identify the association between high (n=14) and low (n=14) gene expression and overall survival using the log-rank test. Statistical significance was assumed at $p < 0.05$. This analysis was done by Anna Maria Birkl-Toeglhofer.

3.6 Protein isolation and immunoblot

For total protein isolation, cell lines were washed in ice-cold PBS, scraped and lysed in Nonidet P-40 lysis buffer (0.05 M Tris-HCl, 5 mM NaCl, 0.5% NP-40, 0.1 mM Pefabloc, 1 mM DTT, cOmplete Mini and PhosSTOP) for 30 min, followed by subsequent centrifugation. For trichloracetic acid (TCA) precipitation, serum-free cell culture supernatants were collected, and TCA was added to a final concentration of 10% and incubated overnight at -20°C.

Tissues were homogenized using MagNA Lyser homogenizer (Roche Diagnostics, Risch-Rotkreuz, Switzerland) in 1 mL Nonident P-40 lysis buffer, followed by subsequent centrifugation. The supernatant was collected, and protein concentration was determined with the Bradford protein assay (Biorad Protein Assay Dye Reagent; BioRad Laboratories GmbH, Munich, Germany). Between 15 and 30 µg of total protein lysate was applied to a 12.5 % sodium-dodecyl-sulfate polyacrylamide gel electrophoresis (SDS-PAGE; 30% Acrylamid/Bisacrylamid solution; ROTH, Karlsruhe, Germany) in a Mini-vertical electrophoresis unit (Hoefer Inc, Richmond, USA). The setup for the electrophoresis was 120 V until the running front reached the bottom of the gel. Afterwards, the proteins were blotted onto a poly(1,1-difluoroethylene) (PVDF) membrane (Immobilin-P Transfer Membrane; Millipore, Massachusetts, USA) using 80 mA for 1.5 h in a semi-dry blotting unit (V20-SDB; Scieplas, Cambridge, UK). The membranes were stained with a methanol/Ponceaou S solution (Sigma-Aldrich, St. Louis, USA) to verify protein transfer, destained and blocked for 1 h at room temperature with 5% non-fat dried milk (AppliChem; Darmstadt, Germany) in 0.1% TBS-Tween 20 (TBS-T). Primary antibodies (Table 2) were diluted in 5% bovine serum albumin (BSA; Roche Diagnistics GmbH, Mannheim, Germany) or 5% non-fat dried mild in 0.1% TBS-T and incubated overnight at 4°C under vigorous shaking. On the next day, the membranes were washed and incubated with matching secondary antibody (Table 2) for 1 h at room temperature. Visualization of the proteins was done with the chemiluminescence Amersham ECL Prime Western Blotting Detection Reagent (GE Healthcare Life Science, Buckinghamshire, UK) and exposed in the Image Quant LAS 500 (GE Healthcare Life Science, Buckinghamshire, UK).

Table 2: Antibodies used in this study. [Published in Kleinegger *et al.*, 2019]

Antibody	Species	Dilution	Distributor
IL-6Rα (4-11)	mouse	1 µg/mL	Described elsewhere (138,190)
p-STAT3 (Tyr705)	rabbit	1:2 000	Cell Signaling (Danvers, USA)
p-STAT3 (Ser727)	rabbit	1:1 000	Cell Signaling (Danvers, USA)
STAT3	mouse	1:1 000	Cell Signaling (Danvers, USA)
gp130 (E-8)	mouse	1:1 000	Santa Cruz Biotechnology (Dallas, USA)
SOCS3	rabbit	1:1 000	Cell Signaling (Danvers, USA)
GAPDH	rabbit	1:1 000	Cell Signaling (Danvers, USA)
ECL™ Anti-mouse IgG HRP	sheep	1:3 000	GE Healthcare (Buckinghamshire,UK)
ECL™ Anti-rabbit IgG HRP	donkey	1:5 000	GE Healthcare (Buckinghamshire,UK)
Vimentin	mouse	ready to use	Linaris (Dossenheim, Germany)
E-Cadherin	mouse	ready to use	Dako (Santa Klara, USA)
Cytokeratin 7	mouse	1:100	Dako (Santa Klara, USA)
Cytokeratin 19	mouse	1:100	Dako (Santa Klara, USA)

3.7 RNA isolation

For total RNA isolation, cell lines were washed with ice-cold PBS, scraped, and the cell pellet was resuspended in 1 mL TRIzol® reagent (Life Technologies; Woolston, UK). RNA isolation of human tissues was performed by homogenization in 1 mL TRIzol® reagent using a MagNA Lyser homogenizer.

Subsequently, 200 µL chloroform was added. After phase separation by centrifugation, the aqueous phase was precipitated with 500 µL ice-cold isopropanol. The pellet was washed with 80% ethanol and dissolved in RNAse-free water. Total RNA concentrations were measured using a Nanodrop1000 (Thermo Fischer Scientific Inc., Waltham, USA), and samples were stored at -80°C prior cDNA synthesis.

3.8 cDNA synthesis and quantitative real-time PCR

One µg RNA was reverse transcribed to cDNA using the High-Capacity cDNA Reverse Transcription Kit (Applied Biosystems, Foster City, USA) containing RNAse inhibitors (Applied Biosystems, Foster City, USA) in a GeneAmp 9700 Thermocycler (Applied Biosystems, Foster City, USA) according to the manufacturer's instructions. The setup for the thermocycler was as follows: 10 min at 25°C, 120 min at 37°C and 5 min at 85°C. For quantitative real-time PCR (qRT-PCR), 5 ng cDNA for human

tissue or 2.5 ng cDNA from cell lines was used together with the Power SYBR™ Green PCR Master Mix Kit (Applied Biosystems, Foster City, USA) and 5 µM primers in a total volume of 20 µL. The qRT-PCR was performed in a QuantStudio™ 7 Flex Real-Time PCR System (Applied Biosystems, Foster City, USA). Primers are listed in Table 3 and were checked for specificity and efficiency. Out of four different housekeeping genes, NormFinder (98) calculated *GAPDH* to be the most stable endogenous control. The relative gene expression levels were calculated by the $2^{-\Delta\Delta CT}$ method (191) and are represented as x-fold change.

Table 3: Used primers for qRT-PCR. [Published in Kleinegger *et al.*, 2019]

Gene name	RefSeq no.	Sequence 5´-3´	Amplicon size [bp]
IL-6Rα	NM_000565.3	GGGTTGTGGAATCTTGCAGC	93
		TCTTGCCAGGTGACACTGAG	
IL-6 (RTPrimerDB ID 3545)	NM_001318095.1	GGCACTGGCAGAAAACAACC	85
		GCAAGTCTCCTCATTGAATCC	
gp130	NM_001190981.1	ACCCCAAAGTTTGCTCAAGGA	96
		AAAGCAGAACAGCACTCCCA	
JAK1	NM_001321853.1	CTTTGCCCTGTATGACGAGAAC	101
		ACCTCATCCGGTAGTGGAGC	
JAK2	NM_001322196.1	TCTGGGGAGTATGTTGCAGAA	130
		AGACATGGTTGGGTGGATACC	
TYK2	NM_003331.4	GAGATGCAAGCCTGATGCTAT	76
		GGTTCCCGAGGATTCATGCC	
STAT3	NM_139276.2	CAGCAGCTTGACACACGGTA	150
		AAACACCAAAGTGGCATGTGA	
SOCS3	NM_003955.4	GATTCGGGACCAGCCCCC	121
		AACTTGCTGTGGGTGACCAT	
ADAM17	NM_003183.5	ACCGAATGCTGCTGGATATT	150
		CCTATTCCTGACCAGCGTG	

3.9 DNA isolation and cell line characterization

Cells were grown under standard conditions, washed, harvested, and genomic DNA was isolated using the QIAamp® DNA Mini Kit (Qiagen, Hilden, Germany) according to the manufacturer´s instructions. Isolated DNA was dissolved in DNAse free-water, and concentration was determined with a Nanodrop1000 (ThermoFischer Scientific, Massachusetts, USA).

3.9.1 Short tandem repeat analysis

This analysis was performed at the Institute for Human Genetics (Medical University of Graz). For cell line identification, short tandem repeat analysis was chosen using a PowerPlex® 16 HS System (Promega, Madison, USA) according to the manufacturer´s instructions. 0.5 ng DNA was mixed with primers and mastermix in a final volume of 10 µL. After PCR, 1 µL of the product was mixed with Hi-Di formamide (Applied Biosystems Inc., Foster City, US) and Internal Lane Standard (ILS600). After denaturation and fractionation on an ABI 3730 Genetic Analyzer (Applied Biosystems Inc., Foster City, US), the resulting data was analyzed and evaluated with the ABI Genemapper 4.0 (Applied Biosystems Inc., Foster City, US).

3.9.2 Mutational analysis by next-generation sequencing

This analysis was performed at the Laboratory for Molecular Diagnostics at the Diagnostic and Research Institute of Pathology (Medical University of Graz). Therefore, NGS libraries were prepared using the AmpliSeq library kit 2.0 (Thermo Fisher Scientific, Waltham, USA) and the Ion Ampliseq Cancer Hotspot Panel V2 (CatNr: 4475346) primer pool covering hotspot mutations in 50 genes implicated in cancer. Sequencing was performed on an Ion Proton benchtop sequencer (Thermo Fisher Scientific, Waltham, USA) to a length of 200 base pairs. Initial data analysis was done using the Ion Torrent Suite Software Plug-ins (Thermo Fisher Scientific, open source, GPL, https://github.com/iontorrent/). Briefly, this included base calling, alignment to the reference genome (HG19) using the TMAP mapper and variant calling by a modified diBayes approach taking into account the flow space information. Called variants were annotated using open source software ANNOVAR (192) and SnpEff (193). All coding, nonsynonymous mutations were further evaluated and visually inspected in IGV (http://www.broadinstitute.org/igv/), and variant calls resulting from technical read errors or sequence effects were excluded from the analysis.

3.10 Flow cytometry

3.10.1 Cell surface staining

Cells were grown under standard conditions, washed with warm PBS and detached using 10 nM EDTA in PBS. Afterwards, samples were incubated in blocking buffer (10% FBS, 0.1% NaN_3 in PBS) for 10 min on ice, dissociated by cell strainer, counted, and $1x10^6$ cells were re-suspended in Cell Staining Buffer (BioLegend, San

Diego, USA). 5 µL APC anti-human CD126 antibody (BioLegend, San Diego, USA) or 5 µL APC mouse IgG1, κ isotype control (BioLegend, San Diego, USA) was added to the cell suspension and incubated for 1 h on ice under light protection. After subsequent washing steps, measurement was performed with a CytoFLEX S (Beckman Coulter, Brea, USA) flow cytometer using CytExpert software (Beckman Coulter, Brea, USA).

3.10.2 Cell cycle analysis

To analyze the phases of cell cycle upon treatment, between $2x10^4$ and $5x10^4$ cells were seeded into 6-well plates, allowed to adhere overnight and serum starved for 24 h. Subsequently, cells were treated with Hyper-IL-6 (15 ng/mL), IL-6 (100 ng/mL), Tocilizumab (25 µg/mL) and sgp130Fc (25 µg/mL) for 72 h under serum-starved conditions, detached using trypsin (Gibco, Life Technologies, Darmstadt, Germany), washed with PBS, and re-suspended in hypotonic propidium iodide (PI) lysis buffer containing 0.1% sodium citrate, 0.1% Triton-X, 100 µg/mL RNAseA and 50 µg/mL PI. After several washing steps, measurement of cell cycle was performed on a BD LSRII (BD Bioscience, Brea, USA) flow cytometer. Therefore, living cell population was gated, and doublet discrimination was done using a PE-A/PE-W scatter plot. To obtain cell cycle phases, counts were blotted against PE-A signals. Evaluation of different cell cycle phases was done using the ModFit LT software version 5.0 (Verity Software House, Topsham, USA).

3.11 Immunofluorescence staining

Between $2x10^3$ and $5x10^3$ cells were seeded on sterile Flex IHC microscope slides (Dako, Agilent Santa Clara, USA) in a flexiPERM® (Sarstedt, Nuembrecht, Germany) chamber and allowed to adhere overnight. After several washing steps with ice-cold PBS, cells were fixed for 20 min with ice-cold methanol at -20°C. Samples were permeabilized with 1% Triton X-100 (Sigma-Aldrich, St. Louis, USA), and blocking was performed for 1 h with 5% horse serum (ThermoFischer Scientific, Massachusetts, USA). Primary antibody (mouse anti-human IL-6Rα (4-11), 4 µg/mL) was incubated overnight at 4°C in a humid atmosphere. After several washing steps, secondary antibody (AlexaFluor®488 goat anti-mouse IgG, Invitrogen ThermoFischer Scientific, Massachusetts, USA; 1:500) was added and incubated for 1 h at room temperature followed by counterstaining using 4′,6-Diamidin-2-phenylindol (DAPI, Sigma Life Science, St. Louis, USA). Fluorescence microscopy was performed using

an LSM 510 Meta microscope (Zeiss, Oberkochen, Germany). The same setup was used for all cell lines to avoid data manipulation.

3.12 Electrochemiluminescence immunoassay

To quantify the amount of secreted IL-6 in the cell culture supernatant, $5x10^4$cells were seeded in 6-well plates and allowed to adhere overnight. Cells were serum-starved for 24 h, and medium was refreshed afterwards. After 24 h, the supernatant was collected, centrifuged and stored at -80°C prior to electrochemiluminescence immunoassay (ECLIA) (194). The amount of secreted IL-6 was analyzed automatically using the COBAS® immunoassay system (Roche Diagnostics, Risch-Rotkreuz, Switzerland). The CalSet IL-6 Elecsys® (Roche Diagnostics, Risch-Rotkreuz, Switzerland) was used for calibration. This assay was performed by Tobias Niedrist.

3.13 Cell viability assay

Viable cells were analyzed by mitochondrial reduction of 3-(4,5-dimethylthiazol-2-yl)-2,5-diphenyltetrazolium bromide (MTT, Sigma Aldrich, Missouri, USA) to (E,Z)-5-(4,5-dimethylthioazol-2-yl)-1,3-diphenylfromazan. Therefore, between $1x10^4$ and $5x10^4$ cells/well were seeded in 96-well plates and allowed to adhere for 24 h. After serum starvation overnight, cells were treated for 24 h, 48 h and 72 h with increasing concentrations of all four compounds (5, 15, 30 ng/mL for IL-6 and Hyper-IL-6; 1, 10, 25 µg/mL for Tocilizumab and sgp130Fc) under serum depletion. At indicated time points, cells were incubated for 2 h with 5.5 mg/mL MTT at 37°C. Afterwards, the supernatant was removed, and cells were lysed in 3% SDS. The violet formazan crystals were dissolved in a 4 mM isopropanol/HCl solution under vigorous shaking. Absorption was measured at 570 nm in a Synergy™4 spectrometer (BioTek, Winooski, USA).

3.14 Proliferation assay

For the measurement of real time proliferation, xCELLigence DP device (OLS Omni Life Science, Bremen, Germany) was used. $5x10^3$ cells per well were seeded in electronic microtiter plates (E-Plate™, OLS) and allowed to adhere for 24 h, followed by serum starvation for 24 h. Afterwards, cells were treated with all compounds (15 ng/mL Hyper-IL-6, 100 ng/mL IL-6, 25 µg/mL Tocilizumab or 25 µg/mL sgp130Fc) under serum depletion. Every 20 min for 72 h, the cell density was measured through

the whole experiment, including adherence of the cells and serum starvation. Normalization was performed directly after treatment. The slope of the logarithmic phase of the growth curve and the population doubling time (PDT) were calculated with the RTCA software version 2.0 (ACEA Biosciences, Inc., San Diego, USA).

3.15 Apoptosis assay

To investigate changes in apoptotic signals, the intercalation of YoPro©-1 iodide (491/509) (Thermo Fisher Scientific, Massachusetts, USA) in DNA of cells after 24 h, 48 h and 72 h treatment with Hyper-IL-6 (5 ng/mL, 15 ng/mL and 30 ng/mL), IL-6 (15 ng/mL, 50 ng/mL and 100 ng/mL), Tocilizumab (1 µg/mL, 10 µg/mL and 25 µg/mL) and sgp130Fc (1 µg/mL, 10 µg/mL and 25 µg/mL) was measured fluorometrically on a Synergy™4 spectrometer (BioTek, Winooski, USA). Therefore, between $1x10^4$ and $5x10^4$ cells/well were seeded in clear bottom black 96-well plates and allowed to adhere, followed by serum starvation overnight and treatment (5, 15, 30 ng/mL for IL-6 and Hyper-IL-6; 1, 10, 25 µg/mL for Tocilizumab and sgp130Fc). Afterwards, the cells were washed with PBS, and YoPro©-1 iodide (491/509) was added. After 15 min of incubation, the cells were washed, and fluorescence was measured.

3.16 Wound healing assay

To investigate differences in migration upon treatment of cell lines, wound healing assay (scratch assay) was performed. Therefore, between $5x10^5$ and $1x10^6$ cells were seeded in 6-well plates. On the next day, cells were checked for 100% confluency and serum starved overnight. Afterwards, the cell layer was wounded using a 200 µL tip and treated with 15 ng/mL Hyper-IL-6, 100 ng/mL IL-6, 25 µg/mL Tocilizumab, 25 µg/mL sgp130Fc or in combination under FBS depletion. Pictures were taken with an Olympus Inverse IX53 microscope (Tokyo, Japan) after 24 h, 48 h and 72 h of treatment. Opened wound area was calculated using the TScratch software version 1.0 (195).

3.17 Statistical analysis

Statistical analysis was performed with GraphPad Prism version 5.01 (GraphPad Software, La Jolla, USA) if not mentioned otherwise. The proper tests were selected regarding data distribution of each analysis. $p < 0.05$ was considered statistically significant.

4. Results

4.1 Analysis of patient derived tumor tissue

4.1.1 The IL-6Rα is expressed in GBC tissue and correlates with overall survival of GBC patients

To investigate the potential of IL-6Rα as a possible biomarker for overall survival, FFPE material of 367 GBC samples and 61 NNTs was examined due to IL-6Rα immunoreactivity and correlated to patients' overall survival. The patients´ characteristics are listed in Table 1.

Positive IL-6Rα immunoreactivity was seen as clear cytosolic or membranous staining (Figure 8A). 365 out of 367 GBC samples (99.4%) showed positive IL-6Rα immunoreactivity, indicating the presence of IL-6Rα in GBC tissue. For further analysis, staining intensity was grouped as low IL-6Rα expression (no and weak staining intensity) and high IL-6Rα expression (moderate and strong staining intensity). High IL-6Rα expression was found in 305 samples (83.1%), whereas 60 samples (16.3%) showed low IL-6Rα expression. Analysis regarding the survival rate of GBC patients revealed a significant ($p < 0.001$) association between high IL-6Rα expression and better survival probability (Figure 8B). Subdivision of GBC into low (G1-G2) and high (G3-G4) grade tumors, as well as IL-6Rα expression, revealed similar results (Figure 8C), whereas patients suffering from low grade GBC showed longer overall survival. GBC occurs predominantly in women. Therefore, survival analysis was done regarding gender, the presence of IL-6Rα and survival probability. No gender-specific differences were found in the cohort analyzed (Figure 8D). These findings indicate that IL-6Rα might be a prognostic factor for GBC overall survival independent of tumor grade and patients´ gender.

In order to find out whether IL-6Rα is GBC-specific, survival analysis of the TCGA database regarding *IL-6Rα* gene expression was performed on 28 Caucasian patients suffering from known primary CCA. The analysis showed no significant difference between *IL-6Rα* gene expression and CCA patients´ overall survival (Figure 8E), which may be due to a low sample number.

To gain information on signaling downstream IL-6Rα, the JAK/STAT3 cascade was analyzed in fresh frozen GBC samples.

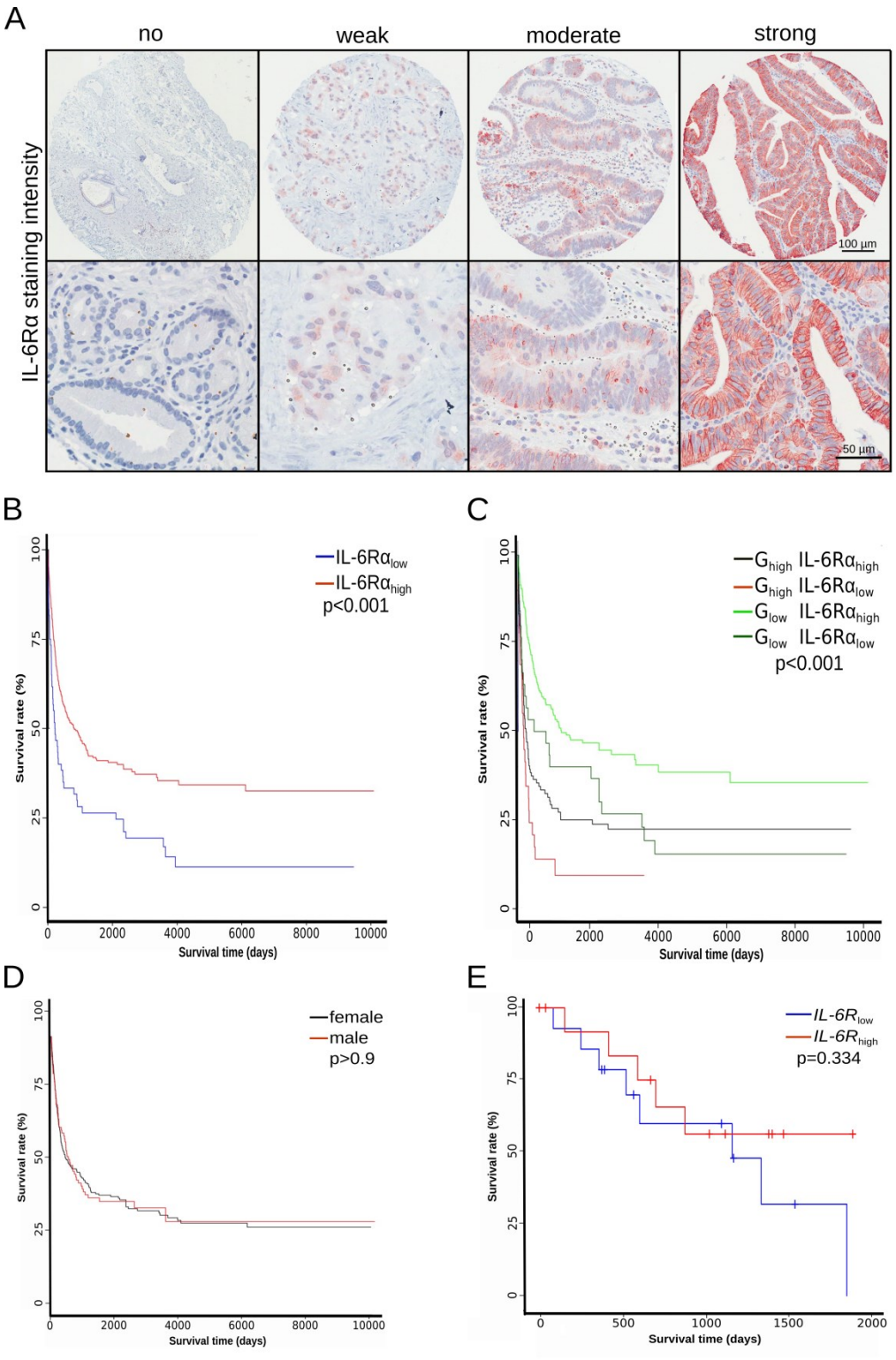

Figure 8: Evaluation of GBC FFPE tissue regarding IL-6Rα staining intensity. (A) Representative immunohistochemistry of no, weak, moderate and strong IL-6α immunoreactivity in GBC. (B) Survival Analysis of GBC patients grouped as high and low IL-6Rα staining intensity. (C) Kaplan-Maier analysis of low and high grade GBC patients distributed in high and low IL-6Rα staining intensity. (D) Overall survival of GBC patients based on positive IL-6Rα staining intensity distributed by gender (E) *IL-6Rα* gene expression related to overall CCA patients' survival using TCGA database. Bar = 100 or 50 µm. [Published in Kleinegger *et al.*, 2019]

4.1.2 The IL-6Rα is downregulated in GBC tissue and might cause decreased STAT3 activation

IL-6Rα signaling is often dysregulated in carcinomas. Therefore, analysis of the downstream signaling cascade was performed in fresh frozen GBC tissue and compared to NNT.

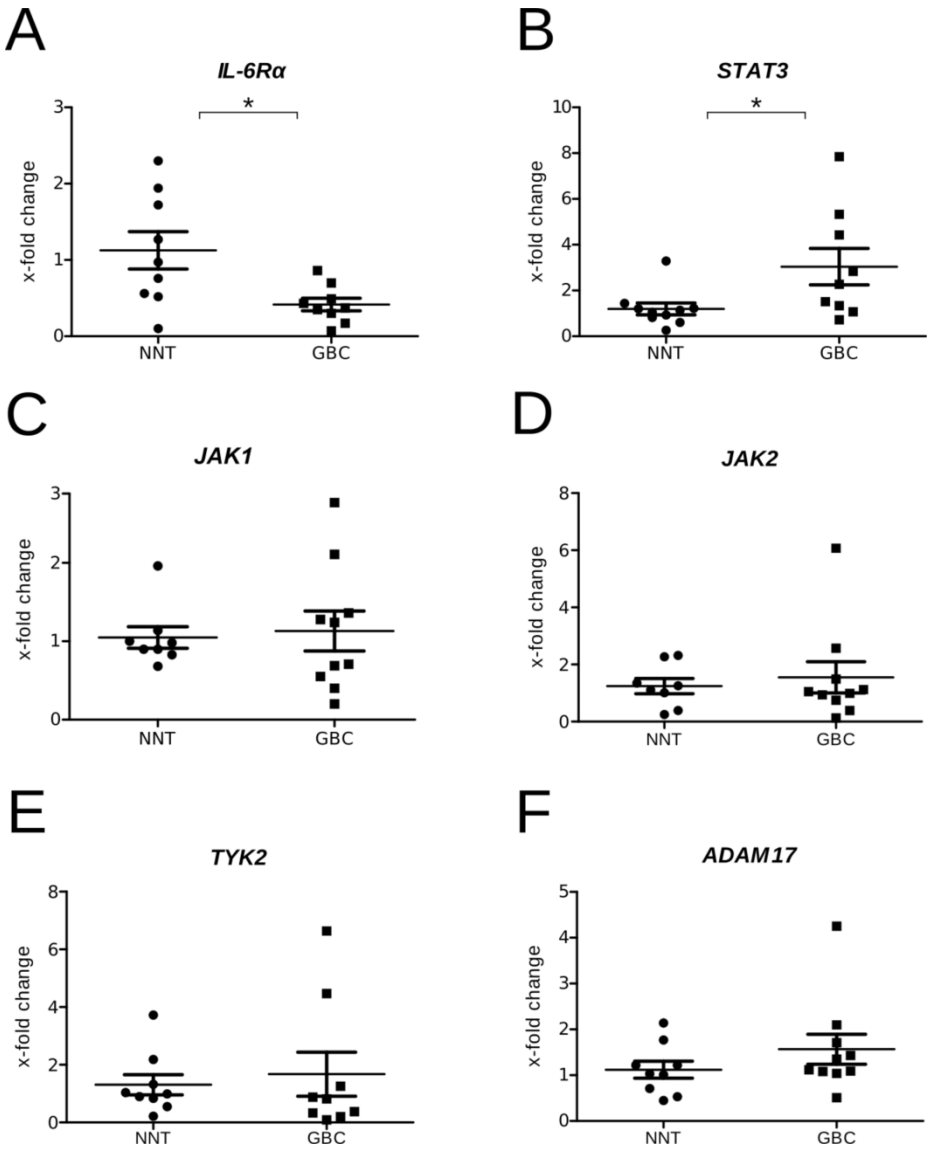

Figure 9: Gene expression analysis of fresh frozen GBC tissue compared to NNT. Graphs represent x-fold change of (A) *IL-6Rα*, (B) *STAT3*, (C) *JAK1*, (D) *JAK2*, (E) *TYK2*, and (F) *ADAM17* gene expression calculated using the $2^{-\Delta\Delta Ct}$ method. Bars represent mean ± SEM. Statistical analysis: t-test/Mann-Whitney U test. * $p < 0.5$. [Published in Kleinegger *et al.*, 2019]

On mRNA level, a significant downregulation ($p < 0.05$) of *IL-6Rα* was found in GBC compared to NNT (Figure 9A). The expression of *STAT3* was found to be significantly ($p < 0.05$) upregulated (Figure 9B). Analysis of kinases (Figure 9C-E) responsible for STAT3 activation revealed no significant alterations during

carcinogenesis. The result was the same for the gene expression of the metalloprotease *ADAM17* (Figure 9F).

To gain information about the two forms of the IL-6Rα and the activation (phosphorylation) of STAT3, 12 NNT and 14 GBC samples were immunoblotted (Figure 10A).

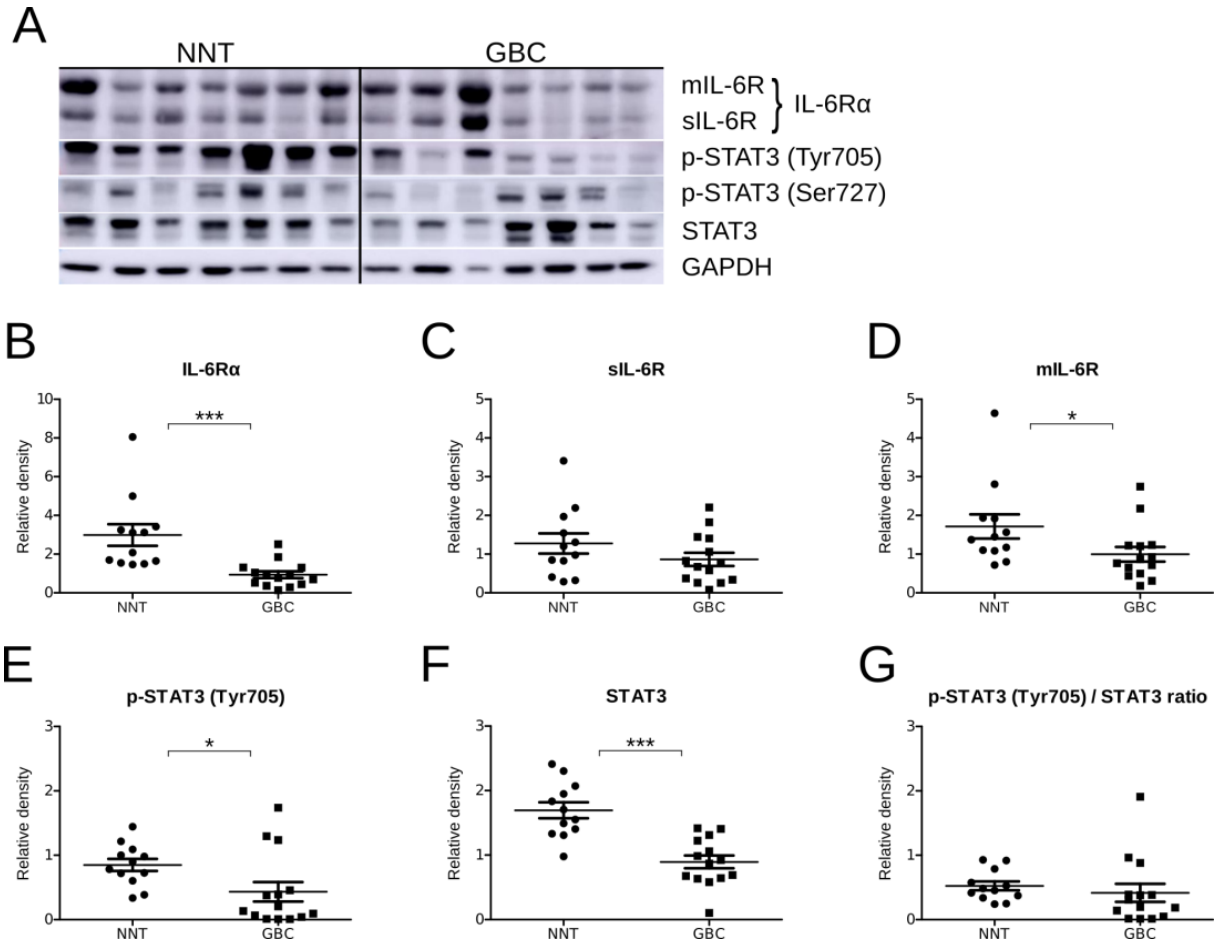

Figure 10: Protein expression analysis of fresh frozen GBC tissue compared to NNT. (A) Representative immunoblot of non-neoplastic, non-inflamed gallbladder tissue (n=12) and gallbladder cancer tissue samples (n=14). Densitometric analysis of (A) IL-6Rα and its two different forms (C) sIL-6R and (D) mIL-6R. Analysis of (E) p-STAT3 (Tyr705), (F) total STAT3 and the calculated ratio of (G) p-STAT3 (Tyr705)/STAT3. Bars represent mean ± SEM. Statistical analyses: t-test/Mann-Whitney U test, * $p < 0.05$, *** $p < 0.001$. [Published in Kleinegger *et al.*, 2019]

This analysis revealed the expression of both IL-6Rα forms in NNT and GBC, whereby a significant IL-6Rα downregulation ($p < 0.001$) was seen in GBC samples after densitometric analysis (Figure 10B). Differentiating both IL-6Rα forms revealed no significant alterations in the soluble form of the IL-6R (Figure 10C) and a significant ($p < 0.05$) downregulation of the membranous form (Figure 10D). STAT3

was found to be significantly ($p < 0.05$) less activated in GBC compared to NNT (Figure 10E). The same significant ($p < 0.001$) finding was observed for total STAT3 (Figure 10F). However, by calculating the ratio of p-STAT3 (Tyr705) and STAT3, no significant alterations were observed between the two groups (Figure 10G).

Taken together, the tissue analyses results revealed the presence of IL-6Rα and it both forms in GBC tissue. However, the receptor is downregulated in GBC tissue compared to NNT on protein and mRNA level. Cholangiocarcinogenesis affects mIL-6R more intensely than sIL-6R, indicating a leading role of IL-6 classic signaling. Furthermore, the receptor serves as a good prognostic marker for overall survival of GBC patients independent of grade and gender.

4.2 *In vitro* experiments

Prior to *in vitro* experiments, five different CCA cell lines, TFK-1, EGI-1, Mz-ChA-1, Mz-ChA-2 and SK-ChA-1, were characterized regarding their origin, BTC marker expression and mutations, followed by detailed analysis of IL-6Rα mediated signaling.

4.2.1 Genetic profiling and tumor marker expression of CCA cell lines

In order to prove the origin of cell lines, DNA was isolated, followed by STR analysis. Results are shown in Table 4.

Table 4: STR profiling of the cell lines used. All cell lines revealed a unique STR profile on 16 different loci, analyzed by the PowerPlex® 16HS System.

STR-Locus	TFK-1	EGI-1	Mz-ChA-1	Mz-ChA-2	SK-ChA-1
D3S1358	17, 18	17	15	18	15
TH01	6	6, 9	7	8	6
D21S11	30	28, 33.2	28	28	28
D18S51	16	14, 16	14	15	16
Penta E	5, 18	5, 11	9, 12	14, 17	17
D5S818	9, 12	13	11	10	11, 13
D13S317	14	11	8, 10	12, 13	10
D7S820	10	9, 13	13, 14	11, 12	10
D16S539	9	12, 13	11, 12	11	9,13
CSF1PO	10	12, 13	11	12	12, 13
Penta D	13, 14	7, 9	12	9, 12	2.2
Amelogenin	X, Y	X, Y	X	X	X
vWA	14, 17	17, 18, 19	15, 19	15, 17	16, 18
D8S1179	13, 14	11, 16	13	13	13, 14
TPOX	8	8, 11	8	8, 11	8
FGA	20, 23	20, 25	20, 23	22, 24	25

All cell lines were tested for a specific STR profile, indicating that no cross-contamination occurred during culture. Alignment of the obtained STR profile with available cell line databases verified the cell lines. To get more information about mutations in the cell lines used, analysis of 50 oncogenes and tumor-suppressor genes was performed. The results, including the exact mutation and swift score, are listed in Table 5.

Table 5: Mutational analysis of the CCA cell lines used. All cell lines were analyzed regarding their mutational profile (Ion AmpliSeq Cancer HotSpot Panel v2), revealing a deletion of *CDKN2A* and mutated *TP53* in all tested cell lines. Values represent the exchanged nucleotide, including swift score in brackets. WT = Wildtype. [Published in Kleinegger *et al.*, 2019]

Genes	TFK-1	EGI-1	Mz-ChA-1	Mz-ChA-2	SK-ChA-1
ABL1	WT	WT	WT	WT	WT
AKT1	WT	WT	WT	WT	WT
ALK	WT	WT	WT	WT	WT
APC	WT	WT	WT	WT	WT
ATM	WT	WT	WT	WT	WT
BRAF	WT	WT	WT	WT	**G1780A (0)**
CDH1	WT	WT	WT	WT	WT
CDKN2A	**Deletion**	**Deletion**	**Deletion**	**Deletion**	**Deletion**
CSF1R	WT	WT	WT	WT	WT
CTNNB1	WT	WT	WT	WT	WT
EGFR	WT	WT	WT	WT	WT
ERBB2	WT	**Amplification**	**Amplification**	WT	**Amplification**
ERBB4	WT	WT	WT	WT	WT
EZH2	WT	WT	WT	WT	WT
FBXW7	WT	WT	WT	WT	WT
FGFR1	WT	WT	WT	WT	WT
FGFR2	WT	WT	WT	WT	WT
FGFR2	WT	WT	WT	WT	WT
FLT3	WT	WT	WT	WT	WT
GNA11	WT	WT	WT	WT	WT
GNAQ	WT	WT	WT	WT	WT
GNAS	WT	WT	WT	WT	WT
HNF1A	WT	WT	WT	WT	WT
HRAS	WT	WT	WT	WT	WT
IDH1	WT	WT	WT	WT	WT
IDH2	WT	WT	WT	WT	WT
JAK2	WT	WT	WT	WT	WT
JAK3	WT	WT	WT	WT	**C395A (0.39)**
KDR	WT	WT	WT	WT	WT
KOIT	WT	WT	WT	WT	WT
KRAS	WT	**G35A (0)**	WT	WT	WT
MET	WT	WT	WT	WT	WT

MLH1	WT	WT	WT	WT	WT
MPF	WT	WT	WT	WT	WT
NOTCH1	WT	WT	WT	WT	WT
NPM1	WT	WT	WT	WT	WT
NRAS	WT	WT	WT	WT	WT
PDGFRA	WT	WT	WT	WT	WT
PIK3CA	WT	WT	WT	WT	WT
PTEN	WT	WT	WT	WT	WT
PTPN11	WT	WT	WT	WT	WT
RB1	WT	WT	WT	WT	WT
RET	WT	WT	WT	WT	WT
SMAD4	WT	WT	**C725G (0.14)**	WT	WT
SMARCB1	WT	WT	WT	WT	WT
SMO	WT	WT	WT	WT	WT
SRC	WT	WT	WT	WT	WT
STK11	WT	WT	WT	WT	WT
TP53	**G273A (0.19)**	**G818A (0.01)**	**G828T (0)**	**C535T (0)**	**C844T (0)**
VHL	WT	WT	WT	WT	WT

All cell lines were found to have deleted *CDKN2A* and mutated *TP53*. SK-ChA-1 cells were the only cells tested and found to have a mutation in *JAK3*. *ERBB2* (also known as *HER2/neu*) was found to be amplified in three out of five cell lines.

CCA is pathologically diagnosed using the markers cytokeratin 7 (CK7) and cytokeratin 19 (CK19). Therefore, cells were seeded on coated IHC slides, fixed and stained for CK7, CK19 and the epithelial-to-mesenchymal transition (EMT) markers E-cadherin and Vimentin. Representative pictures of the immunohistochemistry are shown in Figure 11.

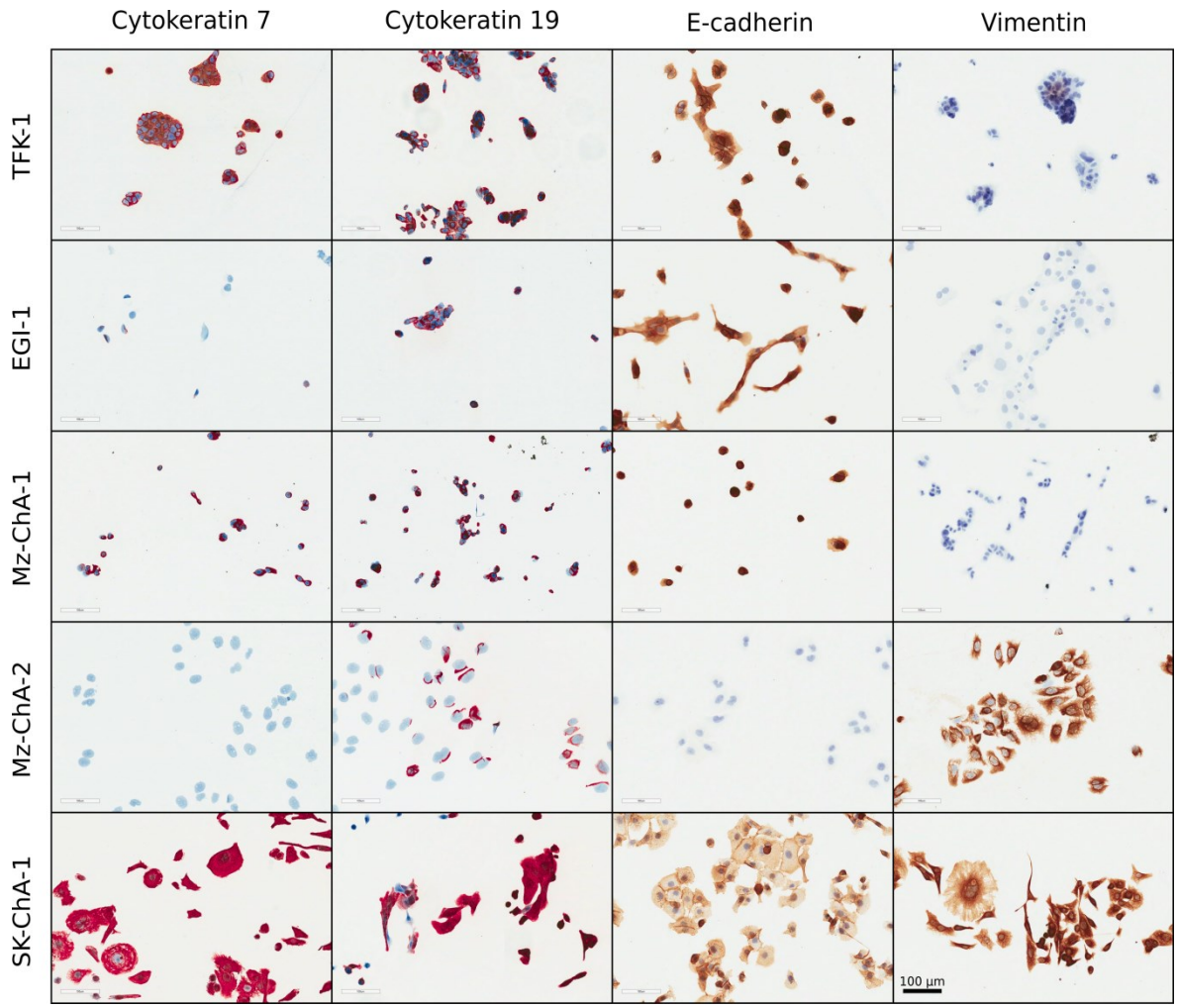

Figure 11: Immunohistochemical evaluation of BTC marker expression in cholangiocarcinoma cell lines. Cells were seeded on IHC slides, fixed with 4% formalin and stained for Cytokeratin 7 and 19, E-cadherin and Vimentin. Bar = 100 µm.

SK-ChA-1 was the only cell line which showed a positive immunoreactivity for all four tested markers. TFK-1 and Mz-ChA-1 had positive immunoreactivity for CK7 and CK19, whereas EGI-1 and Mz-ChA-2 were exclusively positive for CK19. Besides SK-ChA-1, only Mz-ChA-2 expressed Vimentin, which gives this cell line a mesenchymal character. E-cadherin was positive in TFK-1, EGI-1 and Mz-ChA-1 cells. These findings proved the CCA marker expression in all cell lines and indicate their different status regarding EMT.

4.2.2 Characterization of CCA cell lines regarding IL-6Rα mediated signaling

For detailed information of IL-6 mediated signaling in the used cell lines, different methods were applied. First, the cells were analyzed for the expression of IL-6,

IL-6Rα, gp130, STAT3, including phosphorylation sides, and SOCS3 on mRNA level (Figure 12) and protein level (Figure 13).

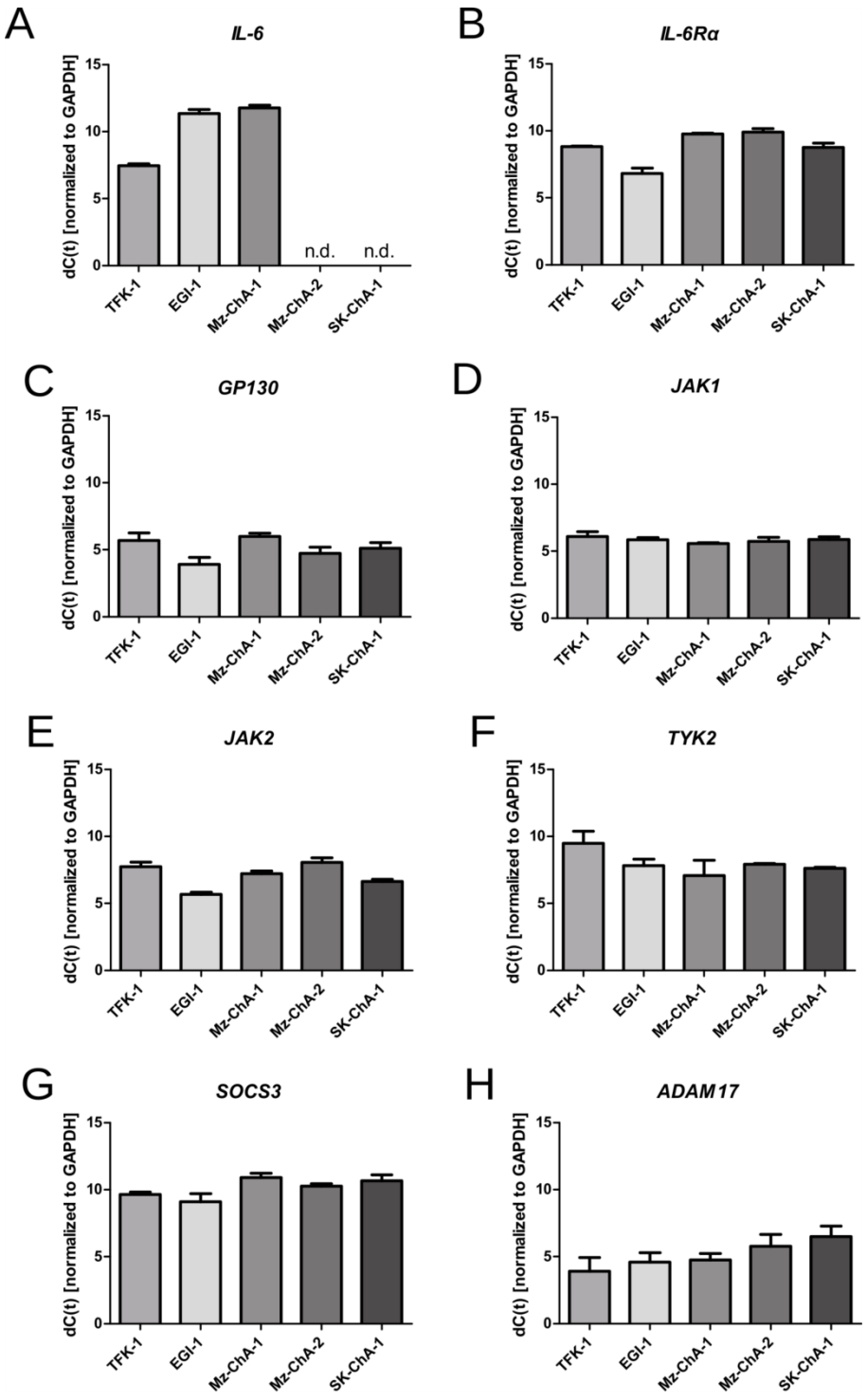

Figure 12: Gene expression profile of IL-6 signaling cascade in CCA cell lines. Gene expression was analyzed using qRT-PCR. (A) *IL-6*, (B) *IL-6Rα*, (C) *GP130*, (D) *JAK1,* (E) *JAK2,* (F) *TYK2,* (G) *SOCS3,* and (H) *ADAM17* mRNA levels were analyzed and normalized to *GAPDH*. n.d. = not detectable. Graphs represent Mean ± SD. [Parts are published in Kleinegger *et al.*, 2019]

Three out of five cell lines were found to express *IL-6* (Figure 12A). The other analyzed genes were found to be expressed in all five cell lines (Figure 12B-H). Except for *JAK1* (Figure 12D), all tested genes were found to be differentially expressed through all cell lines.

To gain information about the protein levels of IL-6Rα in these cell lines, immunofluorescence staining was performed. All cell lines showed positive cytosolic/membranous immunoreactivity for IL-6Rα, which is in line with *IL-6Rα* gene expression data (Figure 13A).

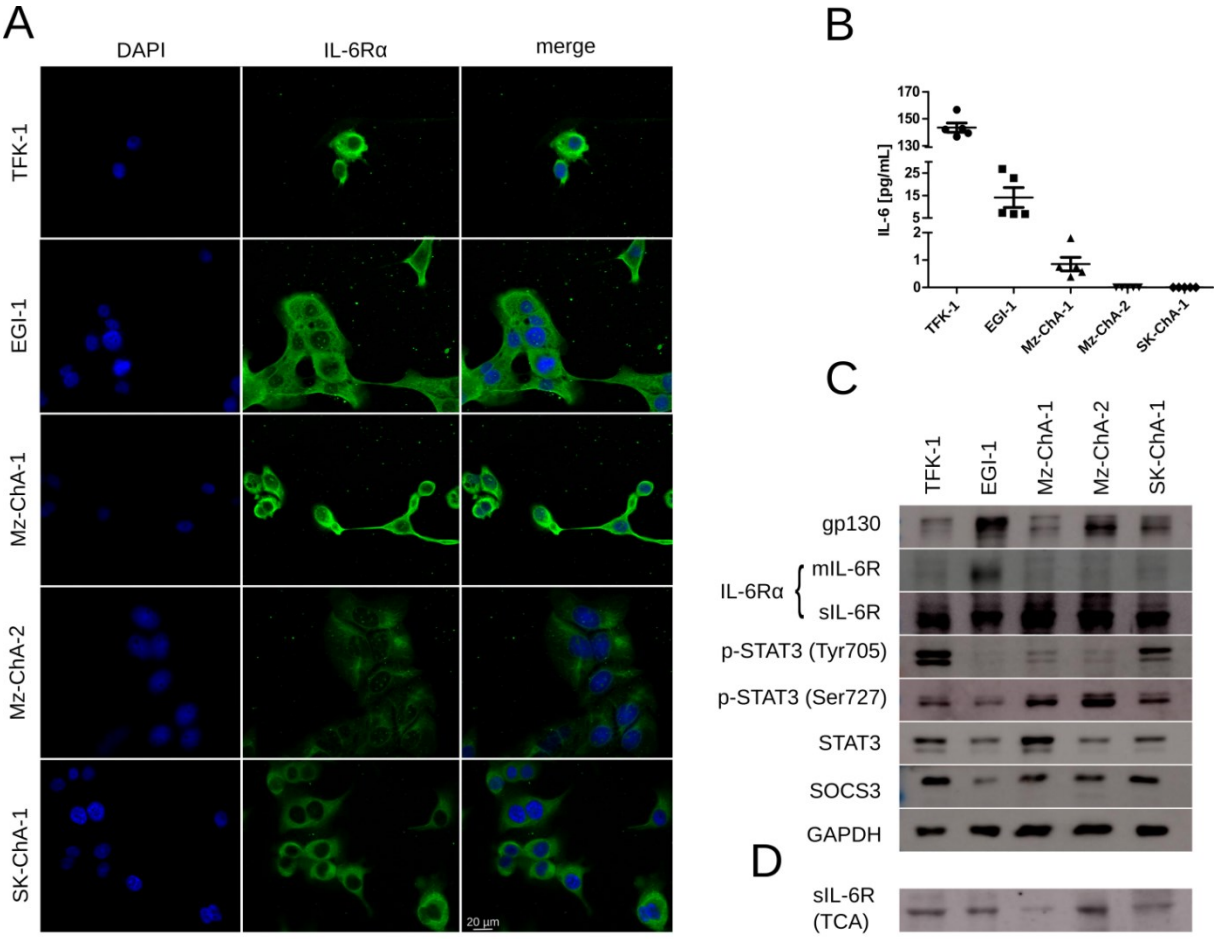

Figure 13: Expression analysis of the IL-6 pathway in CCA cell lines. (A) Immunofluorescence staining of the IL-6Rα on all tested cell lines. (B) Quantification of IL-6 in the serum-free cell culture supernatants of cell lines using ECLIA. (C) Immunoblot analysis of IL-6 and its mediated signaling. (D) Analysis of the sIL-6R in the cell culture supernatant using TCA precipitation followed by immunoblotting. [Published in Kleinegger *et al.*, 2019]

As the differences were found to be strongest for *IL-6* gene expression (Figure 12A), the cell culture supernatant was quantified regarding cell line secreted IL-6 (Figure 13B). Indeed, IL-6 was found in three out of five cell lines, confirming gene expression data. The cell line TFK-1 was found to secret the highest amount of IL-6 (143 pg/mL), followed by EGI-1 (14 pg/mL) and Mz-ChA-1 (1 pg/mL). As *IL-6* expression data suggested, IL-6 was not detectable in the supernatant of Mz-ChA-2 and SK-ChA-1 cells.

To investigate activation of STAT3 and upstream signaling, cell whole protein lysates were immunoblotted (Figure 13C).

All cell lines were found to express gp130, STAT3 and SOCS3. Differentiation by size gave information on the two IL-6R forms. The five cell lines express sIL-6R and mIL-6R, whereas the strongest expression was seen in EGI-1 cells. Strong tyrosine phosphorylation (activation) of STAT3 was found in TFK-1 and SK-ChA-1 cells, whereas all other cell lines showed little activation. Serine phosphorylation of STAT3 was found in all cell lines. Since the sIL-6R is shed, cell culture supernatant was precipitated using TCA and immunoblotted, revealing the presence of sIL-6R in the supernatant of all tested cell lines (Figure 13D).

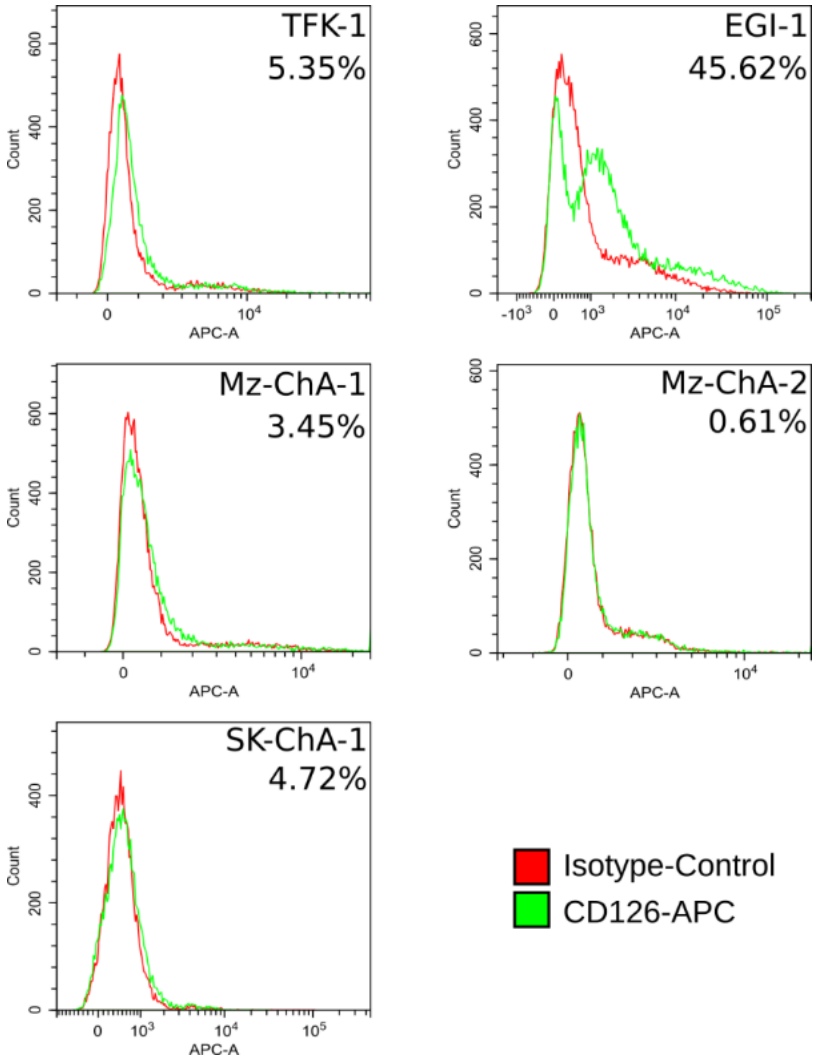

Figure 14: Flow cytometric analysis of the IL-6Rα on the cell culture surface. Cells were stained using a CD126-APC antibody against the IL-6Rα, and the presence of the IL-6Rα on the cell surfaces was analyzed. Percentage of $CD126^{+}$ positive cells was calculated with CytExpert software and compared to the isotype control. [Published in Kleinegger *et al.*, 2019]

To prove the presence of the IL-6Rα on the cell´s surface, flow cytometric analysis was performed. The analysis of positive cells ranged between 0.61 % (Mz-ChA-2) and 45.62 % in EGI-1 cells (Figure 14). This finding confirmed the immunoblot and qRT-PCR data by highlighting EGI-1 as the cell line that shows the highest expression of IL-6Rα in all cell lines tested.

Due to the weaker IL-6Rα expression and weak activation of STAT3, Mz-ChA-2 cells were chosen as a tool to study the differences between STAT3 activation by IL-6 and Hyper-IL-6. TFK-1 cells served as a model suitable for the inhibition of IL-6 signaling using Tocilizumab and sgp130Fc due to high expression of IL-6 and autocrine activation of STAT3.

4.2.3 Analysis of *in vitro* effects of activation and inhibition of IL-6 classic signaling and IL-6 trans-signaling on CCA cell lines

For the analysis of potential differences in the activation of STAT3, Mz-ChA-2 cells were treated with equal concentrations of either IL-6 or Hyper-IL-6 over 1 h, 6 h and 24 h and immunoblotted.

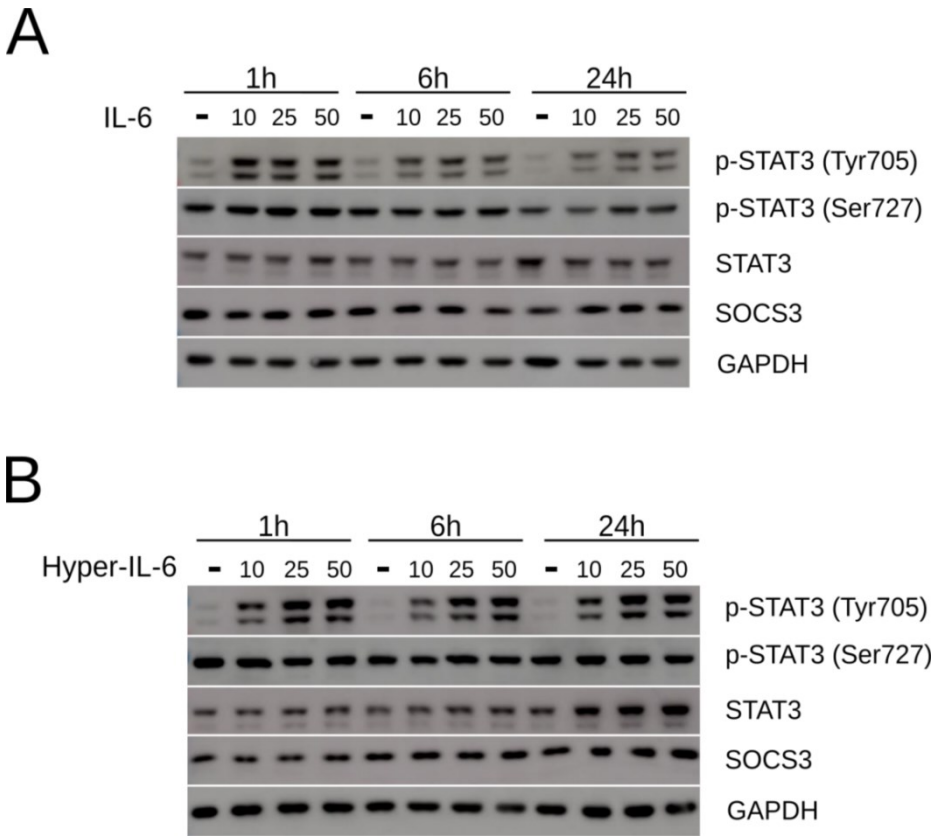

Figure 15: Immunoblot analysis of STAT3 activation induced by IL-6 and Hyper-IL-6 in Mz-ChA-2 cells over time. (A) Mz-ChA-2 cells were treated with 10, 25, 50 ng/mL IL-6, harvested and immunoblotted. (B) Mz-ChA-2 cells were cultivated in the presence of 10, 25 or 50 ng/mL Hyper-IL-6, harvested after indicated time points and immunoblotted. [Published in Kleinegger *et al.*, 2019]

IL-6 treatment led to an activation of p-STAT3 (Tyr705), with the strongest effects seen after 1 h of incubation (Figure 15A). Interestingly, the p-STAT3 (Tyr705) signal upon IL-6 decreased over time independent of concentration. In contrast, Hyper-IL-6 led to a more stable and stronger activation of p-STAT3 (Tyr705) compared to IL-6 (Figure 15B). Both compounds affected neither the phosphorylation of STAT3 on serine 727 nor the expression of total STAT3 and SOCS3.

In order to prove the function of the used inhibitors Tocilizumab and sgp130Fc, Mz-ChA-2 cells were pretreated with the inhibitors for 6 h, followed by incubation with either IL-6 or Hyper-IL-6 prior to immunoblotting (Figure 16).

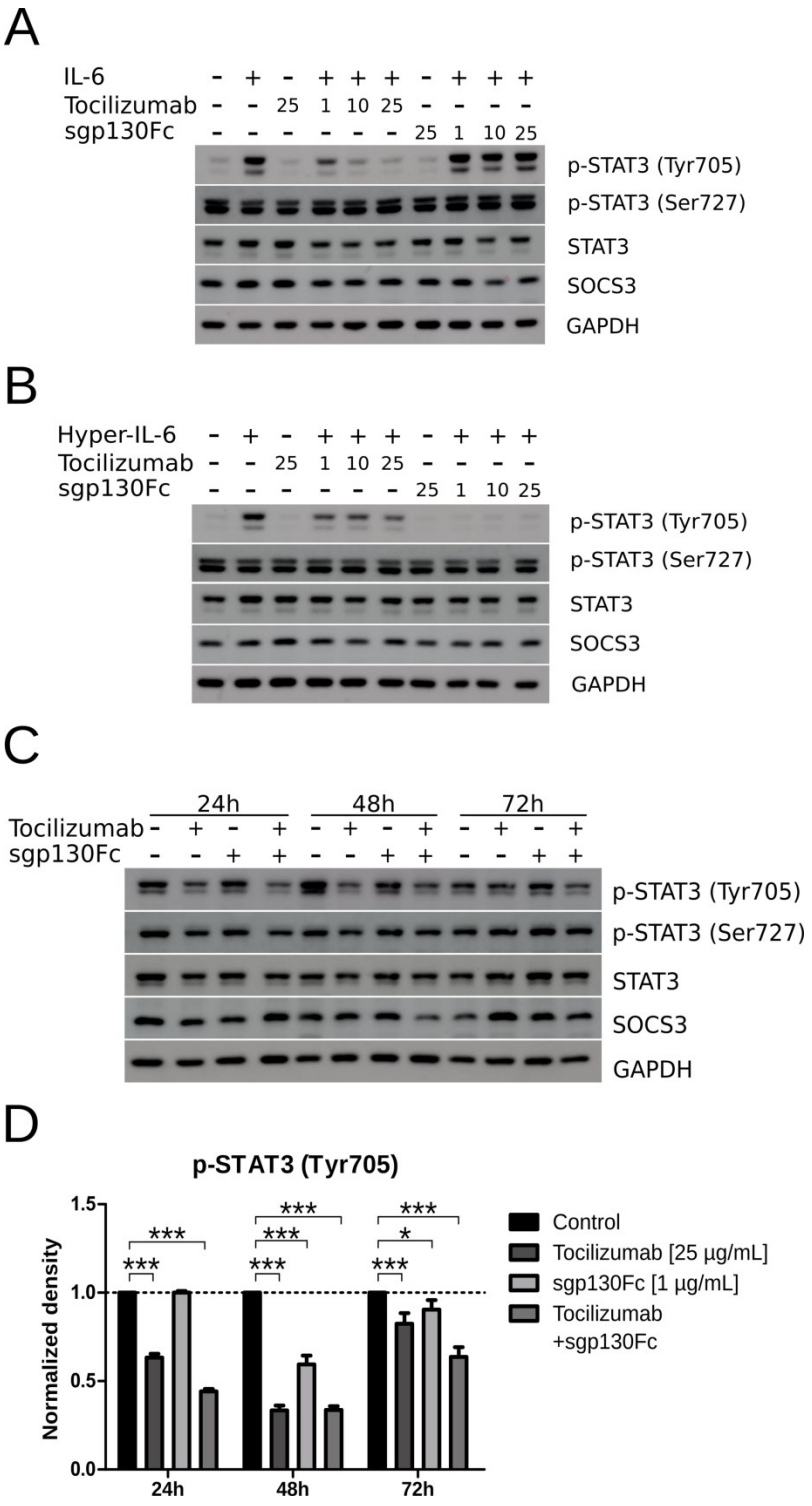

Figure 16: Effects of IL-6R inhibition on induced STAT3 activation in CCA cell lines. Mz-ChA-2 cells were pretreated with 1, 10 or 25 µg/mL Tocilizumab or sgp130Fc for 6 h followed by incubation with (A) 100 ng/mL IL-6 or (B) 15 ng/mL Hyper-IL-6. (C) Competitive inhibition of autocrine IL-6Rα signaling in TFK-1 cells, treated for 24 h, 48 h and 72 h with Tocilizumab (25 µg/mL) and/or sgp130Fc (15 µg/mL). (D) Densitometric analysis of p-STAT3 (Tyr705) signal after treatment with Tocilizumab (25 µg/mL) and/or sgp130Fc (15 µg/mL) over 24 h, 48 h or 72 h. Bars represent mean ± SEM. * $p < 0.05$, ** $p < 0.01$, *** $p < 0.001$. Statistical analysis: One-way ANOVA. [Published in Kleinegger *et al.*, 2019]

A concentration of 10 µg/mL Tocilizumab was able to block IL-6 induced STAT3 activation, which was not influenced by the presence of sgp130Fc (Figure 16A). In contrast, sgp130Fc was able to inhibit Hyper-IL-6 induced STAT3 activation at a concentration of 1 µg/mL (Figure 16B). This effect was mitigated by administration of Tocilizumab in a concentration-independent manner. Neither Tocilizumab nor sgp130Fc influenced the expression levels of p-STAT3 (Ser727), total STAT3 and SOCS3 (Figure 16A-B).

In order to investigate the inhibitory effects of Tocilizumab and sgp130Fc on autocrine IL-6 signaling, TFK-1 cells were incubated with either 25 µg/mL Tocilizumab, 15 µg/mL sgp130Fc or a combination of both compounds for 24 h, 48 h and 72 h prior to immunoblotting (Figure 16C). Tocilizumab treatment was able to reduce STAT3 tyrosine phosphorylation by 40% after 24 h. In contrast, sgp130Fc treatment revealed the same result after 48 h. The effect was strongest when using a combination of both compounds after 24 h by a reduction of p-STAT3 (Tyr705) of 60% (Figure 16D). Interestingly, neither blocking IL-6 classic signaling nor IL-6 trans-signaling influenced the levels of p-STAT3 (Ser727), total STAT3 and SOCS3.

Due to these findings, which revealed differences in IL-6 class signaling and IL-6 trans-signaling on STAT3 activation in CCA cell lines, further investigations regarding cellular processes were performed. Therefore, cells were seeded and allowed to adhere overnight, followed by 24 h serum starvation and treatment with all four compounds over 72 h prior to subsequent analysis.

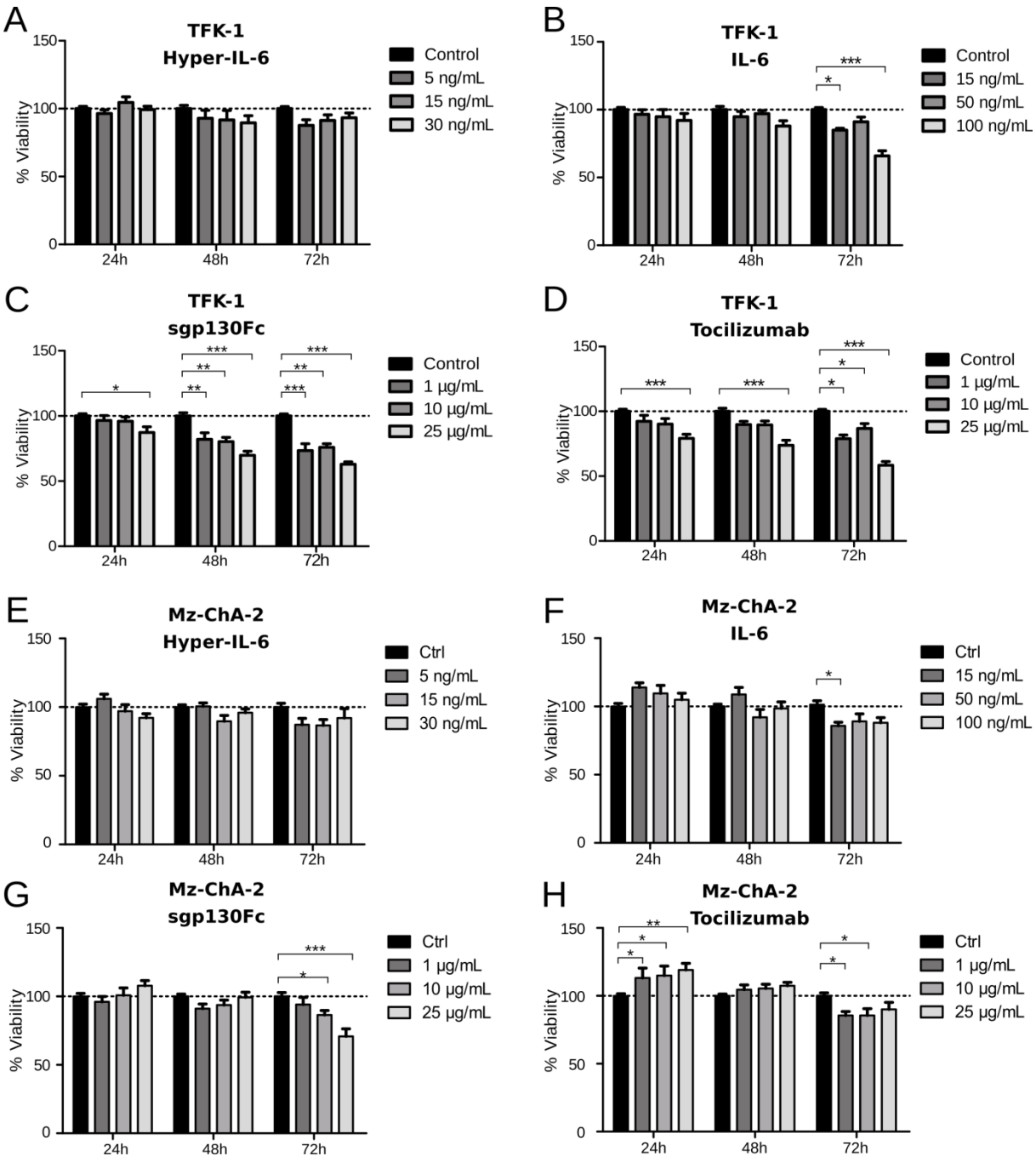

Figure 17: Effects of activation and inhibition of IL-6 classic signaling and IL-6 trans-signaling on cell viability. Cells were seeded for 24 h prior to overnight serum starvation. TFK-1 cells were treated with indicated concentrations of (A) Hyper-IL-6, (B) IL-6, (C) sgp130Fc or (D) Tocilizumab, and cell viability was analyzed using MTT assay after 24 h, 48 h and 72 h treatment. Mz-ChA-2 cells were treated using (E) Hyper-IL-6, (F) IL-6, (G) sgp130Fc or (H) Tocilizumab with indicated concentrations over 24 h, 48 h and 72 h, followed by subsequent MTT assay. Bars represent mean ± SEM. * $p < 0.05$, ** $p < 0.01$, *** $p < 0.001$. Statistical test: one-way ANOVA. Each experiment was performed three independent times. [Published in Kleinegger *et al.*, 2019]

Hyper-IL-6 had no effect on TFK-1 cell viability within 72 h (Figure 17A). Interestingly, after 72 h of incubation with IL-6, a significant decrease in cell viability was observed

using 15 ng/mL and 100 ng/mL (Figure 17B). Blocking IL-6Rα mediated signaling with sgp130Fc (Figure 17C) or Tocilizumab (Figure 17D) significantly reduced TFK-1 cell viability after 24 h, whereas the strongest effect was seen by using 25 µg/mL of the inhibitory compounds after 72 h.

Mz-ChA-2 cell viability was found to be independent of the presence of Hyper-IL-6 (Figure 17E). IL-6, in contrast, significantly reduced cell viability after 72 h (Figure 17F). As in TFK-1 cells, Mz-ChA-2 cell viability was reduced upon 10 µg/mL and 25 µg/mL sgp130Fc after 72 h (Figure 17G). Treatment with Tocilizumab after 72 h led to the same finding (Figure 17H).

After analysis of cell viability, cell apoptosis was investigated upon treatment of all compounds.

Apoptosis was exclusively independent of Tocilizumab in TFK-1 cells (Figure 18D). All other compounds (Hyper-IL-6, IL-6 and sgp130Fc) influenced apoptotic signals in TFK-1 cells (Figure 18A-C). High concentrations of Hyper-IL-6 weakened the apoptotic signals (Figure 18A), whereas low concentrations of IL-6 showed the same effect (Figure 18B). Inhibition of IL-6 trans-signaling by a concentration of 25 µg/mL sgp130Fc was only able to significantly decrease apoptosis by 25% after 24 h (Figure 18C). Inhibition of IL-6 signaling by Tocilizumab did not alter apoptotic signals in TFK-1 cells (Figure 18D).

The analysis of apoptotic signals in Mz-ChA-2 cells revealed that only low concentrations of Hyper-IL-6 were able to reduce apoptotic signals (Figure 18E). IL-6 did not induce any changes in apoptosis of Mz-ChA-2 cells (Figure 18F). Blocking of IL-6 trans-signaling using 1 µg/mL sgp130Fc increased apoptotic signals in Mz-ChA-2 cells by 5% after 48 h (Figure 18G). Inhibition of IL-6Rα signaling by 25 µg/mL Tocilizumab was able to significantly lower the apoptosis by approximately 15% after 24 h (Figure 18H).

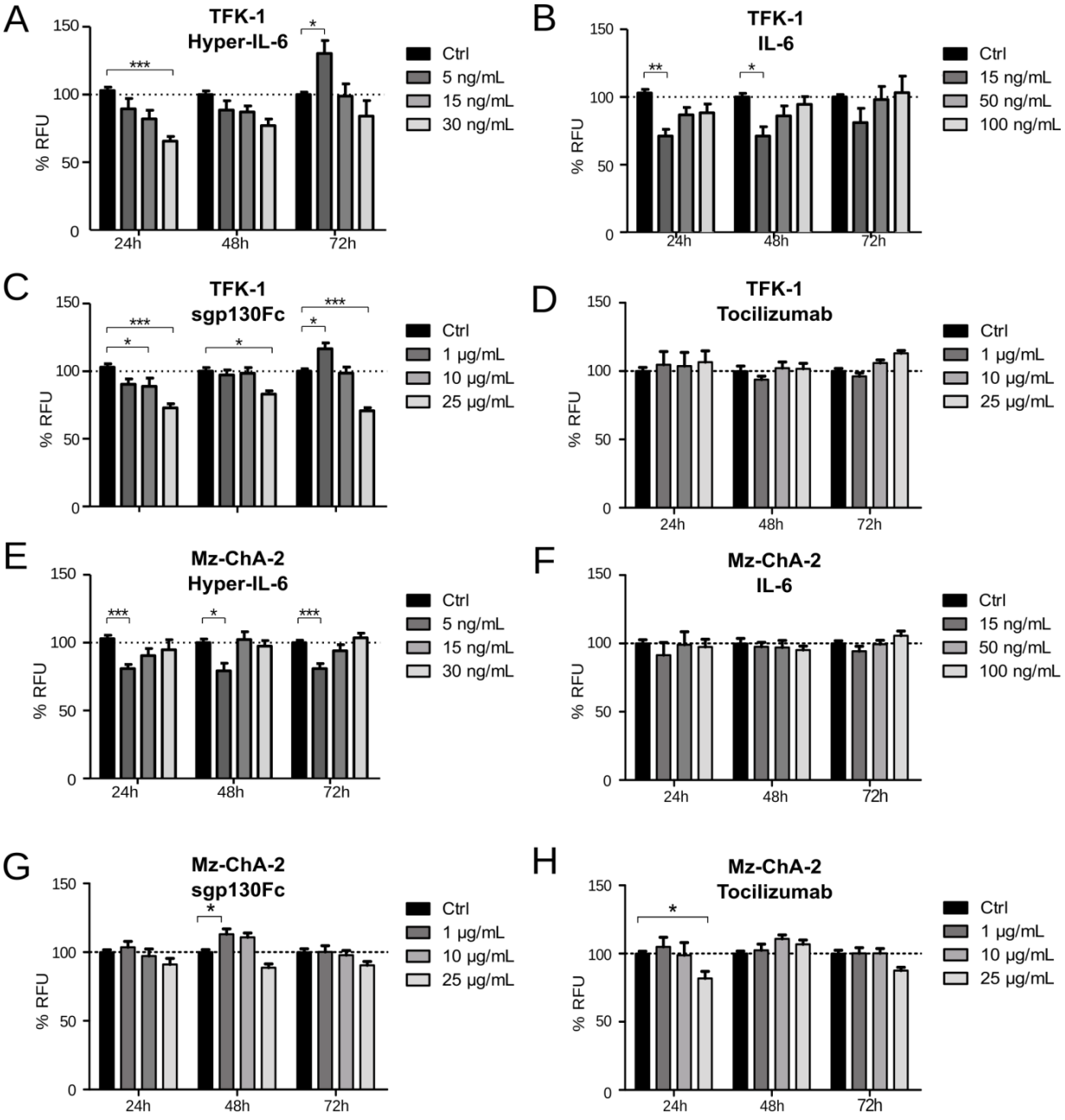

Figure 18: Analysis of apoptotic signals of CCA cell lines upon activation and inhibition of IL-6 classic signaling and IL-6 trans-signaling. Cells were seeded, serum starved and treated for 24 h, 48 h and 72 h with all four compounds. TFK-1 cells were incubated prior to analysis with indicated concentrations of (A) Hyper-IL-6, (B) IL-6, (C) sgp130Fc and (D) Tocilizumab. Mz-ChA-2 cells were treated using (E) Hyper-IL-6, (F) IL-6, (G) sgp130Fc and (H) Tocilizumab for 24 h, 48 h and 72 h with indicated concentrations. Bars represent mean ± SEM. * $p < 0.05$, ** $p < 0.01$, *** $p < 0.001$. Statistical test: one-way ANOVA. Each experiment was performed three independent times. [Published in Kleinegger *et al.*, 2019]

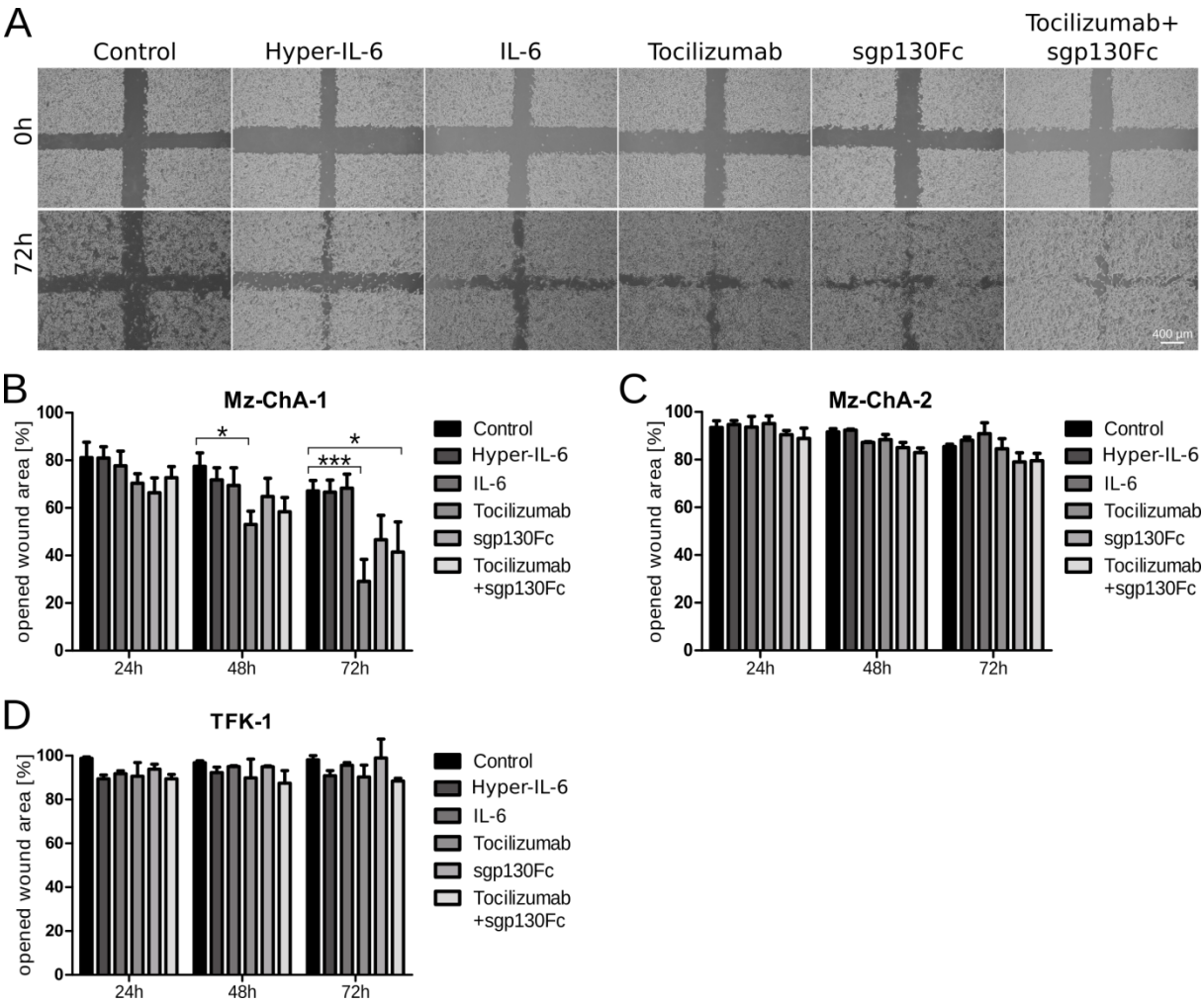

Figure 19: Effects of inhibition and activation of IL-6 classic signaling and IL-6 trans-signaling on CCA cell lines. Cells were grown to 100% confluency, wounded and treated with all four compounds (15 ng/mL Hyper-IL-6, 100 ng/mL IL-6, 25 µg/mL Tocilizumab or 25 µg/mL sgp130Fc). Every 24 h, pictures were taken, and wound closure was observed. (A) Representative images of start (0 h) and end point (72 h) of the migration assay. Calculated percentage of opened wound area of (B) Mz-ChA-1, (C) Mz-ChA-2 and (D) TFK-1 cells. Bar = 400 µm. Bars represent mean ± SEM. * $p < 0.05$, ** $p < 0.01$, *** $p < 0.001$. Statistical test: one-way ANOVA. Each experiment was performed three independent times. [Published in Kleinegger *et al.*, 2019]

To investigate changes in cell motility, cells were grown confluent and wounded under serum-free conditions. Treatment was performed over 72 h, and pictures were taken every 24 h. Mz-ChA-1 cells were chosen due to their phenotype obligatory for this assay. This cell line grows as monolayer and has high motility. As seen in Figure 19A, blocking IL-6Rα signaling increased cell motility, with a stronger effect achieved by sgp130Fc than by Tocilizumab (Figure 19B) after 72 h. Activation of IL-6 classic signaling and IL-6 trans-signaling did not affect cell motility. The tendency was the

same in Mz-ChA-2 (Figure 19C) and TFK-1 (Figure 19D) cells, however, these cell lines show low to near motility as seen by comparing the controls over time.

After analysis of cell motility, real-time cell proliferation was observed upon treatment.

Changes in cell proliferation upon inhibition and activation of IL-6 classic signaling and IL-6 trans-signaling were observed in real-time using xCELLigence technique (Figure 20). Representative growth curves for the activation of IL-6 signaling are shown in Figure 20A. Growth curves influenced by inhibition of IL-6Rα are shown in Figure 20B. Inhibiting IL-6Rα significantly increased the growth curves slope of TFK-1 cells within 72 h (Figure 20C). As a consequence of the increased slope, the PDT of TFK-1 cells was reduced by 10 h (Figure 20D). Interestingly, adverse effects were observed in Mz-ChA-2 cells except for the combination of Tocilizumab and sgp130Fc (Figure 20E-F). Activation of STAT3 by IL-6 or Hyper-IL-6 had no significant influence on proliferation of both cell lines.

In order to investigate whether the observed findings are caused by cell cycle alterations, TFK-1 and Mz-ChA-2 cells were analyzed regarding cell cycle distribution upon treatment (Figure 21A). None of the four compounds had an effect on the G0/G1 phase, neither in Mz-ChA-2 cells (Figure 21B) nor in TFK-1 (Figure 21E). The strongest effect was seen by the inhibitory compounds Tocilizumab and sgp130Fc. These compounds increased S-phase of Mz-ChA-2 (Figure 21C) and TFK-1 (Figure 21F) cells by approximately 15%. Moreover, after normalization, G2/M-phase was significantly decreased by approximately 20% (Figure 21D and Figure 21G). IL-6 and Hyper-IL-6 did not significantly affect cell cycle phases.

In summary, the *in vitro* results achieved by activation and inhibition of both IL-6 signaling forms proved that IL-6 classic signaling and IL-6 trans-signaling differentially influence CCA.

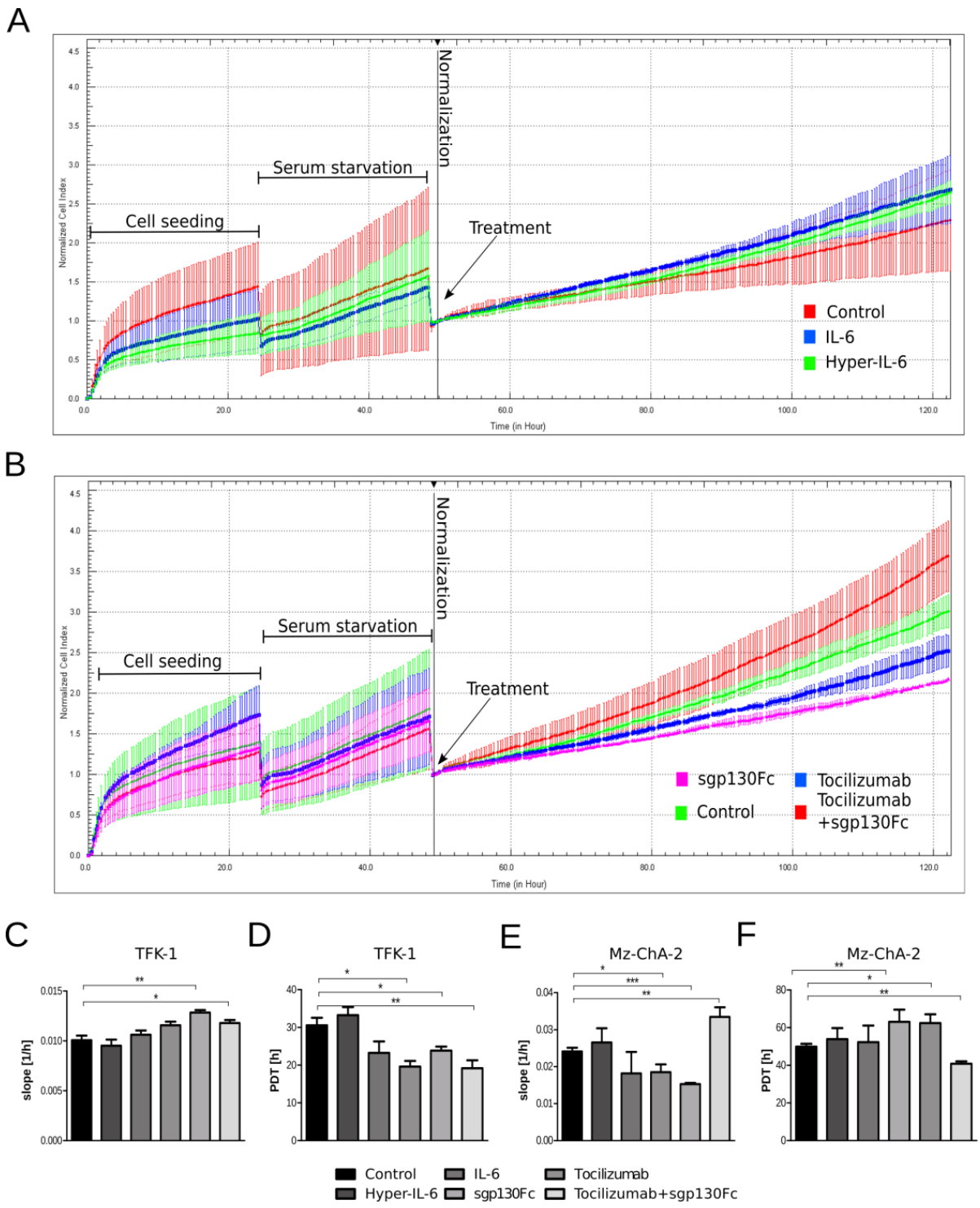

Figure 20: Effects on real-time proliferation of IL-6 classic signaling and IL-6 trans-signaling in CCA cells. Cell lines were seeded, serum-starved for 24 h, treated with all four compounds (15 ng/mL Hyper-IL-6, 100 ng/mL IL-6, 25 µg/mL Tocilizumab or 25 µg/mL sgp130Fc) and real-time proliferation was observed. (A) Representative growth curve of IL-6 and Hyper-IL-6 treated cells. (B) Representative growth curve of sgp130Fc, Tocilizumab and in-combination-treated cells. (C) Calculated slope of TFK-1 cell growth curve. (D) Population doubling time (PDT) of TFK-1 cells upon treatment. (E) Slope of treated Mz-ChA-2 cells. (F) Calculated PDT of treated Mz-ChA-2 cells. Bars represent mean ± SEM. * $p < 0.05$, ** $p < 0.01$, *** $p < 0.001$. Statistical test: one-way ANOVA. Each experiment was performed three independent times. [Published in Kleinegger *et al.,* 2019]

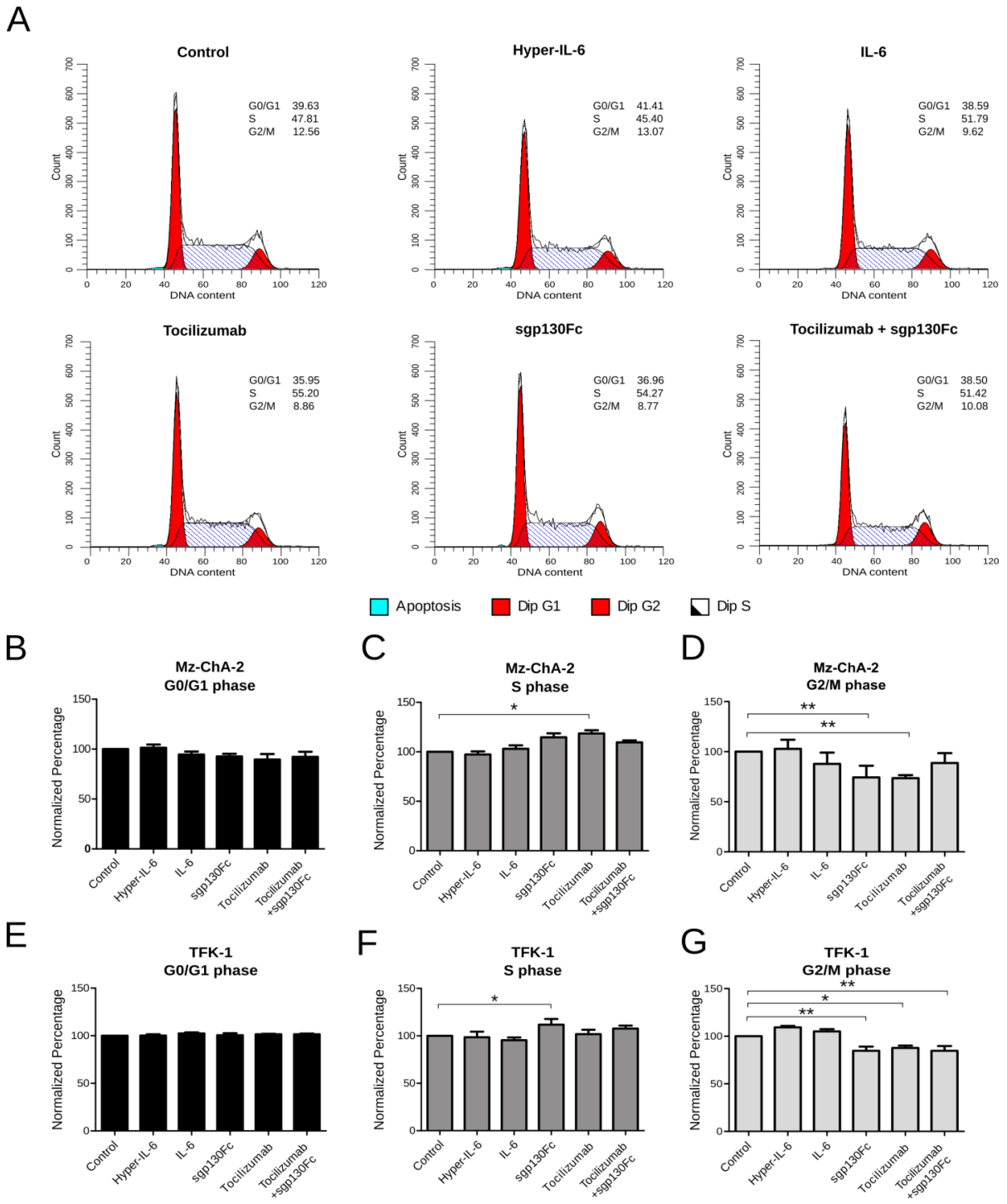

Figure 21: Cell cycle analysis of CCA cell lines upon IL-6, Hyper-IL-6, sgp130Fc and Tocilizumab. Cells were seeded, serum-starved and treated (15 ng/mL Hyper-IL-6, 100 ng/mL IL-6, 25 µg/mL Tocilizumab or 25 µg/mL sgp130Fc) for 72 h prior to cell cycle analysis by flow cytometry. (A) Representative cell cycle measurements validated by ModFit LT. (B) Normalized G0/G1 phase of Mz-ChA-2 cells upon treatment. (C) Normalized S-phase of Mz-ChA-2 cells. (D) Normalized G2/M phase of Mz-ChA-2 cells. (E) G0/G1 phase of TFK-1 cells upon treatment. (F) Normalized S phase of TFK-1 cells. (G) G2/M phase after normalization of TFK-1 cells upon treatment. Bars represent mean ± SEM. * $p < 0.05$, ** $p < 0.01$, *** $p < 0.001$. Statistical test: one-way ANOVA. Each experiment was performed three independent times. [Published in Kleinegger *et al.*, 2019]

5. Discussion

Parts of the discussion resemble the discussion section in Kleinegger *et al.* 2019 (1).

BTCs represent the second most primary liver cancer with a strong link to inflammation. As the disease is poorly understood, a better understanding of the underlying pathological mechanisms is urgently needed. Two main hypotheses were addressed within this study: first, IL-6Rα plays a pivotal role in BTC and second, IL-6 classic signaling and IL-6 trans-signaling have a different impact on cellular processes of BTC cell lines.

5.1 Analysis of IL-6Rα mediated signaling in patient derived GBC tissue

Most patients suffering from BTC are affected by unresectable tumors, which might be a result of late detection. BTC is lacking successful treatment options and reliable biomarkers making this tumor entity highly interesting for basic research. The IL-6/IL-6Rα/gp130/STAT3 axis has been shown to play a pivotal role in BTC. However, only the presence of proteins obligatory for IL-6 signal transduction was correlated with patients´ characteristics, but the implications of functional signaling were not elucidated.

For instance, the expression of IL-6 was proven to correlate with GBC patients' overall survival by analysis of 20 GBC cases and adjacent tissues, suggesting a rather tumor-supportive role of IL-6 in GBC (196). In this study, the data were confirmed by analyses of fresh frozen GBC specimens. Moreover, this study was the first to illustrate the association between IL-6Rα expression and GBC patients´ overall survival. Compared to NNT, GBC showed a downregulation of IL-6Rα on mRNA and protein level, and a correlation between high IL-6Rα expression and better overall survival of GBC patients was found. This finding was corroborated by correlation of *IL-6Rα* gene expression with CCA patients' overall survival. Other studies reported identical findings in ovarian (161) and breast cancer (197). Moreover, Becker *et al*. described a downregulation of mIL-6R in colon cancer compared to adjacent normal mucosa tissue (198), suggesting IL-6Rα as possible therapeutic target. Similar findings were achieved in GBC tissues within this study.

ADAM17 is more active in cancer and associated with shorter overall survival of CCA patients (199). The presence of *ADAM17* mRNA in GBC and the downregulation of

mIL-6R on protein level indicate a potential receptor-shedding mechanism in GBC. Compared to IL-6 classic signaling, IL-6 trans-signaling is ten times more potent. Malignantly transformed cholangiocytes would be able to induce an inflammatory surrounding, leading to wound healing or tissue remodeling. In order to prove this, it would be of great interest to study sIL-6R and gp130 serum concentrations of patients suffering from GBC or BTC in general. The source of the IL-6Rα could further represent an immunotherapeutic target. Taken together, these data highlight that not only IL-6 but also IL-6Rα might be important in different solid tumor types, including BTC, and represent a novel biomarker for biliary tract cancers.

In GBC, increased *STAT3* gene expression was found. On protein level, STAT3 expression was shown to be decreased. However, the ratio of total STAT3 and activated STAT3 was found to be unaltered in GBC compared to NNT. This finding proves the activation of STAT3 in both GBC and NNT. Gene expression of important kinases responsible for STAT3 activation was also found to be unaffected by cholangiocarcinogenesis, underlining the theory that the IL-6Rα is the cause of decreased STAT3 activation. Another reasonable explanation for this finding could be the presence of bile acids. It was shown that hydrophobic bile acids are able to inhibit IL-6 induced STAT3 signaling in rat hepatocytes (200). However, bile acid analysis of patient derived tissues was not part of this study. Xin-wei *et al.* analyzed STAT3 in iCCA and found an increased expression of STAT3 as well as stronger phosphorylated STAT3 in tumorous tissue compared to adjacent liver tissue, which does mainly comprise of hepatocytes not cholangiocytes. However, this study does not even provide any information of the analyzed phosphorylation site of STAT3 (179). Moreover, Dokduang *et al.* found p-STAT3 (Tyr705) in 18% of the analyzed CCA cases, whereas higher STAT3 activation was seen in the inflammatory precancerous lesions (178).

It is noteworthy that analysis of fresh frozen tissue alone can lead to different results compared to FFPE material data obtained by IHC. Frozen tissue analysis resembles the state of protein expression in all cell types within the tumor, including the tumor microenvironment. Cells of the tumor microenvironment are able to influence results by harboring greater effects on the proteins of interest compared to tumor cells. It is not possible to distinguish between tumor cells and other cell types within the tumor by gene expression or immunoblot analysis of whole fresh frozen tissue specimens. To clarify in which cells an observed effect occurs, tumor tissues have to be, for

instance, dissected using laser capture microdissection for mRNA/DNA analysis or IHC should be performed to identify cells of interest due to their specific morphology. A study highlighting this issue was conducted by Andersen *et al.,* who used laser capture microdissection to identify 1 442 differentially expressed genes, including IL-6, between stroma and epithelium of 23 CCA tumor tissues (177). This method would further clarify if there is a difference in the IL-6Rα expression in cells of tumor microenvironment. A loss of IL-6Rα on cells of the tumor microenvironment might lead to possible IL-6 trans-signaling within BTC.

Overall, these findings, which are limited by a low number of available fresh frozen tissue samples on the one hand, but strengthened by a large amount of GBC FFPE material on the other hand, demonstrate the effects of cholangiocarcinogenesis on IL-6Rα.

5.2 Dissecting between IL-6 classic signaling and trans-signaling *in vitro*

5.2.1 Authentication and characterization of CCA cell lines

Over the last decades, cell lines have been considered to be representable *in vitro* tools for certain organs and tissues, and became indispensable for life science research. To maintain their specific biology, cell lines should be tested regarding their origin and function. Moreover, the international cell line authentication committee (http://iclac.org/) lists over 480 misidentified or cross-contaminated cell lines. Therefore, it is obligatory to ensure that the cell line is correct (201). For this purpose, the used CCA cell lines were characterized regarding their STR profiles, CK7 and CK19 expression, and genetic mutations. The revealed STR profiles matched available databases, and the expression of CK7 and CK19 confirmed the biology of CCA. Except for EGI-1, no mutational data of all cell lines were available in databases. Interestingly, all cell lines showed loss of *CDKN2A.* Farshidfar *et al.* reported that *CDKN2A* was deleted, silenced or mutated in 47% of their analyzed human CCA specimens (202). Borger *et al.* revealed *IDH1/2* mutations by mutational analysis of CCA tissue samples (203). They reported differences in the *IDH1/2* mutation status of CCA tissue depending on its anatomical location. Frequent *IDH1/2* mutations were found predominantly in iCCA but not in eCCA (203). In this study, none of the tested cell lines was found to be *IDH1* or *IDH2* mutated. Interestingly, all

tested cell lines originate from extrahepatic biliary tract cancers, which might explain the presence of wild type *IDH1/2* in the tested cell lines.

ERBB2 (*HER2/neu*) expression plays a major role in breast cancer in which ErbB2 targeting antibodies are used as treatment (204). Several studies suggest ErbB2 as new therapeutic approach in BTC (205,206). This study showed the amplification of the *ERBB2* gene in three out of five CCA cell lines. Two of the ERBB2 expressing cell lines have not yet been reported to express ERBB2, which corroborates the theory of a possible implication of HER2/neu therapy in BTC.

Taken together, the characterized cell lines resemble the biology of BTC and are suitable tools for the study of cholangiocarcinoma.

In order to characterize the cell lines used with regard to IL-6 signaling, gene expression of involved proteins was analyzed using qRT-PCR, and whole protein lysates were immunoblotted. Moreover, the presence of the IL-6Rα and its two forms was analyzed. All cell lines expressed IL-6Rα, gp130, JAK1, JAK2 and TYK2. SOCS3, the regulator of STAT3 phosphorylation, was ubiquitously expressed.

Isomoto *et al.* analyzed the CCA cell line Mz-ChA-1 and CC-LP-1 for SOCS3 protein expression and compared the cell lines to an immortalized non-malingnant cholangiocyte cell line H69 (173). This study showed no detectable protein levels of SOCS3 in the malignant cell lines, which was restored by the use of a nucleoside DNA methylation inhibitor. They concluded that SOCS3 is epigenetically silenced in CCA (173). This thesis was able to detect SOCS3 mRNA levels in 5 different CCA cell lines. The cell line Mz-ChA-1 was established from a GBC abdominal wall metastasis and the cell line CC-LP-1 from an primary iCCA (187,207,208). This thesis investigated SOCS3 expression on mRNA and protein level, which was found in all tested cell lines. Different used cell passages or different cultivation conditions might be the reason for this controversies (209,210).

Strong differences in IL-6 expression were found. SK-ChA-1 was the only cell line harboring activated STAT3 in the absence of IL-6. A *JAK3* (C395A) mutation was found exclusively in this cell line. This specific mutation possibly rearranges the SH2 domain of JAK3, causing a potential activation of STAT3 without the presence of IL-6.

Some of the tested cell lines harbor two signals by analyzing p-STAT3 (Ser727). This STAT3 phosphorylation is possible in STAT3α but not STAT3β, which is lacking the TAD domain. One possible explanation might be the other STAT3 isoforms, STAT3γ and STAT3δ. The serine phosphorylation of these isoforms might be detected in the used cell lines.

The presence of the IL-6Rα (CD126) on the cell surface was analyzed by flow cytometry. Interestingly, the percentage of $CD126^+$ cells seems to be quite low, ranging from 0.61% (Mz-ChA-1) to 45.62% (EGI-1). The low positivity might have several reasons. First, the detachment process of adherent cells induces stress signals, which, in turn, can lead to enhanced ADAM17 activation leading to IL-6Rα shedding (211). Second, the IL-6Rα is able to internalize via endocytosis, which makes it undetectable using surface staining (212). A study on HepG2 cells revealed a low percentage of $CD126^+$ by flow cytometry, indicating the challenge of CD126 surface staining on adherent cell lines (213). Another study was not able to detect CD126 on the surface of colon cancer cell lines, although IL-6Rα mRNA expression was proven in the same study (183). However, all methods used for the analysis of IL-6Rα expression showed similar expression patterns amongst the CCA cell lines used, proving the expression and presence of the IL-6Rα in the tested cell lines.

Due to the differences in IL-6 expression and STAT3 activation, two cell lines were chosen for *in vitro* experiments, Mz-ChA-2 and TFK-1. One exception was made due to the phenotype and growth pattern of Mz-ChA-2 and TFK-1 cells. Mz-ChA-1 cells grow as monolayer in single cells, which makes exclusively this cell line suitable for wound healing assays.

5.2.2 *In vitro* studies of IL-6 classic signaling and IL-6 trans-signaling

According to several studies, IL-6 plays a pivotal role in BTC. However, the differences between the two modes of IL-6 signaling and their influence on BTC remained unclear. Activation of IL-6 trans-signaling via Hyper-IL-6 induced a stronger and prolonged STAT3 activation compared to IL-6. Holmer *et al.* described the same effect of strong STAT3 phosphorylation by even lower concentrations of Hyper-IL-6 in the colorectal cancer cell line HT29p (183). Another study investigating primary hippocampal neurons found comparable differences in STAT3 activation upon IL-6 and Hyper-IL-6 (214). The IL-6 induced p-STAT3 (Tyr705) signal decreased over time. It was shown that IL-6 internalizes in rat hepatocytes followed by degradation

(215). Dittrich *et al.* suggests that the internalization of IL-6 might be due to down-regulation of the surface receptor to prevent cells from over-stimulation (216). The question of whether internalization of IL-6 or protein stability causes the attenuation of the p-STAT3 (Tyr705) signals needs to be clarified in future experiments.

Tocilizumab reduced p-STAT3 (Tyr705) signals in TFK-1 cells after 24 h, as shown in other neoplasms like chronic lymphocytic leukemia (217) and non-small lung cancer (218). Total STAT3 deactivation upon Tocilizumab was achieved neither in this study, nor in other studies. This could be due to technical reasons. IL-6 leads to STAT3 activation within 5 minutes in CCA cell lines (data not shown). The time needed for washing and harvesting of treated cell lines prior to immunoblot analysis is sufficient for autocrine secreted IL-6 to induce STAT3. Interestingly, sgp130Fc was able to increase STAT3 activation only after 48 hours of incubation. This leads to the suggestion that TFK-1 cells perform autocrine IL-6 classic signaling to a greater extent than IL-6 trans-signaling *in vivo.*

Activation of IL-6 trans-signaling did not alter the expression of any analyzed signaling related proteins nor did it induce noteworthy alterations in the cellular processes observed. This finding might indicate that in BTC, IL-6 trans-signaling-induced STAT3 activation might play only a minor role. However, p-STAT3 (Ser727) was persistent and not influenced by any IL-6 signaling form in the cell lines tested. This phenomenon might indicate that mitochondrial STAT3, which is triggered by STAT3 serine phosphorylation, could play an important role in BTC. CCA cell viability was found to be reduced upon IL-6Rα blockage. Mitochondrial STAT3 interacts with enzymes of Complex II of the electron transport chain. The same enzymes are the basis for the viability assay used (94,219). However, details of mitochondrial STAT3 in CCA were not further addressed in this study but opens future research opportunities.

Meng *et al.* showed that IL-6 overexpressing Mz-ChA-1 cells resulted in increased cell growth and tumor growth in vivo, leading to the conclusion that IL-6 enhances cell survival (166). The same research group published a theory about a connection between exogenous IL-6 and increased CCA cell proliferation (167). The results demonstrated increased proliferation upon IL-6 treatment. However, decreased cell viability was found under influence of IL-6, without affecting cell cycle and migration

of CCA cells. Moreover, apoptotic signals were decreased by low dosages of IL-6, indicating a tumor-supporting function of IL-6 *in vitro*.

Tocilizumab is an immunosuppressive agent used as treatment for rheumatoid arthritis. It inhibits the interaction between IL-6 and IL-6Rα, independent of whether a membranous or soluble receptor form is present. Over the last decades, Tocilizumab has been proven to be a successful treatment agent for many diseases, including cancer. For instance, in non-small cell lung cancer cells, Tocilizumab induced a sub-G1 cell cycle arrest and reduced cell line viability (218). In chronic lymphocytic leukemia, an increased number of cells in G1 phase was found upon Tocilizumab promoting cell cycle re-entrance of cells (217). In this study, Tocilizumab was proven to affect S and G2/M phases of CCA cell lines, leading to increased cell proliferation. Indeed, the PDT of TFK-1 cells was increased as a consequence of Tocilizumab treatment. This effect was found only for sgp130Fc-treated Mz-ChA-2 cells, indicating that the effect observed in TFK-1 cells might be due to the ability of Tocilizumab to block IL-6 trans-signaling. Tocilizumab decreased constitutive active STAT3 tyrosine phosphorylation in TFK-1 cells by 60% after 72 h. However, the fact that activation of STAT3 was still present may be due to autocrine IL-6 activation loop. Inhibition of IL-6 trans-signaling by sgp130Fc led to a 40% reduction of STAT3 activation only after 48 h. This indicates that IL-6 trans-signaling is minor to IL-6 classic signaling in CCA cells *in vitro.* Tocilizumab has been shown to enhance chemotherapy efficacy in pancreatic ductal adenocarcinoma (220). To date, no study has investigated a connection between IL-6 signaling blockade and chemotherapy resistance in BTC, which could be used as future perspective.

Distinction between the two modes of IL-6 signaling is of growing interest (142). In order to differentiate between IL-6 classic signaling and IL-6 trans-signaling, sgp130Fc was compared with Tocilizumab. Inhibition of IL-6 trans-signaling by sgp130Fc increased migration of Mz-ChA-1 cells and decreased STAT3 activation in TFK-1 cells. Tocilizumab treatment showed similar effects in the observed cellular processes like sgp130Fc. This indicates that the observed effects induced by Tocilizumab might be due to its ability to block the soluble IL-6R.

6. Conclusion

Analysis of 26 fresh frozen tissues and 367 GBC FFPE samples for IL-6 signaling revealed a downregulation of IL-6Rα in GBC and a correlation between high IL-6Rα expression and patients´ overall survival. Therefore, I conclude that IL-6Rα might represent a novel prognostic biomarker for overall survival in BTC. By differentiation between activation/inhibition of IL-6 classic signaling and IL-6 trans-signaling, I concluded that activation of IL-6 classic signaling might be superior to activation of IL-6 trans-signaling. Since similar results were achieved by treating CCA cell lines with Tocilizumab and sgp130Fc, I conclude that blocking IL-6 trans-signaling might be tumor-promoting. A schematic overview of the differences in tumor-promoting activity of both IL-6 signaling forms is shown in Figure 22.

Taken together, these findings suggest that GBC patients or other patients suffering from known precursors of BTC should be excluded from IL-6Rα inhibitor therapy.

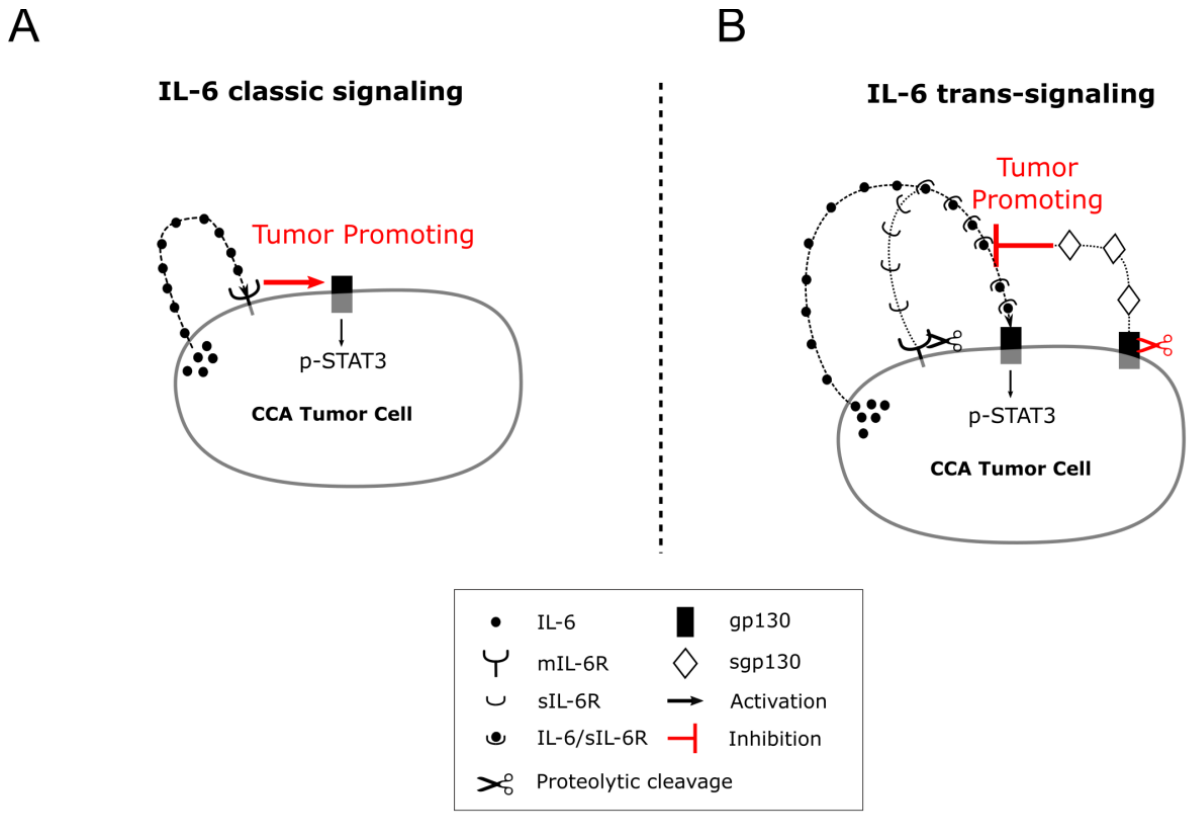

Figure 22: Tumor promoting activity of IL-6 classic signaling and IL-6 trans-signaling in CCA *in vitro*. (A) Activation of IL-6 classic signaling showed tumor promoting activity. (B) Inhibition of IL-6 trans-signaling might be tumor promoting. [Published in Kleinegger *et al.*, 2019]

7. Future perspectives

In view of future studies on IL-6R mediated signaling in BTC, it would be of highest interest to perform gain and loss of function experiments. This study proved the downregulation of IL-6Rα in GBC, and gain and loss of function experiments might clarify whether loss of function promotes tumor cell growth and *vice versa*. Moreover, the question arises whether blockage of IL-6 signaling influences the chemotherapy resistance of tumor cells. Future research could aim at the mechanisms lying behind IL-6Rα downregulation. Therefore, analyses of promoter regions should be performed.

JAKs are able to interact with other signaling cascades like, the RAS/RAF/MEK/ERK pathway. Therefore, it would be interesting to see if activation IL-6 trans-signaling influences for instance ERK1/2.

Nowadays, 3D cell culture is used as tool to mimic *in vivo* situations better than 2D culturing systems. I recommend a comparison between IL-6Rα expression of 2D cultured cells and tumor spheroids. Moreover, co-cultivation of malignant cholangiocytes and stromal cells could give insights into tumor-stroma interactions and their influence on IL-6Rα expression and STAT3 signaling *in vitro*.

One limitation of this study is that patient samples of only one BTC subtype were tested. I highly recommend analysis of iCCA and eCCA samples. This would clarify the question of whether the results obtained by tissue analysis are GBC specific or applicable to BTC in general.

Finally, I recommend analysis of circulating sgp130 and sIL-6R serum levels of BTC patients during therapy and disease progression to investigate their possible function as predictive and prognostic biomarker.

8. References

1. Kleinegger F, Hofer E, Wodlej C, Golob-Schwarzl N, Birkl-Toeglhofer AM, Stallinger A, et al. Pharmacologic IL-6Rα inhibition in cholangiocarcinoma promotes cancer cell growth and survival. Biochim Biophys Acta - Mol Basis Dis. 2019;1865(2):308–21.
2. Lefkowitch JH. Anatomy and Function. In: Dooley JS, Lok ASF, Burroughs AK, Heathcote EJ, editors. Sherlock's Diseases of the Liver and Biliary System, 12th Edition. Oxford, UK: Wiley-Blackwell; 2011. p. 1–19.
3. Masyuk AI, Masyuk T V, LaRusso NF. Physiology of Cholngiocytes. In: Physiology of the Gastrointestinal Tract. Sixth Edit. Elsevier; 2018. p. 1003–23.
4. Kanel GC. Liver: anatomy, microscopic structure, and cell typesle. In: Podolsky DK, Camilleri M, Fitz JG, Kalloo AN, Shanahan F, Wang TC, editors. Yamada' s Textbook of Gastroenterology. John Wiley & Sons, Ltd; 2015. p. 145–60.
5. Welling TH. Gallbladder and biliary tract: anatomy and structural anomalies. In: Podolsky DK, Camilleri M, Fitz JG, Kalloo AN, Shanahan F, Wang TC, editors. Yamada' s Textbook of Gastroenterology. Sixth Edit. Oxford, UK: John Wiley & Sons, Ltd; 2015. p. 133–44.
6. Behar J. Physiology and Pathophysiology of the Biliary Tract: The Gallbladder and Sphincter of Oddi—A Review. ISRN Physiol. 2013;2013:1–15.
7. Crawford JM. Gallbladder , Extrahepatic Biliary Tract , and Pancreas Tissue Processing Techniques , and Normal Histology. In: Odze RD, Goldblum JR, editors. Surgical Pathology of the GI Tract, Liver, Biliary Tract, and Pancreas. Second Edi. Elsevier Inc.; 2009. p. 765–81.
8. Shaffer EA. Review article : control of gall-bladder motor function. Aliment Pharmacol Ther. 2000;14:2–8.
9. Lazaridis KN, Larusso NF, Huch M, Gehart H, van Boxtel R, Hamer K, et al. Biliary differentiation and bile duct morphogenesis in development and disease. Int J Biochem Cell Biol. 2015;43(2):245–56.
10. Maroni L, Haibo B, Ray D, Zhou T, Wan Y, Meng F, et al. Functional and Structural Features of Cholangiocytes in Health and Disease. C Cell Mol Gastroenterol Hepatol. 2015;1(4):368–80.
11. Glaser S, Francis H, DeMorrow S, LeSage G, Fava G, Marzioni M, et al. Heterogeneity of the intrahepatic biliary epithelium. World Journal of Gastroenterology. 2006. p. 3523–36.
12. Schaffner F, Popper H. Electron microscopic studies of normal and proliferated bile ductules. Am J Pathol. 1961;38(4):393–410.
13. Masyuk AI, Masyuk T V., LaRusso NF. Cholangiocyte primary cilia in liver health and disease. Developmental Dynamics. 2008. p. 2007–12.
14. Glaser S, Wang M, Ueno Y, Venter J, Wang K, Chen H, et al. Differential transcriptional characteristics of small and large biliary epithelial cells derived from small and large bile ducts. Am J Physiol Gastrointest Liver Physiol. 2010;299(3):G769–77.

15. Fukushima K, Ueno Y. Bioinformatic approach for understanding the heterogeneity of cholangiocytes. World J Gastroenterol. 2006;12(22):3481–6.

16. Razumilava N, Gores GJ. Cholangiocarcinoma. Lancet. 2014;383(9935):2168–79.

17. DeOliveira ML, Cunningham SC, Cameron JL, Kamangar F, Winter JM, Lillemoe KD, et al. Cholangiocarcinoma. Ann Surg. 2007 May;245(5):755–62.

18. Shin HR, Oh JK, Masuyer E, Curado MP, Bouvard V, Fang YY, et al. Epidemiology of cholangiocarcinoma: An update focusing on risk factors. Cancer Science. 2010. p. 579–85.

19. Marcano-Bonilla L, Mohamed EA, Mounajjed T, Roberts LR. Biliary tract cancers: epidemiology, molecular pathogenesis and genetic risk associations. Chinese Clin Oncol. 2016;5(5):61–61.

20. Siegel RL, Miller KD, Jemal A. Cancer statistics, 2018. CA Cancer J Clin. 2018;68(1):7–30.

21. Valle JW, Borbath I, Khan SA, Huguet F, Gruenberger T, Arnold D. Biliary cancer: ESMO Clinical Practice Guidelines for diagnosis, treatment and follow-up†. Ann Oncol. 2016 Sep;27(suppl_5):v28–37.

22. Bridgewater J, Galle PR, Khan SA, Llovet JM, Park J, Patel T, et al. Guidelines Guidelines for the diagnosis and management of intrahepatic cholangiocarcinoma. J Hepatol. 2014;60(6):1268–89.

23. de Groen PC, Gores GJ, LaRusso NF, Gunderson LL, Nagorney DM. Biliary tract cancers. N Engl J Med. UNITED STATES; 1999 Oct;341(18):1368–78.

24. Hamilton SR, Aaltonen L a, Kleihues P, Cavenee WK. World health organization. Classification of tumours. Pathology and genetics of tumours of the digestive system. Parallel Distrib Process 2008 IPDPS 2008 IEEE Int Symp. 2000;1–8.

25. Nakanuma Y, Sato Y, Harada K, Sasaki M, Xu J, Ikeda H. Pathological classification of intrahepatic cholangiocarcinoma based on a new concept. World J Hepatol. 2010;2(12):419–27.

26. Cancer AJC on. AJCC Cancer Staging Manual. AJCC Cancer Staging Manual. 2017. 873-901 p.

27. Mosadeghi S, Liu B, Bhuket T, Wong RJ. Sex-specific and race/ethnicity-specific disparities in cholangiocarcinoma incidence and prevalence in the USA: An updated analysis of the 2000–2011 Surveillance, Epidemiology and End Results registry. Hepatol Res. 2016;46(7):669–77.

28. Sithithaworn P, Yongvanit P, Duenngai K, Kiatsopit N, Pairojkul C. Roles of liver fluke infection as risk factor for cholangiocarcinoma. J Hepatobiliary Pancreat Sci. 2014;21(5):301–8.

29. Murata M. Inflammation and cancer. Environ Health Prev Med. 2018 Dec 20;23(1):50.

30. Banales JM, Cardinale V, Carpino G, Marzioni M, Andersen JB, Invernizzi P, et al. Expert consensus document: Cholangiocarcinoma: current knowledge and future perspectives consensus statement from the European Network for the Study of Cholangiocarcinoma (ENS-CCA). Nature Reviews Gastroenterology and Hepatology. 2016. p. 261–80.

31. Wardell CP, Fujita M, Yamada T, Simbolo M, Fassan M, Karlic R, et al. Genomic characterization of biliary tract cancers identifies driver genes and predisposing mutations. J Hepatol. 2018;68(5):959–69.

32. Tyson GL, El-Serag HB. Risk factors for cholangiocarcinoma. Hepatology. 2011;54(1):173–84.

33. Hsing AW, Sakoda LC, Rashid A, Chen J, Shen MC, Han TQ, et al. Body size and the risk of biliary tract cancer: A population-based study in China. Br J Cancer. 2008;99(5):811–5.

34. Shebl FM, Andreotti G, Rashid A, Gao Y-T, Yu K, Shen M-C, et al. Diabetes in relation to biliary tract cancer and stones: a population-based study in Shanghai, China. Br J Cancer. 2010;103(1):115–9.

35. American Cancer Society. Survival Rates for Bile Duct Cancer [Internet]. 2018 [cited 2018 Aug 9]. Available from: https://www.cancer.org/cancer/bile-duct-cancer/detection-diagnosis-staging/survival-by-stage.html

36. Noone A, Howlader N, Krapcho M, Miller D, Brest A, Yu M, et al. SEER Cancer Statistics Review [Internet]. National Cancer Institute; [cited 2018 Aug 9]. Available from: https://seer.cancer.gov/csr/1975_2015/

37. Kanthan R, Senger J-L, Ahmed S, Kanthan SC. Gallbladder Cancer in the 21st Century. J Oncol. 2015;2015:1–26.

38. Miller G, Jarnagin WR. Gallbladder carcinoma. European Journal of Surgical Oncology. 2008. p. 306–12.

39. Randi G, Franceschi S, La Vecchia C. Gallbladder cancer worldwide: Geographical distribution and risk factors. International Journal of Cancer. 2006. p. 1591–602.

40. Bridgewater JA, Goodman KA, Kalyan A, Mulcahy MF. Biliary Tract Cancer: Epidemiology, Radiotherapy, and Molecular Profiling. Am Soc Clin Oncol Educ B. 2016;36:e194–203.

41. American Cancer Society. Survival Rates for Gallbladder Cancer. [Internet]. 2018 [cited 2018 Aug 10]. Available from: https://www.cancer.org/cancer/gallbladder-cancer/detection-diagnosis-staging/survival-rates.html

42. Barreto SG, Dutt A, Chaudhary A. A genetic model for gallbladder carcinogenesis and its dissemination. Annals of Oncology. 2014. p. 1086–97.

43. Patel T. Cholangiocarcinoma-controversies and challenges. Nature Reviews Gastroenterology and Hepatology. 2011. p. 189–200.

44. Horgan AM, Amir E, Walter T, Knox JJ. Adjuvant therapy in the treatment of biliary tract cancer: a systematic review and meta-analysis. J Cinical Oncol. 2012;30(16):1934–40.

45. Holliman JH. Principles of Inflammation. In: Pathology. New York: Oklahoma Notes; 1992.

46. Ahmed AU. An overview of inflammation: Mechanism and consequences. Frontiers of Biology in China. 2011. p. 274–81.

47. Coussens LM, Werb Z. Inflammation and cancer. Nature. 2002. p. 860–7.

48. Crusz SM, Balkwill FR. Inflammation and cancer: advances and new agents. Nat Rev Clin Oncol. 2015;12(10):584–96.

49. Balkwill F, Mantovani A. Inflammation and cancer: Back to Virchow? Lancet. 2001. p. 539–45.

50. David H. Rudolf Virchow and Modern Aspects of Tumor Pathology. Pathol Res Pract. 1988;183(3):356–64.

51. Hanahan D, Weinberg RA. Hallmarks of cancer: The next generation. Cell. 2011. p. 646–74.

52. Mantovani A, Allavena P, Sica A, Balkwill F. Cancer-related inflammation. Nature. 2008. p. 436–44.

53. Hussain SP, Harris CC. Inflammation and cancer: An ancient link with novel potentials. International Journal of Cancer. 2007. p. 2373–80.

54. Jaiswal M, LaRusso NF, Burgart LJ, Gores GJ. Inflammatory cytokines induce DNA damage and inhibit DNA repair in cholangiocarcinoma cells by a nitric oxide-dependent mechanism. Cancer Res. 2000;60(1):184–90.

55. Tamir S, Burney S, Tannenbaum SR. DNA Damage by Nitric Oxide. Chem Res Toxicol. 1996 Jan;9(5):821–7.

56. Jaiswal M, LaRusso NF, Shapiro RA, Billiar TR, Gores GJ. Nitric oxide-mediated inhibition of DNA repair potentiates oxidative DNA damage in cholangiocytes. Gastroenterology. 2001;120(1):190–9.

57. Cheng KC, Cahill DS, Kasai H, Nishimura S, Loeb LA. 8-Hydroxyguanine, an abundant form of oxidative DNA damage, causes G → T and A → C substitutions. J Biol Chem. 1992;267(1):166–72.

58. Sirica AE, Dumur CI, Campbell DJW, Almenara JA, Ogunwobi OO, Dewitt JL. Intrahepatic Cholangiocarcinoma Progression: Prognostic Factors and Basic Mechanisms. Clin Gastroenterol Hepatol. 2009 Nov;7(11):S68–78.

59. Leyva-Illades D, McMillin M, Quinn M, Demorrow S. Cholangiocarcinoma pathogenesis: Role of the tumor microenvironment. Transl Gastrointest Cancer. 2012;1(1):71–80.

60. Räsänen K, Vaheri A. Activation of fibroblasts in cancer stroma. Experimental Cell Research. 2010. p. 2713–22.

61. Zhang X fang, Dong M, Pan Y hang, Chen J ning, Huang X qi, Jin Y, et al. Expression pattern of cancer-associated fibroblast and its clinical relevance in intrahepatic cholangiocarcinoma. Hum Pathol. 2017;65:92–100.

62. Fridlender ZG, Sun J, Kim S, Kapoor V, Cheng G, Ling L, et al. Polarization of Tumor-Associated Neutrophil Phenotype by TGF-β: “N1” versus “N2” TAN. Cancer Cell. 2009;16(3):183–94.

63. Bin-Zhi Qian1, Jeffrey W. Pollard. Macrophage Diversity Enhances Tumor Progression and Metastasis. Cell. 2010;141:39–51.

64. Mantovani A, Sica A. Macrophages, innate immunity and cancer: balance, tolerance, and diversity. Current Opinion in Immunology. 2010. p. 231–7.

65. Kitano Y, Okabe H, Yamashita Y, Nakagawa S, Saito Y, Umezaki N, et al. Tumour-infiltrating inflammatory and immune cells in patients with extrahepatic cholangiocarcinoma. Br J Cancer. 2018 Jan 9;118(2):171–80.

66. Zhang Y, Ma C, Wang M, Hou H, Cui L, Jiang C, et al. Prognostic significance of immune cells in the tumor microenvironment and peripheral blood of gallbladder carcinoma patients. Clin Transl Oncol. 2017 Apr 7;19(4):477–88.

67. Techasen A, Loilome W, Namwat N, Dokduang H, Jongthawin J, Yongvanit P. Cytokines released from activated human macrophages induce epithelial mesenchymal transition markers of cholangiocarcinoma cells. Asian Pac J Cancer Prev. 2012;13 Suppl:115–8.

68. Goeppert B, Frauenschuh L, Zucknick M, Stenzinger A, Andrulis M, Klauschen F, et al. Prognostic impact of tumour-infiltrating immune cells on biliary tract cancer. Br J Cancer. 2013;109(10):2665–74.

69. Rabinovich GA, Gabrilovich D, Sotomayor EM. Immunosuppressive Strategies that are Mediated by Tumor Cells. Annu Rev Immunol. 2007 Apr;25(1):267–96.

70. Kumari N, Dwarakanath BS, Das A, Bhatt AN. Role of interleukin-6 in cancer progression and therapeutic resistance. Tumor Biology. 2016. p. 11553–72.

71. Rawlings JS, Rosler KM, Harrison DA. The JAK/STAT signaling pathway. J Cell Sci. 2004;117(8):1281–3.

72. Schindler C, Plumlee C. Inteferons pen the JAK-STAT pathway. Seminars in Cell and Developmental Biology. 2008. p. 311–8.

73. Schindler C, Levy DE, Decker T. JAK-STAT Signaling: From Interferons to Cytokines. J Biol Chem. 2007;282(28):20059–63.

74. Wilks AF, Harpur AG, Kurban RR, Ralph SJ, Zürcher G, Ziemiecki A. Two novel protein-tyrosine kinases, each with a second phosphotransferase-related catalytic domain, define a new class of protein kinase. Mol Cell Biol. 1991;11(4):2057–65.

75. Haan C, Is’Harc H, Hermanns HM, Schmitz-Van de Leur H, Kerr IM, Heinrich PC, et al. Mapping of a Region within the N Terminus of Jak1 Involved in Cytokine Receptor Interaction. J Biol Chem. 2001;276(40):37451–8.

76. Fagerlund R, Mélen K, Kinnunen L, Julkunen I. Arginine/lysine-rich nuclear localization signals mediate interactions between dimeric STATs and importin alpha 5. J Biol Chem. 2002;277(33):30072–8.

77. Johnson DE, O’Keefe RA, Grandis JR. Targeting the IL-6/JAK/STAT3 signalling axis in cancer. Nature Reviews Clinical Oncology. 2018. p. 234–48.

78. Brooks AJ, Dai W, O'Mara ML, Abankwa D, Chhabra Y, Pelekanos RA, et al. Mechanism of activation of protein kinase JAK2 by the growth hormone receptor. Science (80-). 2014;344(6185).

79. Levy DE, Lee C. What does Stat3 do? J Clin Invest. 2002 May;109(9):1143–8.

80. Croker BA, Kiu H, Nicholson SE. SOCS regulation of the JAK/STAT signalling pathway. Seminars in Cell and Developmental Biology. 2008. p. 414–22.

81. Carow B, Rottenberg ME. SOCS3, a major regulator of infection and inflammation. Frontiers in Immunology. 2014.

82. Heinrich PC, Behrmann I, Haan S, Hermanns HM, Müller-Newen G, Scharper F. Principles of interleukin (IL)-6-type cytokine signalling and its regulation. Biochem J. 2003;374(1):1–20.

83. Somers W, Stahl M, Seehra JS. 1.9A crystal structure of interleukin 6: Implications for a novel mode of receptor dimerization and signaling. EMBO J. 1997;16(5):989–97.

84. Jostock T, Müllberg J, Özbek S, Atreya R, Blinn G, Voltz N, et al. Soluble gp130 is the natural inhibitor of soluble interleukin-6 receptor transsignaling responses. Eur J Biochem. 2001;268(1):160–7.

85. Rose AS, Hildebrand PW. NGL Viewer: A web application for molecular visualization. Nucleic Acids Res. 2015;

86. Xu GY, Yu HA, Hong J, Stahl M, McDonagh T, Kay LE, et al. Solution structure of recombinant human interleukin-6. J Mol Biol. 1997;268(2):468–81.

87. Taga T, Kishimoto T. Gp130 and the interleukin-6 family of cytokines. Annu Rev Immunol. 1997;15:797–819.

88. Boulanger MJ, Chow D, Brevnova EE, Garcia KC. Hexameric structure and assembly of the interleukin-6/IL-6 alpha-receptor/gp130 complex. Science. 2003;300(5628):2101–4.

89. Mihara M, Hashizume M, Yoshida H, Suzuki M, Shiina M. IL-6/IL-6 receptor system and its role in physiological and pathological conditions. Clin Sci (Lond). 2012;122(4):143–59.

90. Stahl N, Boulton TG, Farruggella T, Ip NY, Davis S, Witthuhn BA, et al. Association and activation of Jak-Tyk kinases by CNTF-LIF-OSM-IL-6 β receptor components. Science (80-). 1994;263(5143):92–5.

91. Guschin D, Rogers N, Briscoe J, Witthuhn B, Watling D, Horn F, et al. A major role for the protein tyrosine kinase JAK1 in the JAK/STAT signal transduction pathway in response to interleukin-6. EMBO J. 1995;14(7):1421–9.

92. Decker T, Kovarik P. Serine phosphorylation of STATs. Oncogene. 2000. p. 2628–37.

93. Sgrignani J, Garofalo M, Matkovic M, Merulla J, Catapano C V., Cavalli A. Structural biology of STAT3 and its implications for anticancer therapies development. International Journal of Molecular Sciences. 2018.

94. Yang R, Rincon M. Mitochondrial Stat3, the need for design thinking. International Journal of Biological Sciences. 2016. p. 532–44.

95. Wegrzyn J, Potla R, Chwae YJ, Sepuri NBV, Zhang Q, Koeck T, et al. Function of mitochondrial Stat3 in cellular respiration. Science (80-). 2009;323(5915):793–7.

96. Shi W, Akira S, Takeda K, Noguchi K, Matsumoto M, Kishimoto T, et al. Targeted disruption of the mouse Stat3 gene leads to early embryonic lethality. Proc Natl Acad Sci. 2002;94(8):3801–4.

97. Chen X, Zhang H, Mcleish KR, Dascani P, Ding C, Yan J, et al. STAT3 Signaling in B Cells Is Critical for Germinal Center Maintenance and Contributes to the Pathogenesis of Murine Models of Lupus. J Immunol. 2016;196(11):4477–86.

98. Chou WC, Levy DE, Lee CK. STAT3 positively regulates an early step in B-cell development. Blood. 2006;108(9):3005–11.

99. Niwa H, Burdon T, Chambers I, Smith A. Self-renewal of pluripotent embryonic stem cells is mediated via activation of STAT3. Genes Dev. 1998;12(13):2048–60.

100. Cannizzaro LA, Levy DE, Raz R, Lee C-K, d'Eustachio P. Essential role of STAT3 for embryonic stem cell pluripotency. Proc Natl Acad Sci. 2002;96(6):2846–51.

101. Alonzi T, Maritano D, Gorgoni B, Rizzuto G, Libert C, Poli V. Essential Role of STAT3 in the Control of the Acute-Phase Response as Revealed by Inducible Gene Activation in the Liver. Mol Cell Biol. 2001 Mar 1;21(5):1621–32.

102. Alvarez J V., Frank DA. Genome-wide analysis of STAT target genes: Elucidating the mechanism of STAT-mediated oncogenesis. Cancer Biology and Therapy. 2004. p. 1045–50.

103. Carpenter RL, Lo HW. STAT3 target genes relevant to human cancers. Cancers. 2014. p. 897–925.

104. Jung JE, Chung DH, Choi S, Park J-W, Yoon S-H, Lee HG, et al. STAT3 is a potential modulator of HIF-1-mediated VEGF expression in human renal carcinoma cells. FASEB J. 2005;19(10):1296–8.

105. Shaulian E. AP-1 - The Jun proteins: Oncogenes or tumor suppressors in disguise? Cellular Signalling. 2010. p. 894–9.

106. Choi HJ, Han JS. Overexpression of phospholipase D enhances Bcl-2 expression by activating STAT3 through independent activation of ERK and p38MAPK in HeLa cells. Biochim Biophys Acta - Mol Cell Res. 2012;1823(6):1082–91.

107. Lo H-W, Cao X, Zhu H, Ali-Osman F. Cyclooxygenase-2 is a novel transcriptional target of the nuclear EGFR-STAT3 and EGFRvIII-STAT3 signaling axes. Mol Cancer Res. 2010 Feb;8(2):232–45.

108. Bellido T, O'Brien CA, Roberson PK, Manolagas SC. Transcriptional activation of the p21(WAF1,CIP1,SDI1) gene by interleukin-6 type cytokines: A prerequisite for their pro-differentiating and anti-apoptotic effects on human osteoblastic cells. J Biol Chem. 1998;273(33):21137–44.

109. Oh HM, Yu CR, Dambuza I, Marrero B, Egwuagu CE. STAT3 protein interacts with class O forkhead transcription factors in the cytoplasm and regulates nuclear/cytoplasmic localization of FoxO1 and FoxO3a proteins in CD4+ T cells. J Biol Chem. 2012;287(36):30436–43.

110. Garcia R, Bowman TL, Niu G, Yu H, Minton S, Muro-Cacho CA, et al. Constitutive activation of Stat3 by the Src and JAK tyrosine kinases participates in growth regulation of human breast carcinoma cells. Oncogene. 2001;20(20):2499–513.

111. Song L, Turkson J, Karras JG, Jove R, Haura EB. Activation of Stat3 by receptor tyrosine kinases and cytokines regulates survival in human non-small cell carcinoma cells. Oncogene. 2003;22(27):4150–65.

112. Mora LB, Buettner R, Seigne J, Diaz J, Ahmad N, Garcia R, et al. Constitutive activation of Stat3 in human prostate tumors and cell lines: Direct inhibition of Stat3 signaling induces apoptosis of prostate cancer cells. Cancer Res. 2002;62(22):6659–66.

113. Aigner P, Just V, Stoiber D. STAT3 isoforms: Alternative fates in cancer? Cytokine. 2018;

114. Caldenhoven E, Van Dijk TB, Solari R, Armstrong J, Raaijmakers JAM, Lammers JWJ, et al. STAT3β, a splice variant of transcription factor STAT3, is a dominant negative regulator of transcription. J Biol Chem. 1996;271(22):13221–7.

115. Maritano D, Sugrue ML, Tininini S, Dewilde S, Strobl B, Fu X, et al. The STAT3 isoforms α and β have unique and specific functions. Nat Immunol. 2004 Apr 14;5(4):401–9.

116. Hendry L, John S. Regulation of STAT signalling by proteolytic processing. European Journal of Biochemistry. 2004. p. 4613–20.

117. Hevehan DL, Miller WM, Papoutsakis ET. Differential expression and phosphorylation of distinct STAT3 proteins during granulocytic differentiation. Blood. 2002;99(5):1627–37.

118. Babon JJ, Varghese LN, Nicola NA. Inhibition of IL-6 family cytokines by SOCS3. Semin Immunol. 2014 Feb;26(1):13–9.

119. Sasaki A, Yasukawa H, Suzuki A, Kamizono S, Syoda T, Kinjyo I, et al. Cytokine-inducible SH2 protein-3 (CIS3/SOCS3) inhibits Janus tyrosine kinase by binding through the N-terminal kinase inhibitory region as well as SH2 domain. Genes to Cells. 1999;4(6):339–51.

120. Heinrich PC, Behrmann I, Müller-Newen G, Scharper F, Graeve L. Interleukin-6-type cytokine signalling through the gp130/Jak/STAT pathway. Biochem J. 1998;334(2):297–314.

121. Rose-John S, Scheller J, Elson G, Jones S a. Interleukin-6 biology is coordinated by membrane-bound and soluble receptors: role in inflammation and cancer. J Leukoc Biol. 2006;80(2):227–36.

122. Hibi M, Murakami M, Saito M, Hirano T, Taga T, Kishimoto T. Molecular cloning and expression of an IL-6 signal transducer, gp130. Cell. 1990;63(6):1149–57.

123. Rose-John S. Il-6 trans-signaling via the soluble IL-6 receptor: Importance for the proinflammatory activities of IL-6. International Journal of Biological Sciences. 2012. p. 1237–47.

124. Novick D, Engelmann H, Wallach D, Rubinstein M. Soluble cytokine receptors are present in normal human urine. J Exp Med. 1989;170(October):1409–14.

125. Novick D, Engelmann H, Wallach D, Leitner O, Revel M, Rubinstein M. Purification of soluble cytokine receptors from normal human urine by ligand-affinity and immunoaffinity chromatography. J Chromatogr A. 1990;510(C).

126. Rose-John S, Heinrich PC. Soluble receptors for cytokines and growth factors: generation and biological function. Biochem J. 1994;300(Pt 2):281–90.

127. Levine SJ. Molecular mechanisms of soluble cytokine receptor generation. Journal of Biological Chemistry. 2008. p. 14177–81.

128. Mülberg J, Schooltink H, Stoyan T, Günther M, Graeve L, Buse G, et al. The soluble interleukin-6 receptor is generated by shedding. Eur J Immunol. 1993;23(2):473–80.

129. Matthews V, Schuster B, Schütze S, Bussmeyer I, Ludwig A, Hundhausen C, et al. Cellular cholesterol depletion triggers shedding of the human interleukin-6 receptor by ADAM10 and ADAM17 (TACE). J Biol Chem. 2003;278(40):38829–39.

130. Csilla Holub M, Szalai C, Polgár A, Tóth S, Falus A. Generation of “truncated” interleukin-6 receptor (IL-6R) mRNA by alternative splicing; a possible source of soluble IL-6R. In: Immunology Letters. 1999. p. 121–4.

131. Wolf J, Waetzig GH, Reinheimer TM, Scheller J, Rose-John S, Garbers C. A soluble form of the interleukin-6 family signal transducer gp130 is dimerized via a C-terminal disulfide bridge resulting from alternative mRNA splicing. Biochem Biophys Res Commun. 2016;470(4):870–6.

132. Mullberg J, Oberthur W, Lottspeich F, Mehl E, Dittrich E, Graeve L, et al. The soluble human IL-6 receptor. Mutational characterization of the proteolytic cleavage site. J Immunol. 1994;152(10):4958–68.

133. Scheller J, Chalaris A, Garbers C, Rose-John S. ADAM17: A molecular switch to control inflammation and tissue regeneration. Trends in Immunology. 2011. p. 380–7.

134. Dimitrov S, Jones SA, Benedict C, Rose-John S, Born J, Nowell MA, et al. Sleep enhances IL-6 trans-signaling in humans. FASEB J. 2006;20(12):2174–6.

135. Walev I, Vollmer P, Vollmer P, Palmer M, Bhakdi S, Rose-John S. Pore-forming toxins trigger shedding of receptors for interleukin 6 and lipopolysaccharide. Proc Natl Acad Sci U S A. 1996;93(15):7882–7.

136. Matthews V, Schuster B, Schütze S, Kallen K-J, Rose-John S. Cholesterol depletion of the plasma membrane triggers shedding of the human interleukin-6 receptor by TACE and independently of PKC. J Biol Chem. 2003;278(40):38829–39.

137. Vollmer P, Walev I, Rose-John S, Bhakdi S. Novel pathogenic mechanism of microbial metalloproteinases: Liberation of membrane-anchored molecules in biologically active form exemplified by studies with the human interleukin-6 receptor. Infect Immun. 1996;64(9):3646–51.

138. Chalaris A, Rabe B, Paliga K, Lange H, Laskay T, Fielding CA, et al. Apoptosis is a natural stimulus of IL6R shedding and contributes to the proinflammatory trans-signaling function of neutrophils. Blood. 2007;110(6):1748–55.

139. Müllberg J, Schooltink H, Stoyan T, Heinrich PC, Rose-John S. Protein kinase C activity is rate limiting for shedding of the interleukin-6 receptor. Biochem Biophys Res Commun. 1992;189(2):794–800.

140. Fischer M, Goldschmitt J, Peschel C, Brakenhoff JP, Kallen KJ, Wollmer A, et al. A bioactive designer cytokine for human hematopoietic progenitor cell expansion. Nat Biotechnol. 1997;15(2):142–5.

141. Garbers C, Aparicio-Siegmund S, Rose-John S. The IL-6/gp130/STAT3 signaling axis: recent advances towards specific inhibition. Curr Opin Immunol. 2015 Jun;34:75–82.

142. Schmidt-Arras D, Rose-John S. IL-6 pathway in the liver: From physiopathology to therapy. J Hepatol. Elsevier; 2016 Jun 1;64(6):1403–15.

143. Maione D, Di Carlo E, Li W, Musiani P, Modesti A, Peters M, et al. Coexpression of IL-6 and soluble IL-6R causes nodular regenerative hyperplasia and adenomas of the liver. EMBO J. 1998;17(19):5588–97.

144. Peters BM, Schirmacher P, Goldschmitt J, Odenthal M, Peschel C, Fattori E, et al. Extramedullary expansion of hematopoietic progenitor cells in interleukin (IL)-6-sIL-6R double transgenic mice. J Exp Med. 1997;185(4):755–66.

145. Schirmacher P, Peters M, Ciliberto G, Blessing M, Lotz J, Meyer Zum Büschenfelde KH, et al. Hepatocellular hyperplasia, plasmacytoma formation, and extramedullary hematopoiesis in interleukin (IL)-6/soluble IL-6 receptor double-transgenic mice. Am J Pathol. 1998;153(2):639–48.

146. Peters M, Blinn G, Jostock T, Schirmacher P, Meyer zum Büschenfelde KH, Galle PR, et al. Combined interleukin 6 and soluble interleukin 6 receptor accelerates murine liver regeneration. Gastroenterology. 2000;119(6):1663–71.

147. Hecht N, Pappo O, Shouval D, Rose-John S, Galun E, Axelrod JH. Hyper-IL-6 gene therapy reverses fulminant hepatic failure. Mol Ther. 2001;3(5 I):683–7.

148. Galun E, Zeira E, Pappo O, Peters M, Rose-John S. Liver regeneration induced by a designer human IL-6/sIL-6R fusion protein reverses severe hepatocellular injury. FASEB J. 2000 Oct;14(13):1979–87.

149. Padberg F, Feneberg W, Schmidt S, Schwarz MJ, Körschenhausen D, Greenberg BD, et al. CSF and serum levels of soluble interleukin-6 receptors (sIL-6R and sgp130), but not of interleukin-6 are altered in multiple sclerosis. J Neuroimmunol. 1999;99(2):218–23.

150. Waage A, Brandtzaeg P, Halstensen A, Kierulf P, Espevik T. The Complex Pattern of Cytokines in Serum From Patients With Meningococcal Septic Shock. J Exp Med. 1989;169(January):333–8.

151. Nowell MA, Williams AS, Carty SA, Scheller J, Hayes AJ, Jones GW, et al. Therapeutic Targeting of IL-6 Trans Signaling Counteracts STAT3 Control of Experimental Inflammatory Arthritis. J Immunol. 2009;182(1):613–22.

152. Richards PJ, Nowell MA, Horiuchi S, McLoughlin RM, Fielding CA, Grau S, et al. Functional characterization of a soluble gp130 isoform and its therapeutic capacity in an experimental model of inflammatory arthritis. Arthritis Rheum. 2006;54(5):1662–72.

153. Nowell MA, Richards PJ, Horiuchi S, Yamamoto N, Rose-John S, Topley N, et al. Soluble IL-6 Receptor Governs IL-6 Activity in Experimental Arthritis: Blockade of Arthritis Severity by Soluble Glycoprotein 130. J Immunol. 2003;171(6):3202–9.

154. Atreya R, Mudter J, Finotto S, Müllberg J, Jostock T, Wirtz S, et al. Blockade of interleukin 6 trans signaling suppresses T-cell resistance against apoptosis in chronic intestinal inflammation: Evidence in Crohn disease and experimental colitis in vivo. Nat Med. 2000;6(5):583–8.

155. Matsumoto S, Hara T, Mitsuyama K, Yamamoto M, Tsuruta O, Sata M, et al. Essential Roles of IL-6 Trans-Signaling in Colonic Epithelial Cells, Induced by the IL-6/Soluble-IL-6 Receptor Derived from Lamina Propria Macrophages, on the Development of Colitis-Associated Premalignant Cancer in a Murine Model. J Immunol. 2010 Feb 1;184(3):1543–51.

156. Lesina M, Kurkowski MU, Ludes K, Rose-John S, Treiber M, Klöppel G, et al. Stat3/Socs3 Activation by IL-6 Transsignaling Promotes Progression of Pancreatic Intraepithelial Neoplasia and Development of Pancreatic Cancer. Cancer Cell. 2011;19(4):456–69.

157. Lo CW, Chen MW, Hsiao M, Wang S, Chen CA, Hsiao SM, et al. IL-6 trans-signaling in formation and progression of malignant ascites in ovarian cancer. Cancer Res. 2011;71(2):424–34.

158. Ara T, Declerck YA. Interleukin-6 in bone metastasis and cancer progression. Eur J Cancer. Elsevier Ltd; 2010;46(7):1223–31.

159. Guo Y, Xu F, Lu T, Duan Z, Zhang Z. Interleukin-6 signaling pathway in targeted therapy for cancer. Cancer Treat Rev. Elsevier Ltd; 2012 Nov;38(7):904–10.

160. Xu B, Chen Q, Yue C, Lan L, Jiang J, Shen Y, et al. Prognostic value of IL-6R mRNA in lung adenocarcinoma and squamous cell carcinoma. Oncol Lett. 2018;16(3):2935–48.

161. Chen Q, Xu B, Lan L, Yang D, Yang M, Jiang J, et al. High mRNA expression level of IL-6R was associated with better prognosis for patients with ovarian cancer: a pooled meta-analysis. Sci Rep. 2017;7(1):8769.

162. Yokomuro S, Lunz JG, Sakamoto T, Ezure T, Murase N, Demetris AJ. The effect of interleukin-6 (IL-6)/gp130 signalling on biliary epithelial cell growth, in vitro. Cytokine. 2000;12(6):727–30.

163. Yokomuro S, Tsuji H, Lunz JG, Sakamoto T, Ezure T, Murase N, et al. Growth control of human biliary epithelial cells by interleukin 6, hepatocyte growth factor, transforming growth factor β1, and activin A: Comparison of a cholangiocarcinoma cell line with primary cultures of non- neoplastic biliary epithelial cells. Hepatology. 2000;32(1):26–35.

164. Park J, Gores GJ, Patel T. Lipopolysaccharide induces cholangiocyte proliferation via an interleukin-6-mediated activation of p44/p42 mitogen-activated protein kinase. Hepatology. 1999;29(4):1037–43.

165. Pinto C, Giordano DM, Maroni L, Marzioni M. Role of inflammation and proinflammatory cytokines in cholangiocyte pathophysiology. Biochimica et Biophysica Acta - Molecular Basis of Disease. 2018. p. 1270–8.

166. Meng F, Yamagiwa Y, Ueno Y, Patel T. Over-expression of interleukin-6 enhances cell survival and transformed cell growth in human malignant cholangiocytes. J Hepatol. 2006;44(6):1055–65.

167. Park J, Tadlock L, Gores GJ, Patel T. Inhibition of interleukin 6-mediated mitogen-activated protein kinase activation attenuates growth of a cholangiocarcinoma cell line. Hepatology. 1999;30(5):1128–33.

168. Tadlock L. Involvement of p38 mitogen-activated protein kinase signaling in transformed growth of a cholangiocarcinoma cell line. Hepatology. 2002;33(1):43–51.

169. Wehbe H, Henson R, Meng F, Mize-Berge J, Patel T. Interleukin-6 contributes to growth in cholangiocarcinoma cells by aberrant promoter methylation and gene expression. Cancer Res. 2006;66(21):10517–24.

170. Hodge DR, Peng B, Cherry JC, Hurt EM, Fox SD, Kelley JA, et al. Interleukin 6 supports the maintenance of p53 tumor suppressor gene promoter methylation. Cancer Res. 2005;65(11):4673–82.

171. Wang Y, van Boxel-Dezaire AHH, Cheon H, Stark GR, Yang J. STAT3 activation in response to IL-6 is prolonged by the binding of IL-6 receptor to EGF receptor. Proc Natl Acad Sci. 2013;110(42):16975–80.

172. Zhou QX, Jiang XM, Wang ZD, Li CL, Cui YF. Enhanced expression of suppresser of cytokine signaling 3 inhibits the IL-6-induced epithelial-to-mesenchymal transition and cholangiocarcinoma cell metastasis. Med Oncol. 2015;32(4).

173. Isomoto H, Mott JL, Kobayashi S, Werneburg NW, Bronk SF, Haan S, et al. Sustained IL-6/STAT-3 Signaling in Cholangiocarcinoma Cells Due to SOCS-3 Epigenetic Silencing. Gastroenterology. 2007;132(1):384–96.

174. Isomoto H, Kobayashi S, Werneburg NW, Bronk SF, Guicciardi ME, Frank DA, et al. Interleukin 6 upregulates myeloid cell leukemia-1 expression through a STAT3 pathway in cholangiocarcinoma cells. Hepatology. 2005;42(6):1329–38.

175. Goydos JS, Brumfield AM, Frezza E, Booth A, Lotze MT, Carty SE. Marked elevation of serum interleukin-6 in patients with cholangiocarcinoma: validation of utility as a clinical marker. Ann Surg. 1998;227(3):398–404.

176. Cheon YK, Cho YD, Moon JH, Jang JY, Kim YS, Kim YS, et al. Diagnostic utility of interleukin-6 (IL-6) for primary bile duct cancer and changes in serum IL-6 levels following photodynamic therapy. Am J Gastroenterol. 2007;102(10):2164–70.

177. Andersen JB, Spee B, Blechacz BR, Avital I, Komuta M, Barbour A, et al. Genomic and genetic characterization of cholangiocarcinoma identifies therapeutic targets for tyrosine kinase inhibitors. Gastroenterology. 2012;142(4).

178. Dokduang H, Techasen A, Namwat N, Khuntikeo N, Pairojkul C, Murakami Y, et al. STATs profiling reveals predominantly-activated STAT3 in cholangiocarcinoma genesis and progression. In: Journal of Hepato-Biliary-Pancreatic Sciences. 2014. p. 767–76.

179. Feng S, Liang L, Guo-jun H, Qin-guo X, Bao-hua Z, Xin-wei Y, et al. STAT3 overexpression promotes metastasis in intrahepatic cholangiocarcinoma and correlates negatively with surgical outcome. Oncotarget. 2016;8(5).

180. Brooks GD, McLeod L, Alhayyani S, Miller A, Russell PA, Ferlin W, et al. IL6 trans-signaling promotes KRAS-driven lung carcinogenesis. Cancer Res. 2016;76(4):866–76.

181. Bergmann J, Müller M, Baumann N, Reichert M, Heneweer C, Bolik J, et al. IL-6 trans-signaling is essential for the development of hepatocellular carcinoma in mice. Hepatology. 2017;65(1).

182. Becker C, Fantini MC, Schramm C, Lehr HA, Wirtz S, Nikolaev A, et al. TGF-β Suppresses Tumor Progression in Colon Cancer by Inhibition of IL-6 trans-Signaling. Immunity [Internet]. 2004 Oct;21(4):491–501. Available from: http://linkinghub.elsevier.com/retrieve/pii/S1074761304002432

183. Holmer R, Wätzig GH, Tiwari S, Rose-John S, Kalthoff H. Interleukin-6 trans-signaling increases the expression of carcinoembryonic antigen-related cell adhesion molecules 5 and 6 in colorectal cancer cells. BMC Cancer. 2015;15(1):975.

184. Prayong P, Mairiang E, Pairojkul C, Chamgramol Y, Mairiang P, Bhudisawasdi V, et al. An Interleukin-6 Receptor Polymorphism is Associated with Opisthorchiasis-Linked Cholangiocarcinoma Risk in Thailand. Asian Pacific J Cancer Prev. 2014 Jul 15;15(13):5443–7.

185. Saijyo S, Kudo T, Suzuki M, Katayose Y, Shinoda M, Muto T, et al. Establishment of a new extrahepatic bile duct carcinoma cell line, TFK-1. Tohoku J Exp Med. 1995;177(1):61–71.

186. Scherdin G, Garbrecht M, Klouche M. In vitro interaction of á-difluoromethylornithine (DFMO) and human recombinant interferon-a (rIFN-a) on human cancer cell lines. Immunobiology. 1987;175:1–143.

187. Knuth A, Gabbert H, Dippold W, Klein O, Sachsse W, Bitter-Suermann D, et al. Biliary adenocarcinoma. Characterisation of three new human tumor cell lines. J Hepatol. 1985;1(6):579–96.

188. Rubbert-Roth A, Furst DE, Nebesky JM, Jin A, Berber E. A Review of Recent Advances Using Tocilizumab in the Treatment of Rheumatic Diseases. Rheumatol Ther. 2018;

189. Venkiteshwaran A. Tocilizumab. mAbs. 2009. p. 430–5.

190. Garbers C, Jänner N, Chalaris A, Moss ML, Floss DM, Meyer D, et al. Species specificity of ADAM10 and ADAM17 proteins in interleukin-6 (IL-6) trans-signaling and novel role of ADAM10 in inducible IL-6 receptor shedding. J Biol Chem. 2011;286(17):14804–11.

191. Livak KJ, Schmittgen TD. Analysis of relative gene expression data using real-time quantitative PCR and the 2(-Delta Delta C(T)) Method. Methods. 2001;25(4):402–8.

192. Wang K, Li M, Hakonarson H. ANNOVAR: Functional annotation of genetic variants from high-throughput sequencing data. Nucleic Acids Res. 2010;

193. Cingolani P, Platts A, Wang LL, Coon M, Nguyen T, Wang L, et al. A program for annotating and predicting the effects of single nucleotide polymorphisms, SnpEff: SNPs in the genome of Drosophila melanogaster strain w1118; iso-2; iso-3. Fly (Austin). 2012;

194. Prieto B, Miguel D, Costa M, Coto D, Alvarez F V. New quantitative electrochemiluminescence method (ECLIA) for interleukin-6 (IL-6) measurement. Clin Chem Lab Med. 2010;48(6):835–8.

195. Gebaeck T, Schulz MMP, Koumoutsakos P, Detmar M. TScratch: A novel and simple software tool for automated analysis of monolayer wound healing assays. Biotechniques. 2009;46(4):265–74.

196. Zhang M, Gong W, Zhang Y, Yang Y, Zhou D, Weng M, et al. Expression of interleukin-6 is associated with epithelial-mesenchymal transition and survival rates in gallbladder cancer. Mol Med Rep. 2015;11(5):3539–46.

197. Karczewska A, Nawrocki S, Bręborowicz D, Filas V, Mackiewicz A. Expression of interleukin-6, interleukin-6 receptor, and glycoprotein 130 correlates with good prognoses for patients with breast carcinoma. Cancer. 2000;88(9):2061–71.

198. Becker C, Fantini MC, Wirtz S, Nikolaev A, Lehr HA, Galle PR, et al. IL-6 signaling promotes tumor growth in colorectal cancer. Cell Cycle. 2005;4(2):217–20.

199. Jiao X, Yu W, Qian J, Chen Y, Wei P, Fang W, et al. ADAM-17 is a poor prognostic indicator for patients with hilar cholangiocarcinoma and is regulated by FoxM1. BMC Cancer. 2018;

200. Graf D, Kohlmann C, Haselow K, Gehrmann T, Bode JG, Häussinger D. Bile acids inhibit interleukin-6 signaling via gp130 receptor-dependent and -independent pathways in rat liver. Hepatology. 2006;44(5):1206–17.

201. Fusenig NE, Capes-Davis A, Bianchini F, Sundell S, Lichter P. The need for a worldwide consensus for cell line authentication: Experience implementing a mandatory requirement at the International Journal of Cancer. PLoS Biol. 2017;15(4).

202. Farshidfar F, Zheng S, Gingras MC, Newton Y, Shih J, Robertson AG, et al. Integrative Genomic Analysis of Cholangiocarcinoma Identifies Distinct IDH-Mutant Molecular Profiles. Cell Rep. 2017;18(11):2780–94.

203. Borger DR, Tanabe KK, Fan KC, Lopez HU, Fantin VR, Straley KS, et al. Frequent Mutation of Isocitrate Dehydrogenase (IDH)1 and IDH2 in Cholangiocarcinoma Identified Through Broad-Based Tumor Genotyping. Oncologist. 2012;

204. Tan M, Yu D. Molecular mechanisms of ErbB2-mediated breast cancer chemoresistance. Advances in Experimental Medicine and Biology. 2007. p. 119–29.

205. Treekitkarnmongkol W, Suthiphongchai T. High expression of ErbB2 contributes to cholangiocarcinoma cell invasion and proliferation through AKT/p70S6K. World J Gastroenterol. 2010;16(32):4047–54.

206. Nam A-R, Kim J-W, Cha Y, Ha H, Park JE, Bang J-H, et al. Therapeutic implication of HER2 in advanced biliary tract cancer. Oncotarget. 2016 Sep 6;7(36).

207. Zach S, Birgin E, Rückert F. Primary Cholangiocellular Carcinoma Cell Lines. J Stem Cell Res Transplant J Stem Cell Res Transpl. 2015;2(2):1013–1.

208. Shimizu Y, Demetris AJ, Gollin SM, Storto PD, Bedford HM, Altarac S, et al. Two new human cholangiocarcinoma cell lines and their cytogenetics and responses to growth factors, hormones, cytokines or immunologic effector cells. Int J Cancer. 1992;52(2):252–60.

209. American Type Culture Collection. Technical Bulletin No 7: Passage Number Effects In Cell Lines. 2010;3. Available from: https://www.atcc.org/~/media/PDFs/Technical Bulletins/tb07.ashx

210. Mackenzie CG. THE EFFECT OF pH ON GROWTH, PROTEIN SYNTHESIS, AND LIPID-RICH PARTICLES OF CULTURED MAMMALIAN CELLS. J Cell Biol. 1961 Jan 1;9(1):141–56.

211. Rzymski T, Petry A, Kračun D, Rie F, Pike L, Harris AL, et al. The unfolded protein response controls induction and activation of ADAM17/TACE by severe hypoxia and ER stress. Oncogene. 2012;

212. Zohlnhöfer D, Graeve L, Rose-John S, Schooltink H, Dittrich E, Heinrich PC. The hepatic interleukin-6 receptor Down-regulation of the interleukin-6 binding subunit (gp80) by its ligand. FEBS Lett. 1992;

213. Jung YD, Shim JW, Park SJ, Choi SH, Yang K, Heo K, et al. Downregulation of UHRF1 promotes EMT via inducing CXCR4 in human cancer cells. Int J Oncol. 2015;

214. Sun Y, März P, Otten U, Ge J, Rose-John S. The effect of gp130 stimulation on glutamate-induced excitotoxicity in primary hippocampal neurons. Biochem Biophys Res Commun. 2002;295(2):532–9.

215. Nesbitt JE, Fuller GM. Dynamics of interleukin-6 internalization and degradation in rat hepatocytes. J Biol Chem. 1992;267(9):5739–42.

216. Dittrich E, Rose-John S, Gerhartz C, Müllberg J, Stoyan T, Yasukawa K, et al. Identification of a region within the cytoplasmic domain of the interleukin-6 (IL-6) signal transducer gp130 important for ligand-induced endocytosis of the IL-6 receptor. J Biol Chem. 1994;269(29):19014–20.

217. Liu FT, Jia L, Wang P, Farren T, Li H, Hao X, et al. CD126 and targeted therapy with tocilizumab in chronic lymphocytic leukemia. Clin Cancer Res. 2016;22(10):2462–9.

218. Kim NH, Kim SK, Kim DS, Zhang D, Park JA, Yi H, et al. Anti‐proliferative action of IL‐6r-targeted antibody tocilizumab for non-small cell lung cancer cells. Oncol Lett. 2015;9(5):2283–8.

219. Gough DJ, Corlett A, Schlessinger K, Wegrzyn J, Larner AC, Levy DE. Mitochondrial STAT3 supports RasDependent oncogenic transformation. Science (80-). 2009;324(5935):1713–6.

220. Long KB, Tooker G, Tooker E, Luque SL, Lee JW, Pan X, et al. IL6 Receptor Blockade Enhances Chemotherapy Efficacy in Pancreatic Ductal Adenocarcinoma. Mol Cancer Ther. 2017 Sep;16(9):1898–908.

Appendix

Cell numbers for seedings

Cell line	Cell cycle	Scratch assay	Proliferation assay	6-well plate	96-well plate
TFK-1	$4x10^4$	$8x10^5$	$5x10^3$	$3x10^5$	$1*10^4$
Mz-ChA-1	$5x10^4$	$1x10^6$	$5x10^3$	$2.5x10^5$	-
Mz-ChA-2	$2x10^4$	$5x10^5$	$2x10^3$	$1.5x10^5$	$5*10^3$

Immunofluorescence

Preparation of cell seedings on IHC slides

1. Autoclave Flexiperms in ddH_2O
2. Sterilize coated IHC slides using 70% EtOH
3. Put Flexiperms and slides under aseptic conditions together (make sure Flexiperms are tightly attached to slides)
4. UV light sterilization for 20 min (make sure the wells are dry)
5. Wash wells with PBS
6. Pipette cells into wells (appr. $1x10^4$ cells/well)
7. Incubate them until proper morphology is present
8. Fix them with 3.7% formalin in PBS (10 min RT) or ice-cold MeOH (10 min -20°C)
9. Wash with PBS
10. Remove Flexiperm
11. Put them shortly into increasing EtOH concentrations
12. Let them dry
13. Store at RT or -20°C till usage

Staining procedure

1. If stored at -20°C, thaw slides for 10 min
2. Circle wells with PAP-Pen
3. Wash 2x 3 min with 0.1 % TBS-T
4. Permeabilize (if necessary) using 1% Triton X-100 for 15 min at RT
5. Block unspecific signals with 5% horse serum in T-BST for 60 min at RT
6. Dilute primary antibody in 0.1% TBS-T containing 0.2% BSA
7. Incubate with primary antibody overnight at 4°C
8. Wash 3x10 min with TBS-T
9. Dilute secondary antibody (in 0.1 TBS-T containing 0.2% BSA)
10. Incubate secondary antibody for 1h at RT under light protection
11. Wash 3x 10 min with TBS-T
12. Counterstain with DAPI (1:1 000 in TBS-T) for 5 min
13. Wash 3x10 min with TBS-T
14. Mount slides with proper fluorescence mounting medium
15. Seal slides and cover glasses with nail polish
16. Immediately microscope slides or store at 4°C for 1 week prior microscopy

CD126 cell surface Staining:

1. Detach cells enzyme-free with 10 mM EDTA in PBS (containing 0.01% NaN_3)
2. Filter cells with cell strainer, count cells
3. Harvest $2x10^6$ cells by centrifuging 350 x g 5 min @ 4°C, discard supernatant
4. Resuspend cells in 500 µL Blocking Buffer (PBS containing 10% FBS), incubate 10 min on ice
5. Centrifuge 350 x g 5 min @4°C, discard supernatant
6. Resuspend in pre-chilled 200 µL Cell Staining Buffer (PBS containing 5% BSA),
7. Aliquot 2x
   a) Istoype Ctrl
   b) CD126á 100 µL for
8. Add 5 µL CD126-APC antibody to 100 µL cell suspension ($1x10^6$ cells).
9. Incubate 60 min on ice in the dark on ice
10. Wash 2x with ~1mL Cell Staining Buffer by centrifugation @ 350 x g 5min for 5 min
11. Resuspend in 200 µL Cell Staining Buffer
12. Analyze by flow cytometer

Cell cycle analysis

1. Detach cells using trypsin
2. Resuspend in full medium
3. Centrifuge 200 x g 4min at 4°C
4. Resuspend pellet in PBS
5. Centrifuge 200 x g 4min at 4°C
6. Resuspend in 200 µL PI Buffer (0.1% Trisodium citrate, 0. 1% Triton X-100, 100 µg/mL RNAseA and 50 µg/mL PI)
7. Incubate 20 min at RT
8. Measure immediately (latest after 2h on ice with light protection)
9. Analyze cell cycle by ModFit

Cell viability assay (MTT)

1. Cultivate cells in 96-well plate
2. Add 5 mg/mL MTT solution to a final concentration of 0.5 mg/mL per well
3. Incubate plate for 2 h or until violet cells are visible
4. Remove supernatant
5. Add 20 µL 3% SDS to each well
6. Add a 100 µL of a 25:1 mixture isopropanol and 1M HCl (v/v)
7. Shake plate until crystals are dissolved
8. Measure wavelength at 570 nm (Background 650 nm)

Apoptosis assay (YoPro)

1. Cultivate cells in 96-well plate
2. Add YoPro Iodide to a final concentration of final concentration 5 µM to wells
3. Incubate 15 min at 37°C
4. Discard supernatant
5. Add 140 µL PBS
6. Measure 485/528 nm (ex/em)

List of devices

Device	Producer	Place
Biofuge Fresco	Heraeus	Hanau, Germany
Biospectrometer	Eppendorf	Hamburg, Germany
Electrophoresis Powersupply EPS 301	GE Healthcare	Little Chalfont, UK
GeneAmp 9700 Thermocycler	Applied Biosystems	Foster City, USA
Image Quant Las 500	GE Healthcare	Little Chalfont, UK
MagNA LYSER	Roche Diagnostics	Risch-Rotkreuz, Switzerland
Mini-Shaker MS1	Ika	North Carolina, USA
Mini-vertical electrophoresis unit SE250	Hoefer inc.	Richmond, USA
NanoDROP 1000	Thermo Fischer Scientific	Massachusetts, USA
Quant Studio 7 Flex	Applied Biosystems	Foster City, USA
Semi-dry Blotting Unit V20-SDB	Scieplas	Cambridge, UK
Semi-Micro Analytical Balance GR200EC	A&D Company	Tokyo, JAPAN
Thermomixer comfort	Thermo Fischer scientific	Massachusetts, USA
Vertical Shaker Duomax 1030	Heidolph	Schwabach, Germany

List of buffers

Buffer/ Solution	Component	Amount	Final concentration
NP-40 lysis buffer	1 M Tris-HCl (pH 7.5)	50 mL	50 mM
	5 M NaCl	30 mL	150 mM
	NP-40	5 mL	0.5%
	ddH_2O	adjust to 500 mL	
Protein lysis buffer	0.1 M Pefabloc	100µl	1 mM
	1 M DTT	10 µl	1 mM
	1 tablet of cOmplete Mini and PhosSTOP in 1mL		
	ddH_2O	1 ml	10%
	NP-40 lysis buffer	9 mL	
10x SDS-running buffer			
	Tris HCl (pH 8.4)	30.29 g	250 mM
	Glycine	14.13 g	192 mM
	SDS	10 g	1%
	ddH_2O	adjust to 1 L	
Towbin Transfer Buffer			
	Tris	3.03 g	250 mM
	Glycine	14.26 g	190 mM
	Methanol	adjust to 500 mL	1%
10 xTBS Buffer	Tris	24.2 g	0.2 M
	NaCl	80.0 g	1.4 M
		adjust pH 7.6 to 1	
	ddH2O	L	
0.1% TBS-Tween	10x TBS Buffer	100 mL	1x
	Tween-20	1 ml	0.1%
	ddH_2O	adjust to 1 L	

Ethical vote for this study

Ethikkommission

Medizinische Universität Graz

Auenbruggerplatz 2, A-8036 Graz
ethikkommission@medunigraz.at
Tel.: +43 / 316 / 385-13928, Fax: -14348

FOLGEVOTUM

gültig bis 14.03.2020

EK-Nummer:	28-294 ex 15/16
Studientitel:	Biochemische und genetische Analyse von molekulare Signalwege der cholangiozellulären Karzinogenese
Prüfer:	Assoz. Prof. Dr. Dr. Johannes Haybäck Institut für Pathologie
Sponsor:	Institut für Pathologie
Ansprechpartner:	Assoz. Prof. Dr. Dr. Johannes Haybäck, 8036 Graz, Auenbruggerplatz 25
CRO:	-
Antragsteller:	Medizinische Universität Graz
Ansprechpartner:	BSc MSc Florian Kleinegger, 8010 Graz, Neue Stiftingtalstraße 6

Die o.a. Studie wurde von der Ethikkommission erstmals im 'expedited Review' am 22.02.2016 behandelt. Die Ethikkommission ist zu folgendem Schluss gekommen:

Es besteht kein Einwand gegen die Durchführung der Studie in der vorliegenden Form.

Kommissionsmitglieder, die für diesen Tagesordnungspunkt als befangen anzusehen waren und daher gemäß Geschäftsordnung an der Entscheidungsfindung und Abstimmung nicht teilgenommen haben: keine

Zur Beurteilung vorliegende Dokumente:

Dokumente eingegangen am 15.02.2016, begutachtet im 'expedited Review' am 22.02.2016	
✓ Cover Letter Covering Letter_pathways of CCC 1.0	15.02.2016
✓ Antragsformular ECS Teil A unterschrieben	15.02.2016
✓ Antragsformular ECS	15.02.2016
Originalprotokoll Studyprotocol_pathways of CCC 1.0	15.02.2016
Informed Consent Form Patienteninformation_pathways of CCC 1.0	15.02.2016
✓ Conflict of Interest Erklärung Erklärung von Interessenskonflikten_pathways of CCC 1.0	15.02.2016
✓ CV CV_Johannes_Haybaeck 1.0	15.02.2016
✓ Sonstiges: 2. Stellungsnahme Biobank Graz_pathways of CCC 1.1	15.02.2016
✓ Sonstiges: 1.Stellungnahme_Biobank Graz_pathways of CCC 1.0	29.01.2016
✓ Sonstiges: Antrag auf Erlass der Bearbeitungsgebühren_pathways of CCC 1.0	15.02.2016
✓ Sonstiges: Zustimmungserklärung_pathways of CCC 1.0	15.02.2016
✓ Antrag Teil B ECS unterschrieben	15.02.2016
Dokumente eingegangen am 29.02.2016, begutachtet im 'expedited Review' am 14.03.2016	
✓ Originalprotokoll 2.0	26.02.2016
✓ Informed Consent Form 2.0	26.02.2016
✓ Informed Consent Form BIOBANK 4.0	17.10.2010
✓ Sonstiges: Stellungnahme zur Bearbeitungsmitteilung	29.02.2016

Scientific contributions and conference activities (excerpt)

Kleinegger, F; Hofer, E; Wodlej, C; Golob-Schwarzl, N; Birkl-Toeglhofer, AM; Stallinger, A; Petzold, J; Orlova, A; Krassnig, S; Reihs, R; Niedrist, T; Mangge, H; Park, YN; Thalhammer, M; Aigelsreiter, A; Lax, S; Garbers, C; Fickert, P; Rose-John, S; Moriggl, R; Rinner, B; Haybaeck, J.
Pharmacologic IL-6Rα inhibition in cholangiocarcinoma promotes cancer cell growth and survival. Biochim Biophys Acta Mol Basis Dis. 2018; 1865(2):308-321

Jahanafrooz, Z; Stallinger, A; Anders, I; **Kleinegger, F**; Lohberger, B; Durchschein, C; Bauer, R; Deutsch, A; Rinner, B; Kretschmer, N. *Influence of silibinin and β-β-dimethylacrylshikonin on chordoma cells*. Phytomedicine. 2018; 49:32-40

Stallinger, A; **Kleinegger, F**; Brvar, L; Liegl-Atzwanger, B; Prokesch, A; Durschein, C; Bauer, R; Deutsch, A; Kretschmer, N; Rinner, B; *β-β-dimethylacrylshikonin induces Apoptosis in Melanoma Cell lines by NOXA Upregulation,* manuscript submitted

Golob-Schwarzl, N; Wodlej, C; **Kleinegger, F**; Toeglhofer, AM; Krassnig, S; Thalhammer, M; Aigelsreiter, A; Hayback, J. *Eukaryotic Translation Initiation Factors Might Represent a Potential Therapeutic Target for Gallbladder Cancer.* ONCOL RES TREAT. 2018; 41: 68-68.-33.

Kleinegger, F; Schrom, S; Thalhammer, M; Aigelsreiter, A; Haybäck, J; Heitzer, E; Rinner, B.
Establishment of a New Cholangiocarcinoma Cell Line MUG-CCArly1. 21st European Congress on Alternatives for Animal Testing. 2018;

Kleinegger, F; Wodlej, C; Golob-Schwarzl, N; Birkl-Töglhofer, AM; Krassnig, S; Niedrist, T; Thalhammer, M; Aigelsreiter, A; Rose-John, S; Fickert, P; Rinner, B; Haybäck, J.
Classic and Trans Interleukin-6 Signaling Promotes Cholangiocarcinoma.
6th International Students Congress. 2018

Wodlej, C; Krassnig, S; Golob-Schwarzl, N; **Kleinegger, F**; Toeglhofer, AM; Sygulla, S; Singer, G; Till, H; Izycka-Swieszewska, E; Czapiewski, P; Haybaeck, J.
The Role of Eukaryotic Translation Initiation Factors as Potential Targets in Neuroblastoma
ONCOL RES TREAT. 2018; 41: 131-131.-33. Deutscher Krebs Kongress

Kleinegger, F; Golob-Schwarzl, N; Toeglhofer, AM; Baran, P; Krassnig, S; Niedrist, T; Speicher, I; Rinner, B; Thalhammer, M; Aigelsreiter, A; Lackner, C; Scheller, J; Rose-John, S; Fickert, P; Haybaeck, J. *Interleukin-6 Receptor influences cholangiocarcinoma progression*
VIRCHOWS ARCH. 2017; 471: S325-S326.-29th European Congress of Pathology; 2017;